Marine Biofouling Control by Ultraviolet Light: Development, Ecological Impact and Genomic Assessment.

Paul Whitworth

School of Natural and Environmental Sciences

A thesis submitted for the degree of

Doctorate of Philosophy (PhD)

December 2022

Abstract

Biofouling is an issue for any surface within the marine environment, causing environmental and financial ramifications. The harmful effects of ultraviolet (UV) light have been well documented in the literature. Its use as an antifoulant, however, is at a developmental stage. Recent technological advancements have produced smaller and more affordable components which can be developed into new innovations. This study investigated the potential of UV B/C (265-300nm) light-emitting diodes (LEDs) for biofouling prevention. This was achieved by the production and analysis of a reproducible system for UV delivery, determination of irradiance thresholds of effect, analysis of UV damage and diatom repair mechanisms, including genotoxicity, and evaluating biofouling control during field deployments over 12 months and at two environmentally distinct locations.

The development of a UV LED-embedded tile system was challenging with initial designs requiring improvements in surface coverage by UV radiation. Tile developments included producing high irradiance capacities and coverage of target surfaces. Highly turbid conditions were found to restrict the transmission of UV from the tile's surface to < 1cm. Although transmission was recorded up to 14cm in the clearest conditions, the effective threshold was within a working range up to 5cm from the surface. LED integration for UV supply was successful and analysis indicated high capacities whilst minimising exposure towards non-target organisms.

The specific UV threshold for effect on the marine diatom *Navicula incerta* was explored by comparing UV exposure at different duration, pulsing and intensity conditions. Continuous exposure over long periods achieved progressively lower biomass of biofouling. Growth reductions were achievable after 2 hours and growth suppression of 87% was recorded after 24 hours. LED pulsing restricted growth compared to controls in all duty cycles trialled, however, duty cycles required a fluence between 0.94 and 2.34 J/cm^2 to reduce biomass. High irradiance intensities produced greater reductions in biomass more readily than at lower irradiances. Using all three methods, specific doses for the prevention of growth of *N. incerta* were determined to be 20-42 J/cm^2 depending on the delivery method.

Cyclobutane pyrimidine dimer (CPD) formation and photoactive repair for *N. incerta* were quantified at specific irradiance exposures. A linear effect was visible for both damage over time and photoactive repair. Peak CPD concentrations of ~ 180 μg/ml^{-1} were reached after 24 hours of exposure; this was reduced by over 45% during a 24-hour repair period. Mutations

forming single nucleotide polymorphisms (SNPs) were less prominent in the higher exposure samples. Higher SNP counts found in low-exposure treatments suggest that organisms were not resilient to exposures over 60 minutes.

A comprehensive field study revealed the effectiveness of UV during practical application and the extent to which the system was able to operate. The photographic analysis determined a wide range of taxa, ranging from tunicates to tube worms, which colonised controls but were prevented within irradiated chambers. Biological restrictions were reproducible in two distinct geographical locations (Melbourne, Australia and Hartlepool, UK) displaying the universal nature of the application. The metagenetic analysis gave an insight into the microscopic biosphere indicating distinct eukaryotic and prokaryotic community structures.

This project successfully developed and tested an innovative UV tile in two biogeographically distinct locations. The technique displayed a wide spectrum of prevention on fouling taxa including the model species *N. incerta.* This study determined thresholds of effect, mutagenic response and organism resilience. Understanding these biological impacts is paramount when determining the feasibility of a new technology.

Acknowledgements

This project was conducted during an extremely difficult period and as such was met with numerous obstacles in which I required help and support from a range of people to push through to completion.

The 3rd-floor Ridley laboratory team became more than colleagues providing indispensable support, advice and technical expertise where needed.

I express thanks to Jess Clarke and John Finlay for their time and patience whilst conducting field sampling in all weather conditions.

Friends have offered support outside of work to give a well-needed break from the constant grind and to give a good work-life balance. I would like to thank Josh Raine and Stephen Johnston who were 1-2 years ahead of me and kept up the pressure whilst also providing some well-needed breaks from work life.

Supervisors have guided me to focus on the topics at hand and assisted in pushing the project beyond its initial design. Nick Aldred and Tony Clare have been indispensable in their support and supplied much-needed advice with writing and countless changes in drafts.

Finally, all of this would not be possible without my family who has driven me to tackle everything head-on despite the hardships.

I thank you all and everyone else who has assisted me to complete this arduous task.

Publications related to this thesis

Chapter 3 was published in February of 2022 in Frontiers in Marine Science as part of the special article, Impact and Management of Marine Biofouling.

Whitworth, P., Aldred, N., Reynolds, K. J., Plummer, J., Duke, P., & Clare, A. S. (2022). Importance of Duration, Duty-Cycling and Thresholds for the Implementation of Ultraviolet C in Marine Biofouling Control. Frontiers in Marine Science. **DOI:** https://doi.org/10.3389/fmars.2021.809011.

Table of Contents

List of tables and figures

Table 5.1. Average cyclobutane pyrimidine dimers (CPDs) (N=3) and single nucleotide polymorphisms (SNPs) of *Navicula incerta* populations after UV treatment and repair. 92

Table 5.2. Regression statistics for CPD abundances during photoreactivation after eight different UV exposure periods. Coefficient indicates the correlation direction and intensity (positive number = positive correlation, negative number = negative correlation). Significance correlations displayed by . < 0.06, * < 0.05, ** < 0.01. 94

Table of Abbreviations

Term	Abbreviation
Antifouling	AF
Apurine	AP
Base excision repair	BER
Benchmarking universal single-copy orthologs	BUSCO
Cyclobutane pyrimidine dimer	CPD
Defence science and technology laboratory	DSTL
Deoxyribonucleic acid	DNA
Dissolved organic carbon	DOC
Dissolved oxygen	DOC
Double strand break	DSB
Electromagnetic radiation	EMR
Fouling release	FR
Generalized linear modelling	GLM
Global genome repair	GGR
Harmful algal bloom	HAB
Homologous recombination	HR
Ionising radiation	IR
Lethal dose	LD
Light emitting diode	LED
Mismatch repair	MMR
Mycosporine-glutaminol-glucoside	MGG
Mycosporine-like amino acid	MAA
Nephelometric turbidity units	NTU
Non-homologous end joining	NHEJ
Non-indigenous species	NIS
Non-metric multi-dimensional scaling	NMDS
Nucleotide excision repair	NER
Operational taxonomic unit	OUT
Parts per thousand	PPT
Photoactive radiation	PAR
Photoproduct	PP
Polyethylene	PE
Polystyrene	PS
Polyvinyl chloride	PVC
Reactive oxygen species	ROS
Short/long patch.	S/LP
Single nucleotide polymorphisms	SNP
Single stand break	SSB
Standard operating procedure	SOP
Transcription coupled repair	TCR
Translesion DNA synthesis	TLS
Triplet-triplet electron transfer	TTET
Trubutyltin	TBT
Ultraviolet	UV

Ultraviolet radiation	UVR
Vacuum UV	VUV

Preface

The current project was a collaborative venture between Newcastle University, AkzoNobel and the Defence Science and Technology Laboratory (DSTL, UK). During the second year, the Defence Science and Technology Group (DST-G, Au) were encountered at a conference, showing interest and were willing to collaborate so were an added contributor.

The main funding body came from the materials for strategic advantage (MSA) program. This is an initiative run by DSTL to develop new materials for operational advantage. The MSAs' key activities were to develop novel concepts and techniques. This included the analysis and assessment of potential in emerging UK technologies for defence capabilities. The MSA provided dissemination opportunities, networking, and supervision. Dissemination allowed progress to be shared via a poster/oral presentation in years one and four of the project. The supervisory team provided motivation to continually progress, feedback on posters/presentations, and thesis edits towards completion.

Newcastle University offered facilities, molecular and biological expertise, bespoke facilities, and supervisory support. The University provided training workshops to enhance and develop new skills. These skills were to benefit the project and future career opportunities. The marine biofouling research laboratory at Newcastle University provided a team of experts in biology at the water-surface interface, with a focus on surface colonisation and biofouling. The team were able to advise in project development with expertise in biological organisms, polymer chemistry, surface scientists, hydrodynamicists, analytical chemists and molecular biologists. The laboratory had equipment that is custom-made for marine fouling organisms and unique for the project’s requirements. The supervisory team gave constructive feedback and regular project meetings to continually develop and progress the project.

AkzoNobel are an international company that designs and develops antifouling coatings available for the general consumer. AkzoNobel offered their technical expertise, facilities and resources for the development and deployment of equipment. The main contributions from AkzoNobel were the provision of field-testing facilities and the design, production and analysis of the ultraviolet (UV) light-emitting tile.

DST-G became a part of the project in the second year and offered the use of their facilities and personnel to allow a second field site. The team set up facilities, organised microbiology facilities and conducted monthly sampling of the UV system. The personnel, equipment and discussions allowed the project to grow beyond its initial design.

Working in collaboration with industrial, academic and government organisations provided a wide range of expertise. Contributions from a variety of collaborators benefitted the project immensely, enabling a wide spectrum of topics to be covered. The project would not have been as successful without the contributions of all involved.

The main objective of the study was to determine the potential of UVC for the prevention of marine fouling organisms in niche areas of marine vessels. The work was to build upon previous works conducted by Richard Piola and their team (DST-G), who established the concept (Piola *et al*., 2016). This was to be achieved by the design and construction of a UV supply system, analysing of the system's technical capabilities, comparison of UV effect on relevant biological organisms and advancement of the system to rectify any issues identified. This included determining onshore vs offshore transmission, the longevity of equipment and metabolic, genetic and community implications on fouling organisms. Each chapter covered a portion of these and were set out as follows:

Chapter 1:

A comprehensive review of UV was conducted to gain an understanding of the capabilities and uses currently available. Factors were covered including the mechanism of harm, the impact on organisms, biological resilience, how it is being applied, and its potential within biofouling.

Aims:

- To explore UVs mechanisms of effect
- Distinguish biological impact on a range of taxa.
- Determine coping mechanisms to UV damage.
- Explore UV technology with industrial applications.
- Delve into the potential of UV within biofouling.

Objectives:

- Explore literature to identify known mechanisms of effect, UV induced damage, repair mechanisms and methods to cope with UV exposure.
- Explore literature regarding technology using UV for sterilisation and inactivation.
- Summarise marine biofouling and current antifouling methods.
- Compare studies that have explored UV as an antifoulant.

Chapter 2:

UV-producing tiles were designed, development and compared for bench and field scale experiments. This required analysis of each tile's irradiance capacity, surface coverage, heat output, wavelength of emittance, and transmittance through different seawater conditions.

Aims:

- Develop a system for UV to be delivered underwater for the prevention of biofouling accumulation on the surface of the system.
- Determine the coverage of UV emittance and the irradiance output.
- Improve any flaws and engage in enhancement design.

Objectives:

- Produce a laboratory scale UV emitting tile for experimentation.
- Measure the UV output, surface coverage, heat generation and irradiance manipulation through voltage control.
- Produce an improved field scale UV emitting tile.
- Measure the field scale tile for UV output, surface coverage and UV transmission through water at varying turbidity's.

Chapter 3:

Laboratory experimentations were conducted on the biofilm-forming diatom *Navicula incerta* to determine UVs influence on settlement and growth. The section covered different exposure methodologies for UV treatment. The duration of exposure was evaluated to determine the level of prevention associated with different irradiation periods. Duty cycling was tested to give comparatives to duration results and assess if duty cycling could achieve effective biofouling prevention while prolonging LED lifespan. Irradiance intensity was manipulated by voltage control to assess settlement at different fluences over a set period of exposure. Intensity experiments allowed a fluence comparison to try and identify a threshold of effect for restricting the growth of *N. incerta*. A collective comparison between methodologies (duration, intensity and duty cycling) and their respective fluences, was conducted to explore variation between delivery methods.

Aims:

- Determine the level of effect of UV on *N. incerta* in laboratory experiments.
- Explore duration, pulsing and intensity delivery methods.

- Isolate thresholds of effect for each delivery method
- Determine variations between thresholds identified at similar fluences.

Objectives:

- Expose *Navicula incerta*. to UV and analyse survivability across a range of treatments for level of effect on cell densities.
- Alter conditions of exposure duration, pulsing frequency and intensity of irradiance and assess survivability.
- Correlate irradiance between methods to identify thresholds of effect for diatom inactivation.

Chapter 4:

UV exposure on wild-type organisms was assessed to determine the real-world application of UV as an antifoulant system. Environmental data were compared to determine if UV was affecting water conditions. UV exposed and control samples were compared for their community assemblages in different conditions (flow speeds, surface type, and geographical location) to determine coverage variations and identify resilient organisms from UV field treatments.

Aims:

- Ascertain UVs level of effect on wild-type biofouling organisms.
- Identify micro and macro fouling communities impacted by UV exposure.
- Assess differences detected in micro and macrofouling taxa identified through photographic and next generation methods.
- Assess the effectiveness of UV in biofouling prevention at two geographically distinct locations.
- Determine the potential of UVs use as a biofouling preventative within niche areas.
- Recognize environmental condition impacts and environmental-community interactions.

Objectives:

- Measure surface coverages of all identifiable organisms between control and irradiated surfaces to determine level of UV effect.
- Conduct metagenetic analysis to determine presence of taxa unidentifiable under photograph analysis.

- Compare the experimental chambers of control and UV irradiated conditions to assess the level of effect within niche areas.
- Measure and compare water conditions in control and UV irradiated chambers for UV impact on water chemistry.

Chapter 5:

DNA damage and repair were quantified for *N. incerta* after exposure to UV. *C*yclobutane pyrimidine dimer (CPD) formation was measured by measuring CPD abundance at different exposures. CPD repair rate was also evaluated over increasing recovery intervals. Finally, mutagenesis incurred during DNA repair was quantified and compared.

Aims:

- Measure CPD accumulation in *N. incerta* over different fluences.
- Identify the threshold where CPD damage begins to accumulate in *N. incerta.*
- Determine rates of CPD repair over five different repair intervals up to 24 hours.
- Construct a de novo genome and quantify mutagenesis rates concerning CPD formation.

Objectives:

- Expose *N. incerta* to a range UV fluences and quantify DNA damage in the form of CPDs.
- Measure mutations induced by producing a de novo genome and assessing for of single nucleotide polymorphisms (SNPs).
- Compare CPD production to SNPs.
- Allow varying recovery periods for CPD repair and compare CPD levels between recovery periods and freshly exposed diatoms.

Chapter 6:

Data gathered throughout the project was compiled and interacting concepts were presented. Collective information was brought together to further understand the underlying biological mechanics and enable the design of equipment to be more targeted. Modifications that enable substantial and effective improvements in output capacities and coverage of the UV delivery system were explored.

Chapter 1. A Review of Ultraviolet Light and its Industrial Integrations

1.1 Introduction

Solar energy is the driving force for Earth's climate; it warms the ocean, drives winds, melts snow and warms the Earth's atmosphere, as well as being harnessed by plants and microorganisms to power photosynthesis and spread the generated energy throughout the food web (Berens & Molinier, 2020a). Anthropogenic uses of light energy include solar photovoltaics, solar thermal, and agriculture. In agriculture, solar food processing uses the sun to grow, dry and protect crops enabling large-scale yields (Eswara & Ramakrishnarao, 2013). Solar photovoltaics converts sunlight into direct current with semiconductors, whereas solar thermal utilises the heat energy generated from the sun's rays for heating or secondary current conversion (Ahmad *et al*., 2020). The utilisation of solar energy in power generation is not the only form of light manipulation. Solar energy has also been utilised for its detrimental effect on living cells and used as a sterilisation method to benefit a multitude of industries.

Solar energy is electromagnetic radiation (EMR) travelling in the form of a wave with vectors propagating perpendicular to the direction of travel (Maxwell, 1865). A wide spectrum of EMR is produced at different wavelengths, with a small portion of this range being harmful to living organisms (Cheng & Moe, 2020). This harmful region can affect genotypic and phenotypic expression, impacting on growth, reproduction and survival of organisms that are exposed.

Solar radiation can be separated into optical radiation (ultraviolet (UV), visible light and infrared radiation), ionising radiation (x-rays and gamma rays) and longer wavelength sources (microwaves and radiofrequency) (Figure 1.1). UV radiation (UVR) covers a range of

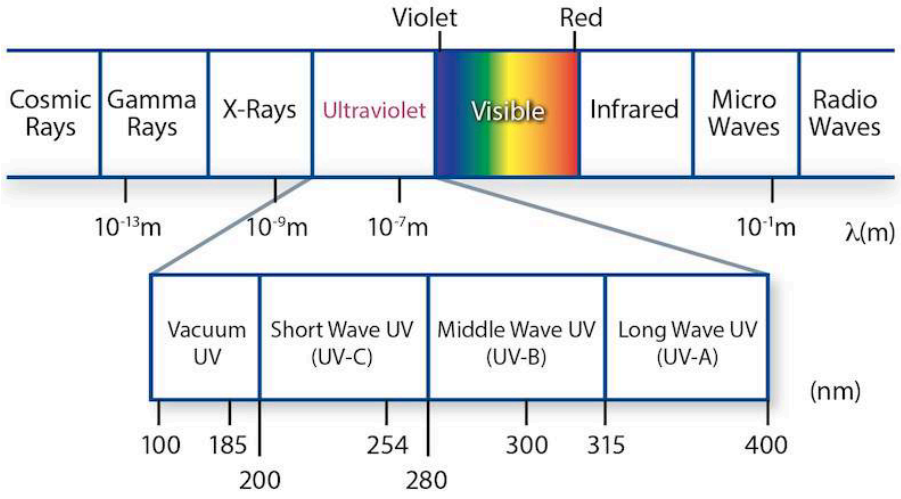

Figure 1.1. Classification of solar radiation with terminology associated with ranges of wavelengths (Cheng and Moe, 2020).

wavelengths from 100-400nm and can be further divided, based on respective wavelengths, into UVA (315-400nm), UVB (280-315nm), UVC (200-280nm) and vacuum UV (100-200nm).

This chapter explores UV's mechanism of damage, the impact it can have on organisms, the defence capabilities of organisms, potential avenues of UV use in industry, and introduces the potential benefits for biofouling control.

1.2 Ultraviolet damage

UV radiation can have positive and negative effects on organisms depending on many factors, including the organism involved, exposure duration and emitting wavelength. Organisms in all extant phylogenetic groups are affected similarly when exposed to UVR. When there is an abundance of neighbouring pyrimidine bases (dipyrimidines, C or T) within the DNA structure, UVR can cause distortions in the double helix. Exposure to electromagnetic waves causes a resonation within the double helix structure to resonate, such that the DNA bases enter a reactive state and undergo photochemical reactions (Berens & Molinier, 2020b). This occurs most prominently at wavelengths between 100–280nm (UVC) causing a range of direct photolesions (isomerising base pairs), or indirect photolesions (creating reactive oxygen species (ROS)) that interact with and alter the DNA structure (Li *et al*., 2006; Schreier *et al*., 2009; Rastogi *et al*., 2010).

The pericyclic reaction converts dipyrimidines into cyclobutane pyrimidine dimers (CPDs) (Rauer *et al*., 2016). This primarily occurs when there are two or more thymine bases adjacent creating thymine dimer formation. The reaction can impact cytosine also, but due to the extra hydrogen bond between the purine and pyrimidine, it is in a more stable state. The dimers formed by this process develop into lesions by altering the shape of the DNA structure. When two adjacent pyrimidines are exposed to UVR, three types of direct photolesions can form; CPDs, (6-4) pyrimidone photoproducts (6-4PP) and pyrimidine(6-4)pyrimidone Dewar isomers (6-4PP Dewar) (Figure 1.2.) (Haiser *et al*., 2012). CPDs form by the C5 and C6 atoms of adjacent pyrimidines binding and forming a stable ring (Schreier *et al*., 2009). This differs from the formation of 6-4 PPs, which are non-cyclic and are developed by the C4 at the 3'-end of an exetane or axetidine intermediate binding with the C6 of the 5'-end pyrimidine (Marguet *et al*., 2003). The Dewar isomers firstly form as the 6-4PP but then the C6 and N3 atoms create weak base pair linkages (Haiser *et al*., 2012). All three forms create lesions in the DNA structure, with the 6-4PPs being the most prominent. All of which can impede cell division and growth, (Rastogi et al., 2010).

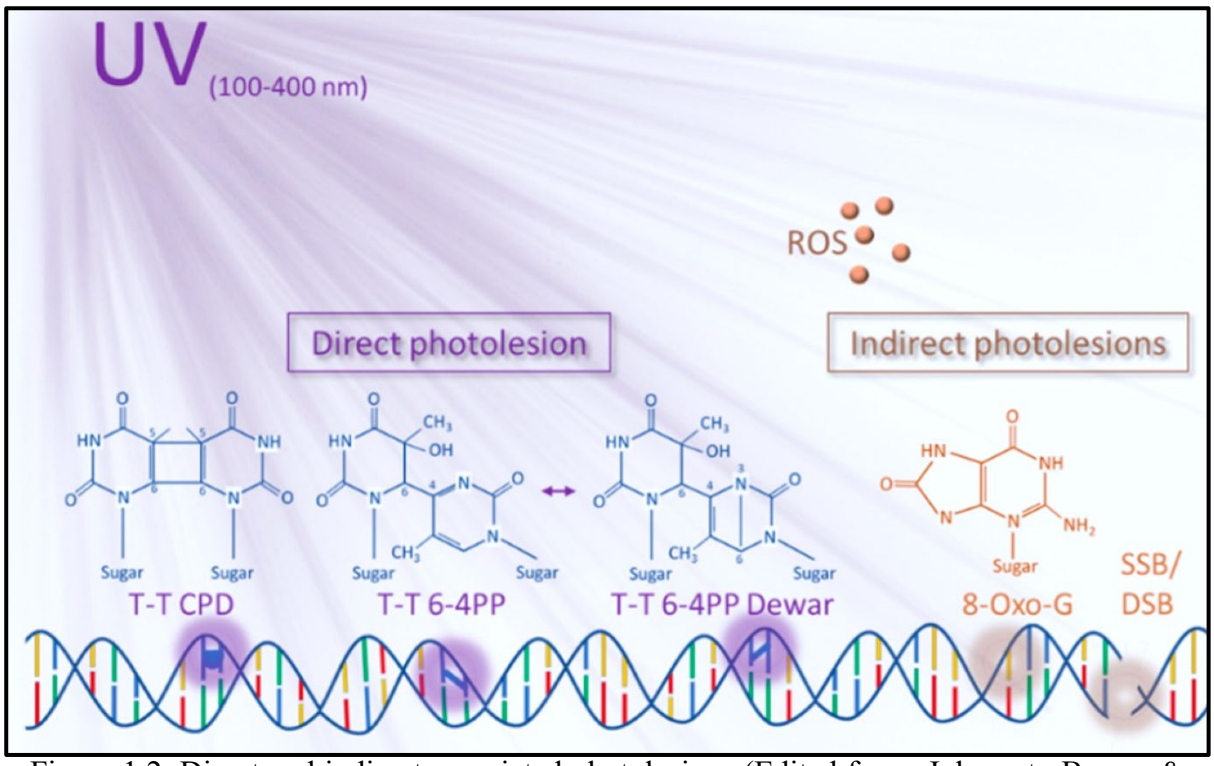

Figure 1.2. Direct and indirect associated photolesions (Edited from: Johann to Berens & Molinier., 2020). ROS = reactive oxygen species, T = Thymine, G = Guanine, CPD = cyclobutane pyrimidine dimer, PP = photoproduct, SSB/DSB = single/double stranded break.

Although UVR is known to induce DNA damage and is primarily absorbed at 254nm, UVR can have damaging effects over a wider range (Berens & Molinier, 2020a). Rochette *et al*. (2003) found that UVA was also able to produce CPDs solely at TT base-pair repetitions but at a significantly lower rate than at UVB and C wavelengths. The light source used by Rochette *et al* (2003) was analysed by Gróf *et al* (2002) who showed that the lowest range of the spectrum was close to the upper limits of UVB (~ 330nm), which may have been the primary spectral region of effect. Indirect photolesions can take several forms that first require photosensitisation or oxidation reactions to react with the UVR-excited biomolecules (Li *et al*., 2006). Triplet-triplet electron transfer (TTET) can create a CPD when UVA causes photosensitisation of benzophenone to react with thymidine in its vicinity (Encinas *et al*., 2004). Other indirect photolesions can occur when UVR is absorbed by chromophores in the presence of hydroxyl radicals and ROS, this leads to the oxidation of purines, pyrimidines and/or the deoxyribose skeleton (Schuch *et al*., 2017).

1.3 UV impact

UV can have lasting impacts on organisms ranging from prokaryotes to mammals (Rastogi et al., 2010). The severity of damage caused can be highly variable between taxonomic groups

and even vary within a species. A wide variation of UV tolerance has been investigated, but no resistant taxonomic group is evident (Sinha & Häder, 2008; Sinha et al., 2008; Häder & Sinha, 2005; Friedberg et al., 2005; Solomon, 2008; Llabrés et al., 2010; D. P. Häder et al., 2007; D.-P. Häder et al., 2007). Factors other than genetic relationship can affect the tolerance of an organism to UV radiation. One factor is the size of the organism exposed. Size can affect the susceptibility of an organism to UV as some smaller organisms cannot produce UV absorbing compounds or must divert more energy to do so (Raven, 1991; Garcia-Pichel, 1994). Bacteria and single-celled organisms are highly susceptible to UV damage, with the rate of lesion formation differing between individuals, and the effects can be dependent on the wavelength of exposure (Tedetti & Semperv, 2006; Tree *et al*., 1997; Santos *et al*., 2013; Joux *et al*., 1999). Photosystem II of smaller cells was found to be more inhibited by UVB irradiance than larger cells in three species of centric diatoms (*Thalassiosira* sp.) (Wu *et al*., 2015). Laurion and Vincent (1998), however, suggested that the cell size of phytoplankton communities was not a good index for UV sensitivity as the pica- and nanoplankton fractions did not differ in response to UV exposure. The study involved a pica plankton community that was dominated by cyanobacteria. Cyanobacteria have ancestors that were present in the Precambrian era when Earth's surface UV levels were higher. As such they have adaptations allowing them to produce mycosporine-like amino acids (MAAs) and scytonemin enabling them to absorb harmful UV rays (Sinha & Häder, 2008). A lower cyanobacterial abundance may have altered the outcome indicated by Laurion and Vincent, (1998), however, *Cyclotella* sp. has indicated an increase in cell size post-UV irradiance (Buma *et al*., 1997) and could also interfere with size-effect determination supporting the conclusion that size as a factor may not be of universal importance.

The peak wavelength that an organism is exposed to can directly affect the intensity of impact. DNA absorbs damaging UVR primarily at ~ 254nm, however, different taxa can display higher impacts at different spectral ranges. UV treatment at 280-320nm caused a significant reduction in growth rate and evidence of cell arrest in the diatom *Cylotella sp*. Thymine dimer content was strongly correlated to growth rate reduction suggesting genetic interference. *Chlorella vulgaris* displayed a linear first-order decrease in photosynthesis upon exposure to different wavelength combinations (PAR < PAR+UVA < PAR+UVA+UVB < PAR+UVA+UVB+UVC) (Forster, 1997). However, *Bacillus pumilus*, when exposed to wavelengths in increments of 10nm from 210-290nm, were inactivated more at 220nm than they were in the expected 250-260nm range (Beck *et al*., 2015). In their study, bacteria and viruses had a higher inactivation at 260-270nm and coliphages were most impacted at < 240nm.

It is clear that when developing the use of UVR as an inhibitor for a specific purpose, it is, therefore, necessary to understand the response of the target organism(s). Operating a wide range of wavelengths may be more effective to target a host of different organisms in a generic community, whereas a narrower more precise wavelength may suit targeting specific organisms if the optimal irradiance wavelength can be determined.

Radiometric units are used to describe UVR. Fluency (the radiant energy received by a surface per unit area in a given time) can be separated into dose (J/m^{-2}) and dose rate (W/m^{-2}) (Thimijan & Heins, 1983). These units are often used to describe the intensity of UV being used. An effective dose pertains to a particular biological effect, which is organism dependent. Zamir Bin Alam *et al*. (2000) found an irradiance level of 370 W/m^{-2} adversely affected the growth of planktonic algae and reduced cell density. *Chlorella vulgaris* displayed inhibition of photosynthesis after exposure to UV between 2 and 10 W/m^{-2} (none weighted to weighted) (Forster, 1997). This fluence can be used as a measure of dose and provides information on thresholds of effect for organisms. As an organism effect is linked with wavelength and intensity, determining the level of effectiveness for specific uses would require optimisation.

An organism can display a range of responses to UV irradiance. *Chlorella vulgaris* had a ~ 75% reduction in concentration within 1 hour of UVC treatment (Chen and Bridgemen, 2017). Zamir Bin Alam *et al. (*2001) found that at irradiance levels over 3.7 W/m-^{2} *Microcystis aeruginosa* cell density was reduced. Chen and Bridgeman. (2017) did not describe the irradiance output from the bulbs used in the experiment, which would be required to effectively compare the exposure. UV treatment of *Ditylum brightwelli* and *M. aeruginosa* affected their ability to remain in suspension, increasing precipitation (Rijstenbil, 2001; Zamir Bin Alam *et al*., 2001). This could potentially remove photosynthetic organisms from the photic zone. Sinking may have been a defensive mechanism to remove algae from the harmful irradiance region and provide respite for recovery. Growth rates, density, and buoyancy alterations are therefore some of the more overt adaptations utilised by organisms to cope with UV exposure.

1.4 UV defences

Life on Earth is estimated to have begun between 3.8 and 2.7 billion years ago (Orgel, 1994). Approximately 2.2–2 billion years ago oxygen levels started to rise which enabled the photosynthetically created O_2 to react with the incoming UVC rays and begin the formation of the ozone layer (Cnossen *et al*., 2007; Rye & Holland, 1998). During the pre-Cambrian period, the lack of an ozone layer allowed UVR of all wavelengths to reach the Earth's surface (Kasting, 1987; Sagan & Chyba, 1997). Early life forms present during this period would have required

adaptions to survive the intense UVC exposures. Organisms that are constituents of the biofilm have evolved adaptations to be particularly resilient to exposure. These adaptations have been inherited by distant ancestors and are still utilised today (Cleaver, 2006).

UVR exposure can cause mutations and alterations in transcription. Inhibition of these genotoxic effects is mediated by DNA repair pathways (Friedberg *et al*., 2005). The repair method varies among organisms with light-independent repair pathways, such as nucleotide excision repair (NER) in mammals and light-dependent photoreactivation being prevalent in single-celled organisms (Mullenders *et al*., 1993, 1997). NER involves enzymic cleavage of the lesioned nucleotides from the DNA strand (Kasting, 1987). Photoreactivation can repair thymine dimers by breaking the bonds between the DNA lesions and causing bonds to reform between the unlinked nucleotides (Banaś *et al*., 2020). CPDs are more difficult to repair than the slower-forming 6-4PP (Kan., 1992).

Resilience to UV involves an organism's ability to recover after exposure and is variable between organisms. Algae have anti-UV properties that enable them to survive in high-intensity UV locations. Kumar *et al. (*2003) provided evidence that the cyanobacterium *Anabaena* BT2 was able to utilise photoactive radiation (PAR) to repair the damage caused by UV irradiance and found that when no PAR was available, cell death was more common.

Damage to the DNA of diatoms can limit the division of cells, halt growth and cause cell arrest (Buma *et al*. 1999) at the G1 or G2 phase of the cell cycle. Cell arrest and growth of a biofilm occur when the irradiance level exceeds the capacity of the repair mechanisms, which are highly variable between species. The quantum yield, a ratio of absorbed photons compared to the emitted photons, can impact whether an organism is susceptible to UVC damage (Koutchma, 2009).

Environmental factors can also impact how organisms are affected, with the tropics having higher UVB exposure year-round than those found further from the equator (Grigalavicius *et al*., 2016). UVA, however, does not follow this trend and has higher irradiances at latitudes around 60ºN and 60ºS during the respective hemispheres' summertime (Grigalavicius *et al*., 2016). Tedetti and Semperv. (2006) found distinctions between different marine locations with the open ocean, coastal and Antarctic waters having clear characteristics in their 10% UV penetration depths. The transmission of UV through water is directly impacted by the composition of the surrounding media. Williamson *et al. (*1996) reported that UVB had a 1% potential penetration depth of 16 m with zero dissolved organic carbon (DOC) present and UVA penetrated 2.5 times deeper. However, with as little as 1-2 mg, L^{-1} DOC that depth reduced to

less than 2 m. DOC can absorb the damaging wavelengths, protecting organisms in even the shallowest water. UV can also affect these DOC, which can be fragmented by UV into smaller subunits and then consumed by bacterioplankton. This could, over time, increase the transmission depth due to less organic matter being present and cause a positive attraction of microorganisms towards the nutrient source (Hadar *et al*., 2007). Consumption of a food source can allow the bioaccumulation of compounds that benefit the predating organism.

Increases in marine plastic pollution have impacted all water bodies including down to the deepest parts of the oceans (Kelly *et al*., 2022). Plastics contain aromatic compounds and through UV degradation these can be released into the surrounding waters (Lomonaco *et al*., 2020). The rise in plastic pollutants is increasing the risk of more of these volatile organic compounds contaminating the oceans. *Mytilus galloprovincialis* has been shown to bioaccumulate waterborne organic UV filters (Vidal-Liñán *et al.* 2018). An increased accumulation of mycosporine-like amino acids in *Artemia* was suggested to improve the tolerance of the organism to UV exposure (Khosravi *et al*., 2013). If there are more volatile organic compounds present due to increases in plastic pollution, then bioaccumulation could also increase and enhance the defence mechanisms of organisms able to readily utilise them.

1.5 UV applications

Anthropogenic use of UVB/C is common and has multiple uses across a broad range of industries. Technological advancements in microelectronics are enabling the introduction of UV into previously unexplored areas. This section briefly covers a range of applications that are being explored.

Polyethylene (PE) is degraded by UV. Exposing PE to wavelengths of 350nm within air began its artificial ageing, which results in polymeric chain branching, oxidation and breakages (Carrasco *et al*., 2001). The photodegradation of polyvinyl chloride (PVC) is also known to occur with UV exposure in the air but the addition of captopril and nickel oxide nanoparticles can provide PVC with some protection (Saleh *et al*., 2022). This has also been implemented for polystyrene (PS) by using cephalexin Schiff bases (Yaseen *et al*., 2021). However, the opposite approach has been suggested to alter the chemical composition such that photodegradation of plastics is less likely (Baum & Deanin, 1973). Although the production of biodegradable plastics has increased, they only represent 0.5% of worldwide plastic production (Chiellini & Corti, 2016). They can be hydro- and oxo-biodegradable with different mechanisms and energetic profiles (Figure 1.3). Exposure to UV increased the photodegradation of oxo-

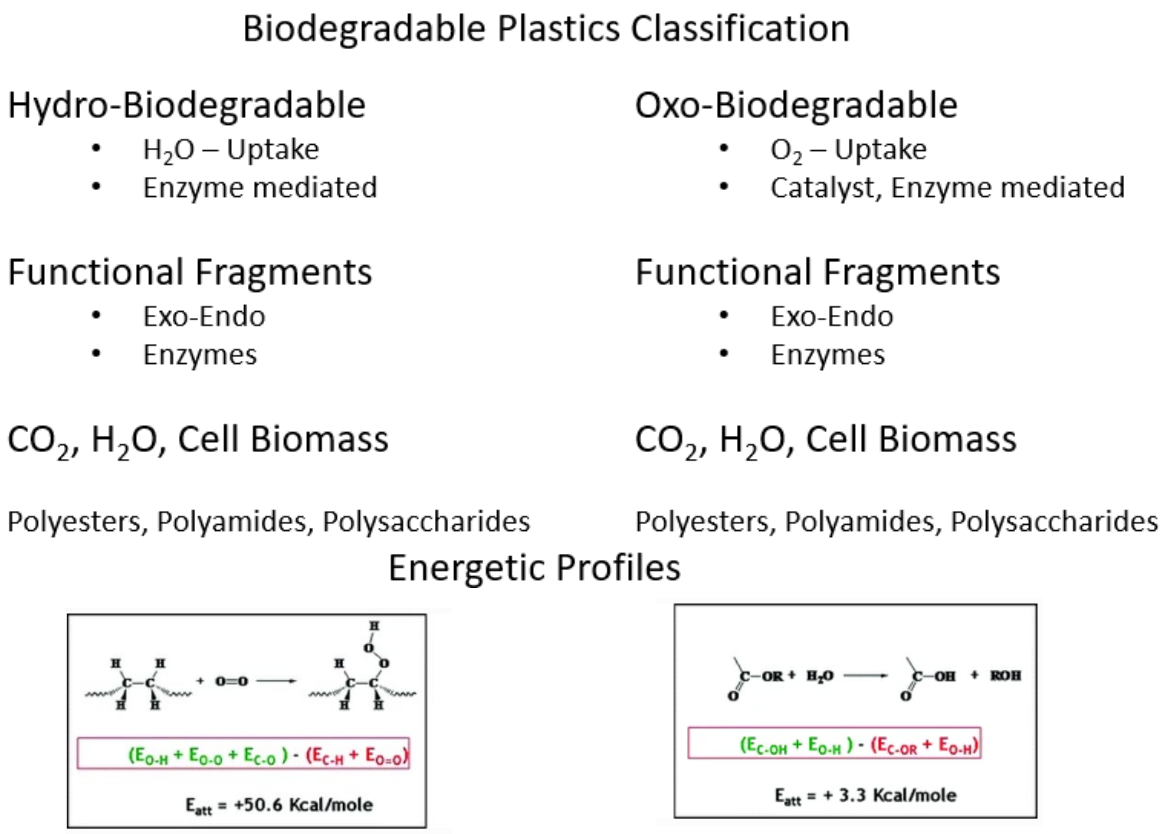

Figure 1.3. Mechanisms for degradation of biodegradable plastic polymers and their energetic profiles (Edited from: Chiellini and Corti, 2016).

biodegradable plastics substantially (Antelava *et al.* 2020). Consequently, these plastics could mitigate plastic pollution. The use of natural UV and microorganisms to help relieve plastic pollution is not a quick solution but is a step toward an energy-efficient solution.

Drinking water must undergo treatment to make it safe for human consumption with some treatments not meeting increasingly stringent regulations (Janasie *et al*., 2021). UV treatment is becoming more common and favourable as it can target organisms such as the intestinal parasites *Cryptosporidium parvum* and *Giardia lamblia*, which chlorine treatment alone cannot (Sarathy & Mohseni, 2006; Bukhari *et al*., 1999; Craik *et al*., 2001). At 325nm, UV can be used to treat triazine-containing pollutants, which are widely used in the textile industry and in herbicides (Chan *et al*., 2019). Distillery wastewater can be refractory to UV treatment and require additional hydrogen peroxide treatment, whereas wastewater from tomato processing plants can be impacted by UV treatment alone (Beltrán *et al*., 1997). Wastewater contains suspended particles which increase the nephelometric turbidity units (NTU) of the water treated. Christensen and Linden. (2003) found that at 10 NTU the lethality of UV could be compromised due to the absorbance and scattering of the UV light. Wastewater can range from 5 -135 NTU, which would render some waters untreatable by UV alone (Bolto, 1990). By using

electrochemical, chemical coagulation or ion exchange methods, NTU and COD can be reduced within highly turbid wastewaters (Lin & Chen, 1997; Hashlamon *et al*., 2017). Natural coagulants or filtration methods could lower the turbidity of waters allowing UV treatment to produce drinkable water. An integrated multi-treatment system would be useful for the comprehensive treatment of highly turbid waters.

Processes that use UV for 'curing' a surface coating, improving the physical and electrical durability, are known as UV assisted processes (Shukla *et al*., 2004). Using light radiation instead of heat on some organic materials, at specific calibrations, can initiate chemical reactions which lead to industrially desirable polymeric materials (Sangermano *et al*., 2014). The most common is photo stabilisation, which occurs by crosslinking reactions across a film and has been used to improve the durability of g-line and l-line photoresists (Waldfried *et al*., 2006). The original objective was to reduce energy use and replacement of solvent-based treatments (Shukla *et al*., 2004). 3D and 4D printing using UV curable resins allow a layer-by-layer treatment to progressively construct a module faster than waiting for each layer to cure via heat curing (Chae *et al*., 2015). 3D printing is not limited to fixed solid structures, with UV curable elastomers enabling an elastic structure to be formed (Patel *et al*., 2017). The combination of fixed and flexible structures has recently been developed as a fast production method to save lives by providing personal protective equipment to medical personnel during a shortage of equipment (Hagen *et al*., 2021). The versatility of UV curable resins enables large- and small-scale production at an affordable rate (Ang & Gan, 2012).

In the medical industry, there are a host of multi-drug-resistant microorganisms that are hard to treat within infected wounds. The application of UVC to localised infections has been proposed as an alternative to drug treatments (Dai *et al*., 2012). The higher susceptibility of microorganisms to UVC combined with the high photoreactivation in mammalian cells is conducive to the treatment of infected areas by UVC (Dai *et al*., 2012). Circumstances may require prolonged exposures for treatments of resistant microorganisms which could result in the host cells being excessively damaged and causing harm to the patient. Altering the wavelength of exposure may allow a less detrimental approach. UV treatment at 200-222nm can have similar antibacterial results to exposures at 256nm, however, due to mammalian cells being larger, the lower wavelengths do not produce premutagenic DNA lesions (Buonanno *et al*., 2020; Welch *et al*., 2018; Buonanno *et al*., 2017, 2013). This can facilitate longer exposures to treat specific UV or drug-resistant bacteria without causing the skin damage that occurs at conventional germicidal wavelengths.

Severe acute respiratory syndrome from Coronavirus 2 (SARS-CoV-2) has had global health implications. SARS-CoV-2 is primarily transmitted via droplet and airborne transmission and can be inactivated whilst it is airborne (Wilson *et al*., 2020). UV technology has been validated as a treatment for SARS-CoV-2 and other pathogens with inactivation rates for the former reported as $1.49 cm^{-2}$ mJ^{-1} (Sneha & Patil, 2022; Ou & Petersen, 2021). Integration of UV treatment into air filtration systems has been investigated with different flow regimes since well before the SARS-CoV-2 pandemic (Taghipour & Mohseni, 2005). To improve on initial designs, computational fluid dynamic models have been used to predict light positioning, flow thickness, flow rates and other factors for efficient sterilization of airborne diseases (Capetillo & Jesus, 2015; Taghipour & Mohseni, 2005). The aerodynamics can affect the results with thin air layers moving through a reactor providing a more uniform effect (Taghipour & Mohseni, 2005). Additionally, the wavelength is important, with the rate of effect being determined best at 267nm ~ 279nm > 286nm > 297nm (Gerchman *et al*., 2020). In circumstances where air treatment through a reactor would not be feasible, another method would be to treat individual rooms. This would be detrimental to inhabitants at the above wavelengths but VUV (222nm) emitting excimer lamps are effective for room-scale reduction in airborne diseases whilst not impacting human health (Eadie *et al*., 2022). However, a crystalline UVC filtration system did not significantly reduce colony-forming bacterial units in a live operating environment (Anis *et al*., 2020). Further optimization of equipment is required but there is a high potential for air treatment to reduce airborne transmitted diseases.

In a world that has undergone a pandemic, sanitation is becoming paramount. Retail and online stores are now able to provide devices to UV sterilise any item of the correct size (McGreer, 2021). This can allow the highest level of hygiene for items such as cutlery and mobile phones that harbour a broad range of microorganisms. UV treatment of materials is used as an accelerated life test by companies aiming to determine the susceptibility of a material to deterioration over a longer time. UV exposure can degrade materials sooner than their expected life span and uses of UV sterilization should, therefore, take into consideration the effect UV sterilization would have on the target surfaces (McGreer, 2021). Printed circuits, seatbelt webbings, silicone rubber and light-emitting diodes are but a few materials that undergo accelerated life tests (Koo & Kim, 2005; Boddy *et al*., 1976; Harm *et al*., 2020; Youn & Huh, 2005). Whilst undergoing life testing using VUV exposure, the crosslink density of silicone increases, which decreases the microwear and smooths the surface altering the water contact angle (Vasilets *et al*., 1998). Surface smoothness and changes in contact angle of rubber and silicone surfaces could be of interest for some industries as water contact angles (as a proxy for

surface free energy) can impact organisms when they attempt to colonize a surface (Finlay *et al*., 2002; Mihm *et al*., 1981). Reductions in microwear of the surfaces along with sterilization could be beneficial. UV sterilization for standard items could have negative effects on the exposed materials, although many polymers are now manufactured to contain anti-UV additives which may protect them (Hsissou *et al*., 2021). If sterilizing causes accelerated ageing and surfaces are overexposed, materials that react more readily to the treatment may have some of the components negatively altered (McGreer, 2021).

Hallegraeff. (2003) found that from the 1980s-2000s the frequency of harmful algal blooms (HABs) increased, although more recently they have discussed that this may be due to intensified monitoring (Hallegraeff *et al*., 2021). Barrado-Moreno, Beltrán-Heredia and Martín-Gallardo. (2017) investigated the use of UVC as a control for harmful algal blooms (HABs) in freshwater environments. Four test species, *Chlorella, Oocystis, Microcystis* and *Scenedesmus*, were all equally affected and reduced in density by ~ 80% when exposed for 30 minutes. Cyanobacteria represent around 45% of harmful algal blooms (HABs), which are detrimental to all animals that contact contaminated waters and have even resulted in human fatalities (Backer *et al*., 2015). Cyanobacteria predate the formation of the ozone layer and are UV tolerant as they possess a rapid repair mechanism. This could be problematic if UV exposure was to promote their proliferation. (Kasting, 1987; Paul, 2008). At rates over 300 mJ/cm^{-2}, UV can reduce the production of the cyanobacterial toxin, cylindrospermopsin, but this irradiance is above levels used in general water treatment capacities (Cheng *et al*., 2009). Phukan, Rai and Syiem. (2019) suggest that too low an irradiance level may be beneficial for the growth of cyanobacteria. Phukan, Rai and Syiem. (2019) did not discuss the irradiance transmission through water, the size of their sterilisation system or the irradiance output of the 254nm lamp used. These factors are of great import for threshold determination, as a high-capacity system would be required to inactivate.

1.6 UVs Potential integration in biofouling

The moment a submerged surface is exposed to the marine environment it begins a process known as biological fouling (biofouling). Marine biofouling is a well-documented phenomenon whereby there is an accumulation of biological material on a substrate (Flemming *et al*., 2009). This can be a newly submerged surface, a recently cleared surface or a newly formed one (Harm *et al*., 2020; Cacabelos *et al*., 2020; Matin *et al*., 2021). Biofouling can impact any industry that interacts with the marine environment including power station cooling intakes, oil rig platforms, floating pontoons, aquaculture fisheries and marine vessels. In aquaculture, biofouling increases the degradation of cages, can inhibit water exchange and increases the potential for

disease (Bannister *et al*., 2019). Powerplant cooling pipes that receive and deposit into the ocean can become clogged, reducing flow, and impacting internal temperature control (Flemming *et al*., 2009). Biofouling can occur on filtration membranes that are used for the desalination of saltwater and reclamation of wastewater (Matin *et al*., 2021). Marine fouling causes data alterations on scientific sensors that are deployed for long durations. The fouling of ships' hulls increases hydrodynamic drag, increasing fuel consumption and pollutant emissions (Munk *et al*., 2009). Fouling of hulls and internal ballast tanks also transports non-indigenous species (NIS), which can be ecologically detrimental to native species, as well as impacting upon farmed aquaculture species, submerged static artificial structures, and presenting risks to marine values (Hopkins *et al*., 2021; Georgiades *et al*., 2021, 2020; Sylvester *et al*., 2011; Piola & Hopkins, 2012). Areas of impact on marine vessels are anywhere below the waterline, including propellers, rudders, the hull and any sea chests, bilges, or cooling intake areas (De Castro *et al*., 2018; Sylvester & MacIsaac, 2010; Frey *et al*., 2014). Once deployed these are difficult and sometimes impossible to conduct regular maintenance or monitoring on. Submerged static artificial structures such as those found in Venice and the Great Lakes are also susceptible to biofouling (Callow & Callow, 2011; Curiel *et al*., 1999). Increased fouling on flotation and support structures can cause negative buoyancy effects and impact structural-water position. Fouling of cooling intakes of power plants can reduce the intake flow of the water and result in overheating of equipment (Moshchenko & Zvyagintsev, 2004). Maintenance of all these structures is costly and labour-intensive (Hopkins *et al*., 2021).

The hulls of vessels are designed to allow a smooth transition and to optimise manoeuvrability. The surface irregularity caused by the biofouling of a hull interrupts the dynamic flow between the hull and the water, creating drag and adding additional weight (Schultz *et al*., 2011; Callow & Callow, 2002; Schultz *et al*., 2015). Algae fouling on ships incurs drag penalties of 11-34 % depending on the level of coverage (Schultz *et al*., 2011; Lebret *et al*., 2009). Fuel consumption equates to 50% of marine vessel transportation costs, and drag penalties affecting fuel consumption can be increased by up to 30% due to the presence of biofilm on a ship's hull (Schultz *et al*., 2015). The added weight and drag cause the vessel to burn more fuel to reach similar speeds to a pristine vessel and, the maximum velocity of the vessel will be reduced. Longer times transporting of goods at a higher fuel expenditure is costly and leads to added greenhouse gas emissions. Marine biofouling was estimated to cost the US Navy $56 million p.a. for the DDG-51 class alone, with estimates as high as ~ $150 billion for annual fuel cost savings to the global shipping fleet derived from effective antifouling coatings (Pritchard, 1988; Maréchal & Hellio, 2009; Schultz *et al*., 2011; Selim *et al*., 2017). Estimates can vary markedly

based on the prevailing oil price. Since 2017 prices have ranged from $11.26- $75.23 per barrel (WTI crude oil) and in 2021 were ~ $25 (60%) per barrel more than when cost estimates were last calculated (Selim *et al*., 2017; MacroTrends, 2021), which could adjust current estimates to as high as ~ $240 billion.

Prevention of biofouling has been documented for thousands of years with Roman ships developing copper-lined hulls as antifoulants (Readman, 2006). To reduce the detrimental effects caused by fouling organisms, there are several available methods but the application of antifoulant paints to a colonisable surface is the primary method used. Contemporary anti-fouling is designed to kill, inhibit, or counter fouling organisms. The knowledge of past, present and future methods has been well covered with multiple comprehensive reviews on known anti-fouling methods (Maréchal & Hellio, 2009; Flemming *et al*., 2009; Hopkins *et al*., 2021; Munk *et al*., 2009; Railkin, 2003; Yebra *et al*., 2004).

Historically tributyltin (TBT) was a highly successful coating used for biofouling prevention. Incorporated as a self-polishing copolymer, the coating had a controlled slow release of a biocide (Evans et al., 2000). The coating could last in excess of 5 years before reapplication was required and was counted as the most effective antifoulant ever devised (Bosselmann, 1996). However, after being in use from the 1960-1990s, TBT was found to have mutagenic implications on a range of nontarget commercially viable species such as fish and oysters (Stroben et al., 1995). Since the 1990s, TBT paints have been incrementally banned by several governments on vessels <25m in length. The Rotterdam Convention and the International Maine Organization (IMO) have attempted a global restriction on TBTs use (IMO, 2008). The environmental impacts caused by TBT paints (Maguire, 1987; Alzieu, 2000), have resulted in restrictions on toxic substances for AF purposes. After the restrictions put on TBT, paint development of new coatings has undergone drastic reformation towards non-toxic replacements. The focus is now toward less detrimental replacements for industry, academic and commercial parties (Clare & Aldred, 2009; Clare *et al*., 1992). Current restrictions on biocides have limited the availability of biocidal coatings (Growcott *et al*., 2017). Currently, the most prevalent method for ships is the use of biocidal paints, which can be used on the hull and in niche areas, such as sea chests (Kiil *et al*., 2002). These paints are optimal for the hull but are often applied to sea chests, even though they are not designed for these areas, and perform poorly due to the different flow regimes (Coutts *et al*., 2003; De Castro *et al*., 2018). The hull experiences smooth flow whilst in motion, but niche areas (propellers, sea-chests, bilge intakes, etc.) are subjected to regimes that can remove or rapidly deplete paints, or restrict paint leaching (Coutts & Taylor, 2004; Coutts & Dodgshun, 2007; Sylvester & MacIsaac, 2010).

Vessel movement enables the translocation of fouling organisms that can be retained within these areas and can introduce non-indigenous species (NIS) globally and negatively impact ecosystems (Fernandes *et al*., 2016; Sylvester & MacIsaac, 2010; Georgiades *et al*., 2020; Cacabelos *et al*., 2020). Niche area fouling is of high concern for translocating NIS and can have implications for ecosystems, port access and economical costs (Fernandes *et al*., 2016). Determining a sufficient treatment method for these complex areas would be economically, and environmentally beneficial.

Fouling-resistant and fouling-release coatings are nontoxic alternatives to biocidal antifouling coatings (FRCs) (Nurioglu & Esteves, 2015). FRCs do not prevent adhesion, but due to hydrophilic polymers that make up the coating, the interfacial bonds between the settling organism and the surface are weaker, allowing the organism to be more easily removed via shear stress (Kavanagh et al., 2005). Unfortunately, FRCs can become swollen in marine environments which alters the mechanical properties and reduces their application (Hu et al., 2020). Also, the low surface free energy also reduces the bond strength between the coating and the surface reducing the length in which it will remain in service. Finally, when in static conditions there is no surrounding flow to create shear stress therefore this can allow a strong adhesion to develop (Brady Jr & Singer, 2000).

The detrimental impact of biocides, reduced effectivity of FRCs and/or the need to be reapplied more frequently than historical methods, requires new methods to be developed to provide a longer lasting nontoxic antifouling method. The development of potential prospects is continuously in development and technological advancements are ever-growing, which expands the anti-fouling potential. The transition throughout time has displayed a wide variety of anti-fouling methodologies with new methods constantly in development.

The potential use of UVC to prevent biofouling in the antifouling industry has been demonstrated with high levels of prevention when integrated correctly (Piola *et al*., 2016; Hunsucker *et al*., 2019; Bueley, 2016; MacKenzie *et al*., 2019). The use of UVC LEDs for biofouling control was investigated by Piola *et al*. (2016), using a tile design that incorporated UVC LEDs in a UV transparent silicone, allowing continual surface irradiance, and investigating settlement diversity over time. The method showed great potential and initially prevented biofouling on the surface. Unfortunately, some LEDs failed during operation. The LEDs that remained operational over the full duration of the project maintained a fouling-free surface within a radius of the light source. From the point source of the LEDs an estimated range of effect was determined and revised tile designs were recommended. Additionally, from this distance an estimated threshold irradiance of 1 $\mu W/cm^2$ was identified for prevention of

biofouling organisms. The low power requirement and high efficacy of the UV sterilization technique confirmed the high potential of UV LEDs as a potential new avenue for the antifouling industry.

The effectiveness is due to the order in which biofouling occurs and the organisms exposed. During biofouling, the surface will be subjected to multiple stages and levels of colonisation that can be successional but is not necessarily so, with some fouling organisms not requiring the surface to be pre-fouled (Roberts *et al*., 1991; Clare *et al*., 1992; Hadfield and Paul, 2001; Callow and Callow, 2011; Salta *et al*., 2013; Piola *et al*., 2016). The successional concept is a simplification of a complex and intertwined process and has been well-researched and reviewed, for further details see (Salta *et al*., 2013; Harm *et al*., 2020; Abelson & Denny, 1997; Callow, 1993; O'Toole *et al*., 2000; Watnick & Kolter, 2000; Suwarno *et al*., 2016).

UVC has been demonstrated as having a high bactericidal effect, which can be used to prevent the initial bacterial colonisation that occurs during marine biofouling. Using UV to stop these fouling organisms is effective and the anti-fouling (AF) capability for the prevention of biofouling formation has been estimated at ~ 0.0001 W/m^{-2} (Piola *et al*., 2016). This was suggested to be an overestimate, with further studies needed to determine a more precise threshold. UV irradiation for sensors and experimental equipment protection is commercially available and is being developed and tested by AML Oceanographic (Bueley, 2016; Bueley *et al*., 2014; Pinnacle, 2016). Although empirical data are not available for their equipment, they have supplied long-term visual comparisons between exposed and control surfaces to demonstrate their operational success (Bueley, 2016). The life span of the UV-generating source could be prolonged by pulsing of the light, but this could lower the fluence. Duty cycling rates of 1:20 are effective on barnacles, bryozoans and tunicates, with a smaller effect on mussels (MacKenzie *et al*., 2019). Duty cycles as low as 1 min/week have indicated reductions in macrofouling growth (Richard *et al*., 2021). Rates for a threshold in the prevention of fouling could provide a target for UV irradiance capacities to lengthen the lifespan of the antifouling devices. Inconclusive thresholds require further exploration in determining the impact of UV on fouling taxa.

1.7 Targeting marine vessel niche areas

Submerged locations on marine vessels that experience unpredictable hydrodynamic flows are known as niche areas (Figure 1.4.). These locations comprise internal pipework and their

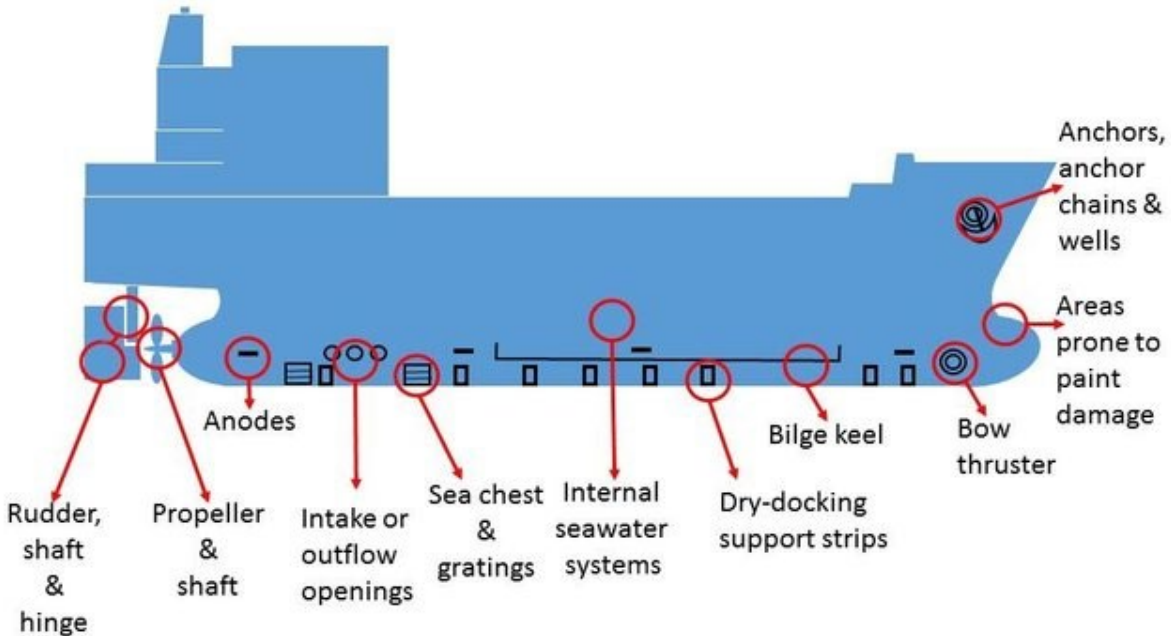

Figure 1.4. Types of niche areas commonly found on domestic vessels. Extracted from (Georgiades & Kluza, 2020)

intakes, rudders, propellers, thrusters, gratings, and sea chests among others. These locations (highlighted in figure 1.4.) do not represent a large proportion of the vessels' wettable surface area (~ 10%) (Moser *et al*., 2017); however, the surfaces are highly susceptible to biological fouling (Georgiades & Kluza, 2020). They can become heavily fouled due to extra exposure to water movement during water intake. Irregular protruding forms experience different hydrodynamics to the hull. Once fouled function of the area can be impeded, sensors can underperform, fouled internal pipework can reduce pumping efficiency and environmental sensors can fail (Growcott *et al*., 2017). Corrosion of pipework and complete blockages can occur which compromises onboard systems and prove costly with unscheduled maintenance. Difficult areas to access, such as sea chests, are problematic to clean once fouled and prevention is key.

To prevent settling organisms it is recommended to have either marine growth prevention systems (MGPSs) or AF coatings (McKenzie *et al*., 2017). A range of MGPSs are available with chemical (Chlorine, chlorine dioxide, bromine, hydrogen peroxide, ferrate, peracetic acid, acetic acid, descalers and quaternary ammonium compounds), physical (physical removal, thermal treatment, deoxygenation, osmotic shock) and cotreatments available (Growcott *et al*., 2017). AF coatings for these areas, tend to be painted with the same AF system as the hull, rather than one specifically designed for the hydrodynamic conditions of the niche area. This can result in the AF coatings underperforming and allowing biofouling to develop (Growcott *et al*., 2019). Physical and chemical treatments can have limitations with large doses required,

increased corrosion to the surfaces, fouling remaining attached once deceased, toxic biproducts, discharges of the chemicals to surrounding waters and other drawbacks. This still may not restrict all fouling with the level of fouling and the implications caused depending on the fouling protection administered.

If biofouling treatment is suboptimal organisms can accumulate. Vessel movement enables the translocation of these organisms and can introduce non-indigenous species (NIS) globally. Transfer of these NIS can have biosecurity risks as they cause detrimental effects on an ecosystem (Georgiades *et al*., 2021). The ascidian *Didemnum vexillum* are native to Japan but have been translocation to the USA, Europe, and Oceania (Griffith *et al*., 2009; Stefaniak *et al*., 2009). The translocation of *D. vexillum* to New Zealand is impacting mussel aquaculture with *Perna canaliculus* being displaced by the invasive (Fletcher *et al*., 2013). Ascidians have broad thermal & saline tolerances, can rapidly reproduce sexually or asexually and can inhabit a broad range of surfaces allowing them to outcompete native species (McKenzie *et al*., 2017). Long-term eradication of *D. vexillum* has failed with chemical and physical processes restricting growth but not being able to treat a large spatial distribution (McKenzie *et al*., 2017). Prevention of introduction pathways of NIS is a priority in restricting the further spread of ecological and economically harmful organisms.

Using UV as a fouling preventative within these areas could restrict fouling build-up and costly maintenance. As UV is damaging to DNA it can be applied to most organisms with high effectiveness. The introduction of UV into sea chests was conducted by Piola *et al. (*2016) who deployed UVC LEDs into a siloxane polymer tile within an artificial sea chest for over 1 year. Equipment failure, unfortunately, prevented some of the LEDs from performing, however, fully operational LEDs indicated high potential as a fouling deterrent. The fouling prevention was successful, however, due to LED failure coverage of the AF system was limited suggesting improved tile designs were required. Building upon this work and elucidating the potential of UV for biofouling prevention is imperative. The foundations of UV antifouling integration have been initiated with a high degree of success, expanding the concept, and investigating the lacking knowledge would be advantageous.

1.8 Summary

The potential for UVs use has been shown to cover a broad range of industries. Biofouling is a global issue that is costly and impacts ecological communities. Ship Niche areas can translocate these organisms which can have economic and environmental ramifications. Within the biofouling industry, UV as an antifoulant is severely underrepresented and requires further

study. Starting within niche areas could enable a broader understanding of UVs potential before integrating the system into larger areas. Retrofitting technology to a structure is not easy and requires small introductions to determine faults and fine-tune system details. Although niche area introduction has shown promise, details are still missing for thresholds of effect, optimal duty cycling, the distance of effect, organic matter disturbances, irradiance coverage, biological tolerance, universal threshold levels, molecular responses, taxonomic variation, UV toxicity, and mutagenic implications. Exploration of these factors is crucial for the application of UV within the biofouling industry and the following chapters investigate these critical gaps.

Chapter 2. Development and Specifications of an Ultraviolet B/C Emitting Tile

2.1 Introduction

Using ultraviolet light as a marine antifoulant is a recently introduced approach (MacKenzie *et al*., 2019; Bueley, 2016; Piola *et al*., 2016; Hunsucker *et al*., 2019; Braga, 2018; Richard *et al*., 2021) that requires a UV light source within a watertight environment and connection to an energy-efficient electrical supply. Light-emitting diodes (LEDs) are powerful semiconductor light sources, which emit light when a current flows through them. LEDs operate when electrons within a semiconductor recombine with electron holes. The energy required to cross the band gap and the semiconductor material determines the wavelength of light emitted (Bourget, 2008). UV-emitting LEDs are a modern invention (April 2000) that allows a low power supply of UV irradiance at a range of wavelengths (Muramoto *et al*., 2014). UV LED technology is considered to be 2-3 generations behind that of current visual light technologies (Hinds *et al*., 2019; Bugbee, 2017). Based on the current visible light market availability, future product development of UV LED size, cost and availability are predicted to be improved in the coming years. IRSTA are currently available as a commercial product (IKEA., 2022), which comprises LED worktop lighting that can uniformly release light across the whole surface from a flexible silicone LED embedded tile. This system is small, lightweight, flexible and can dim the light source for controllable emittance. Another innovative light product, advertised by Design LED, is exterior car lighting systems that are thin, flexible, and waterproof with longer life spans than current OLED products. The development of these cutting-edge products illustrates the future potential of UV LEDs. With the LED market and electronic innovations progressing exponentially it is expected that UV LED capabilities will soon match those currently available for the visible light market. As LEDs are low cost, small, weigh little, have powerful light generation and low power requirements, they are a prime component for tile configuration.

The material used to enclose LEDs requires high light transmission, durability and needs to operate as a sealant. Many halogen light products utilise quartz glass as it is widely accessible. Moreover, quartz has high transmission rates of > 90% of the UV spectrum from > 170nm (Schreiber *et al*., 2005). However, quartz needs to be molten to pour over the LEDs to encapsulate them. Quartz is molten at ~ 1650^{o}C (Beall & Duke, 1969), which exceeds the recommended LED maximum exposure temperature within technical datasheets (Farnell, 2011; Components, 2022). Additionally, the rigidity of quartz could be problematic when trying to install the system in complex shapes and a more flexible encapsulant would be advantageous.

Silicone is used widely as a sealant as it can be fluid at room temperature and once combined with a curing agent can begin to solidify at low temperatures (Johnston *et al*., 2014). Additionally, silicone is more flexible and less dense than quartz, which makes it lighter, and the shape is easily manipulated. However, common silicone products can contain particles that absorb UV light (Lei *et al*., 2018). Some highly transparent silicone polymers are available that have transmittance rates up to 90% depending on the wavelength of light (DeGroot Jr *et al*., 2004). Wu *et al. (*2022) have shown that by encapsulating a LED within a UV-transparent silicone resin, emission could be enhanced by 70% compared to none encapsulated irradiance. The enhancement was achieved by applying a hemispherical encapsulation directly on the LED. This arrangement would not act as a complete sealant to protect a circuit array structure. Wacker Chemie AG have commercially available silicones that can transmit UV with datasheets indicating > 90% transmission (Lorenz & Kandelbauer, 2022). The versatility of silicone which is fluid at low temperature is ideal for LED encapsulation.

To ensure optimal equipment design and manufacture, the current project was a collaboration with AkzoNobel, the Defence Science and Technology Laboratory (DSTL) and the Defence Science and Technology Group (DST-G). This allowed the current project to utilise industrial expertise and specialist recommendations for optimal tile design. There are several requirements for using UV for antifouling in the marine environment. The system would need to operate continuously for extended periods whilst maintaining an effective irradiance level. The light source would need to thoroughly cover the external surface of the material that it is embedded in. To meet these requirements, the current study took inspiration from Piola *et al.* (2016). A method was developed to embed low-powered UVB/C LEDs within a silicone polymer to both protect the electronics and scatter the transmitted light to maximise the affected surface area. To ensure all parameters were met, the study conducted a comprehensive analysis of the tiles and their capacities.

2.2 Tile design and analysis

2.2.1 Laboratory scale UV emitting tile: Materials and process of tile assembly.

This project's initial tile configuration utilised four tiles (A-D, two control and two irradiated) that were manufactured in collaboration with AkzoNobel. Tile development during the project tried to emulate previous project designs utilising the best products available at the time. Due to the rapid evolution in products, materials and equipment that were best at the time of manufacturing may have been superseded by experimental completion. Some of the materials and equipment used herein have been discontinued and are no longer commercially available but more efficient and updated versions could be considered to emulate the current tile designs.

The tile components were comprised of four 278nm, LG LEDs (model: LEUVA66B00HF00) arranged in a 2x2 array. The LEDs were arranged 35mm from each other and 17.5 mm from the tile edge and manually soldered together using a 1 mm solid wire to retain a rigid array (Figure 2.1). The array was soldered to a 0.5m long cable for laboratory experiments and

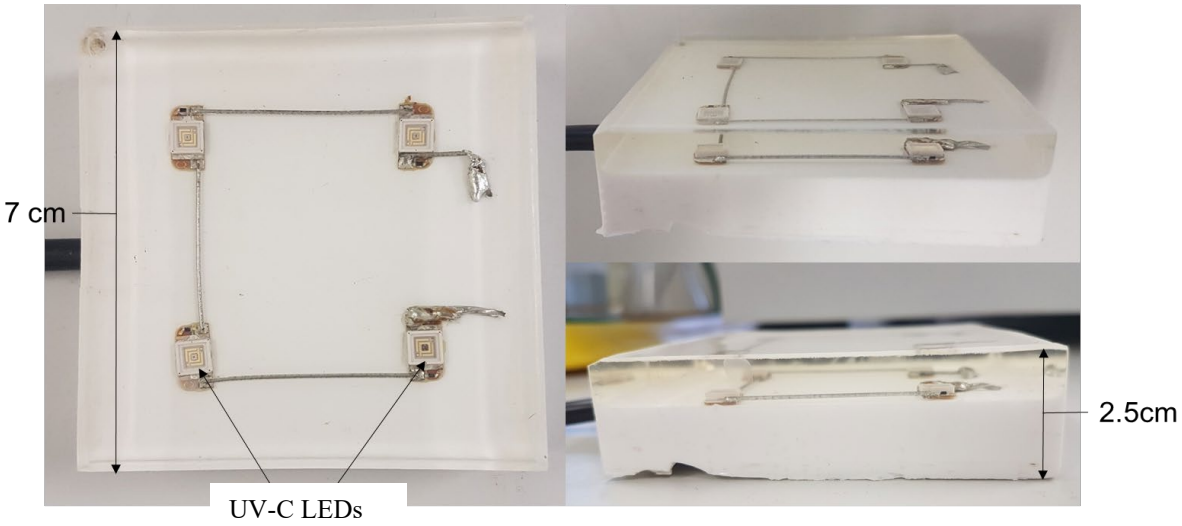

Figure 2.1. Laboratory scale UV emitting tile. UV LEDs embedded within a UV transparent silicone polymer. Four low powered (24-volt, 0.17 amp) UV-B/C LEDs arranged in a 2 × 2 array on a 1.5cm thick opaque silicone polymer and embedded in a 1cm thick UV transparent Lumisil © 400 silicone.

connected to HXT banana plug fittings for integration with a bench power supply unit. The 2x2 arrays were assembled in a dual-layer silicone polymer, with an opaque base layer implemented for enhanced reflectivity and a UV translucent top layer allowing transmittance and partial scattering to amplify the coverage of UV emittance. The opaque base encapsulated the input cable and acted as a surface mount for the LEDs and a protective seal for the base of the array. A total of 50mL of the opaque silicone base was poured into a 70x70x12.5mm acrylic mould. The base layer had internal air pockets removed and silicone cured within a Medline Scientific™ Jeio Tech 665L vacuum oven (OV-12) at -0.1 MPa and 70ºC for 48 hours. The top layer comprised 50mL of Lumisil® 400 (supplied by Wacker Chemie AG) poured onto the opaque layer within a second acrylic mould that was 70x70x30mm and then cured as above. Control and irradiated tiles were built identically, but the control tiles were not initiated for experiments and only Tiles A and B were used. Before experimentation was conducted the mechanical and irradiance attenuation capacities were determined.

2.2.2 Laboratory scale UV emitting tile: methods used for testing the tiles operational capacity.

2.2.2.1 Operational warm up emittance of UV LEDs

To determine exposure rates that exposed organisms would encounter the irradiance capacity needed to be measured. Electronic equipment is known to vary whilst they reach their operational equilibrium, LEDs used for chlorophyll *a* fluorescence stabilised within 5 minutes, with a higher immediate output which can sharply reduce within the first 2-3 minutes (Leeuw *et al*., 2013). Some equipment can take seconds/minutes to stabilise whilst others can take longer. To determine if the irradiance from the LEDs would perform differently at power initialisation as opposed to prolonged use, the tiles were submerged in a container with 50ml of artificial seawater (ASW) and irradiance was measured. Irradiance readings were taken at the tile's surface using a UV SXL 55 Radiometer with a SiC UV air sensor with a parallel 1” area cosine diffuser directly over the LED. Initial measurements were taken whilst powered down then the LED was powered on and left to record in ~ 80mS increments over 2 hours totalling ~ 100,000 recordings per LED.

2.2.2.2 Determination of UV LED heat generation

As electronics generate heat during operation the heat generated can transfer to the surface and affect the surrounding water. To determine heat generation and transfer, water and LED temperature were monitored in powered and control settings over two hours. Tiles were submerged in 50ml of ASW, and LEDs were initiated. Readings were taken directly on the LEDs, central to the tile at distal points from the LEDs and to ensure temperature change was not ambient related, temperatures of a 6 L supply carboy were also taken. Temperatures were logged every minute over the first hour and then at 10-minute increments for a further hour. The temperature was monitored using a digital, non-contact, infrared thermometer temperature gun for LED readings and a mercury thermometer for water readings. Both thermometers were calibrated, before each experiment.

2.2.2.3 Surface coverage of UV LEDs and UV irradiance levels

To determine the UV surface coverage of the tile, the irradiance was measured using a UV SXL 55 Radiometer, scans were taken after 30 mins allowing any initialisation required then measured at 1cm increments across the surface providing an 8x8 matrix (0-7cm). Readings were taken when the tile was submerged in 50ml of ASW and powered at the LED manufacturer's recommended power supply (24V and 0.17 amps). The readings were then analysed using R version 4.2.0 (Bunn, 2013), and the data was interpolated and rasterised using the raster package to give a more resolute UV coverage (Hijmans & van Etten, 2011).

The LED recommendations from the supplier were to operate at 24V to achieve a 10,000-hour L50 irradiance but if operated lower the irradiance life span could be expanded. Operating at lower voltages decreases the fluence rate and can impact the LEDs coverage at the surface of the tiles. To determine irradiance produced whilst extending the LED lifespan by reducing voltage, a series of measurements were taken. An LED was isolated within a PVC pipe to remove any cross-UV contamination and at the surface of the tiles, irradiance readings were taken at different supply voltages varying from 18-24 volts.

2.2.3 Field scale UV emitting tile: Materials and process of tile assembly.

To improve surface coverage an updated tile design was designed to eliminate the dead zone found in the centre of the 2x2 tile versions. These tiles were to be deployed for any field studies and would require operation over 12 months. Due to the COVID pandemic, LEDs (Model: TY-SMD-275nm-3535-B-20mm) were sourced from UVTAO China, which was a different supplier compared to the 2x2 tile LEDs. Based on the technical datasheets provided, an optimal spacing was calculated to cover a 350x350 mm tile. An optical view angle of 130^{o} required spacing of 32.75mm from the perimeter to the centre of LEDs and 67.5mm between LED centres and required a silicone depth of > 15mm to allow the surface to have overlapping irradiance regions. To account for LED and starboard thickness and to encapsulate under the starboard base whilst ensuring sufficient irradiance overlap a total tile thickness of 18mm was applied. This coverage had a minimal depth to achieve sufficient overlap which reduced irradiance loss through scattering and absorption by restricting the distance that the light transmitted through the silicone.

A total of 16 LEDs were manually soldered into a 4x4 array using an MDF wooden template to ensure the replicability of positioning on all tiles. LEDs were secured using a 1mm rigid copper wire to retain the designed spacing. LEDs were numbered from 1 to 16 along a parallel circuit with number 1 starting at the location which was connected to a 1m long power supply cable (Figure 2.2). The LED arrays were then encapsulated within an acrylic mould that was 350x350x25mm deep. To attain the required depth 2.25L of Lumisil® 903 was poured over the array using a Graco PR70 fixed ratio injection pump that delivered and mixed parts A and B in equal measure. The tiles were degassed and cured at -0.1 MPa within a Medline Scientific™ Jeio Tech 665L vacuum oven (OV-12) at 70^{o}C for 48 hours. A total of 18 tiles were produced and a further 18 tiles at a depth of 7mm that consisted of no electronic components to act as controls. All tiles were visually inspected for flaws and then had technical specifications measured.

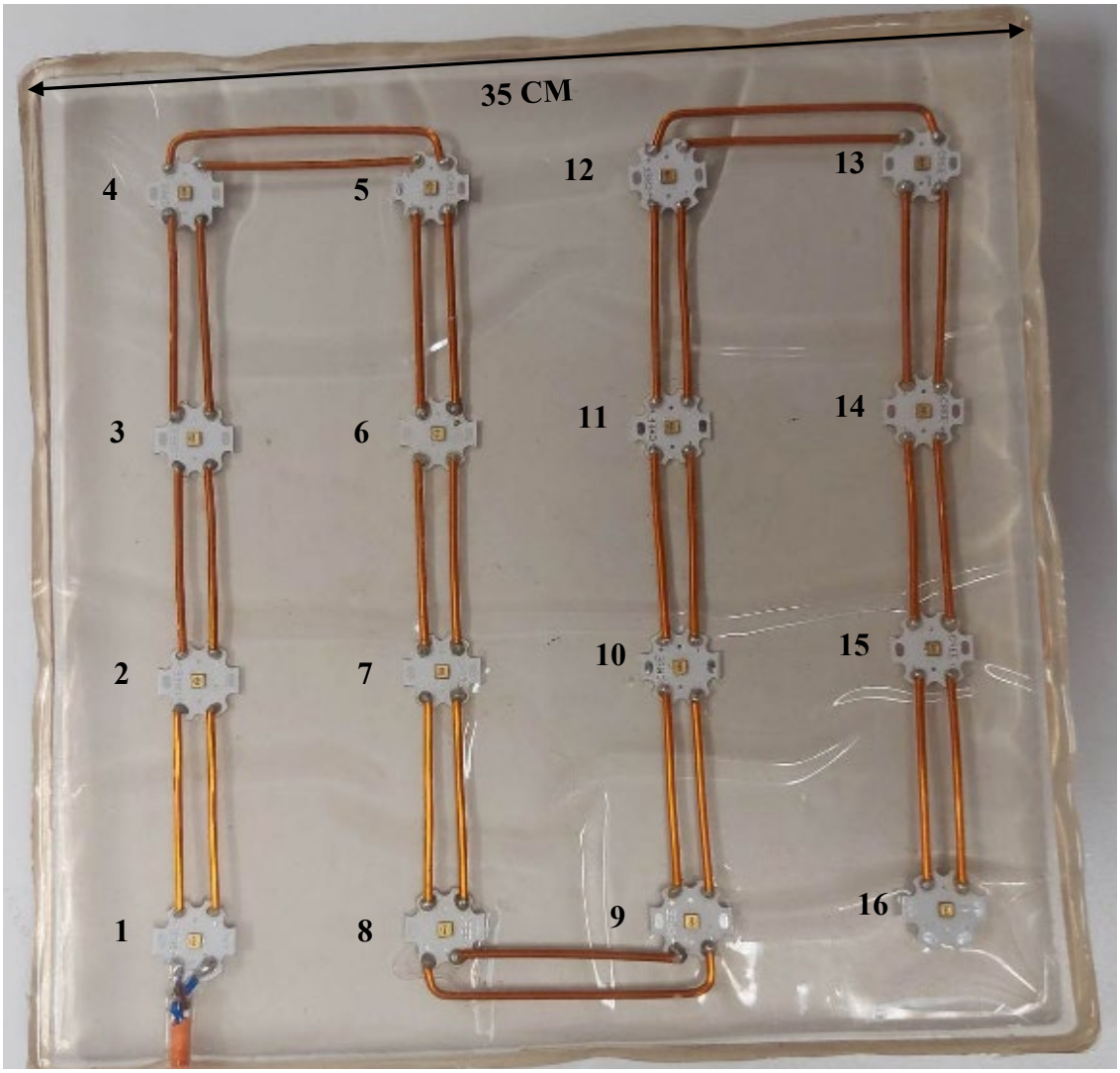

Figure 2.2. Field scale UV emitting tile. UV LEDs embedded within a UV transparent silicone polymer. LED identification numbers arranged from input and ascending around the circuit. Sixteen low powered (6-volt, 0.17 amp) UV-B/C emitting LEDs arranged in a 4 × 4 array embedded in a 1.8 cm thick UV transparent Lumisil © 903 silicone.

2.2.4 Field scale UV emitting tile: methods used for testing tiles operational capacity.

2.2.4.1 Surface coverage of UV LEDs and UV irradiance levels

The silicone polymer (Lumisil® 903) in which the tiles were embedded was indicated to provide > 90% transmission, however, this was conducted at 450nm and through a 1mm film. As our silicone layer would be required to be thicker and the LEDs emitted at a lower wavelength determining irradiance loss was required. Additionally, as LEDs were obtained from a new source their operational capacity needed to be determined. To determine the accuracy of predicted coverage based on the datasheet calculations, readings were taken at the tile surface at 1cm increments across the whole tile. To determine the irradiance and the achieved

transmission rate through the silicone, irradiance readings were taken before and after silicone embedding. Using a UV Touch radiometer scans were taken at 1cm increments starting at the tile edge giving a 36x36 irradiance measurement array. Measurements of all tiles were taken before LED arrays were embedded within the silicone polymer and rescanned after curing. This allowed the determination of UV irradiance lost within the silicone layer and the ability to calculate the transmission. Readings were analysed using R version 4.2.0 (R Core Team, 2013) using the Raster package (Hijmans & van Etten, 2011) and each point was rasterised and interpolated to give a gradient of irradiance. The bare tile had embedded readings subtracted and the difference was plotted to visualise irradiance loss.

2.2.4.2 UV transmission through water and interference of turbidity.

To determine how far the UV light is transmitted through water and to determine how variation between environments with high and low dissolved organic matter may affect the tile's irradiance, a turbidity study was conducted. Three PVC pipes were secured to the surface of one of the tiles to isolate single LED irradiances. Pipes were filled with a formazin standard (4000 NTU) solution which was created by combining analytical grade reagent hexamethylenetetramine ($(CH_2)_6N_4$) (product no. 398160) and hydrazine sulfate ($H_6N_2O_4S$) (product no. 489735) as described by (Thorne, 1961; Kitchener *et al*., 2017). The solution was diluted down in increments giving 4000, 2400, 1200, 720, 360, 220, 110, 50, 10, 1 and 0.1 NTU solutions. At the tile's surface and from 1-15cm from the surface irradiance readings were taken using an ILT 950 radiometer with a SiC UV air sensor with a parallel 1” area cosine diffuser. Readings were analysed within R version 4.2.0 (R Core Team, 2013) using the ggplot package (Wickham *et al*., 2016), data were isolated to the LED emitted UV wavelength range (260-310nm) organised by distance and turbidity then irradiance was summed to determine total irradiance across distances at different turbidity’s.

2.2.5 Statistical analysis

All data was analysed for normal distribution and equal variance before being statistically analysed using ANOVA and Wilcoxon pairwise comparisons with R version 4.2.0.

2.3 Results

2.3.1 Laboratory scale tile assessment.

2.3.1.1 UV irradiance stabilisation.

The readings from the SXL radiometer provided a total irradiance in mW/cm^2 between 230-320 nm but did not provide peak irradiances or wavelength specifics. The initialisation of the LEDs indicated variability between individual LEDs and between stabilisation periods. Each LED

performed differently with three distinct initiation patterns found, these comprised of a slow increase to consistency, an initial high emittance followed by a lower stabilisation and a quick stabilisation. A quick stabilisation was prominent on Tile B, LEDs 1,3 and 4 but LED 2 required a slow increase of ~ 30 minutes to achieve stability. Tile A had LEDs 2 and 4 that were slow to increase to stabilisation requiring durations of 7 minutes and 1 hour respectively to stabilise. On Tile A, LED 3 had a quick stabilisation in less than 1 minute. Tile A, LED 1 was the only output to have an initial high irradiance which then reduced to a stable irradiance after 10 minutes (Figure 2.3.). Both tiles had LEDs with high and low UV irradiances, Tile A, had the highest irradiance but also the lowest output with LEDs 3 and 4 respectively. All LEDs had

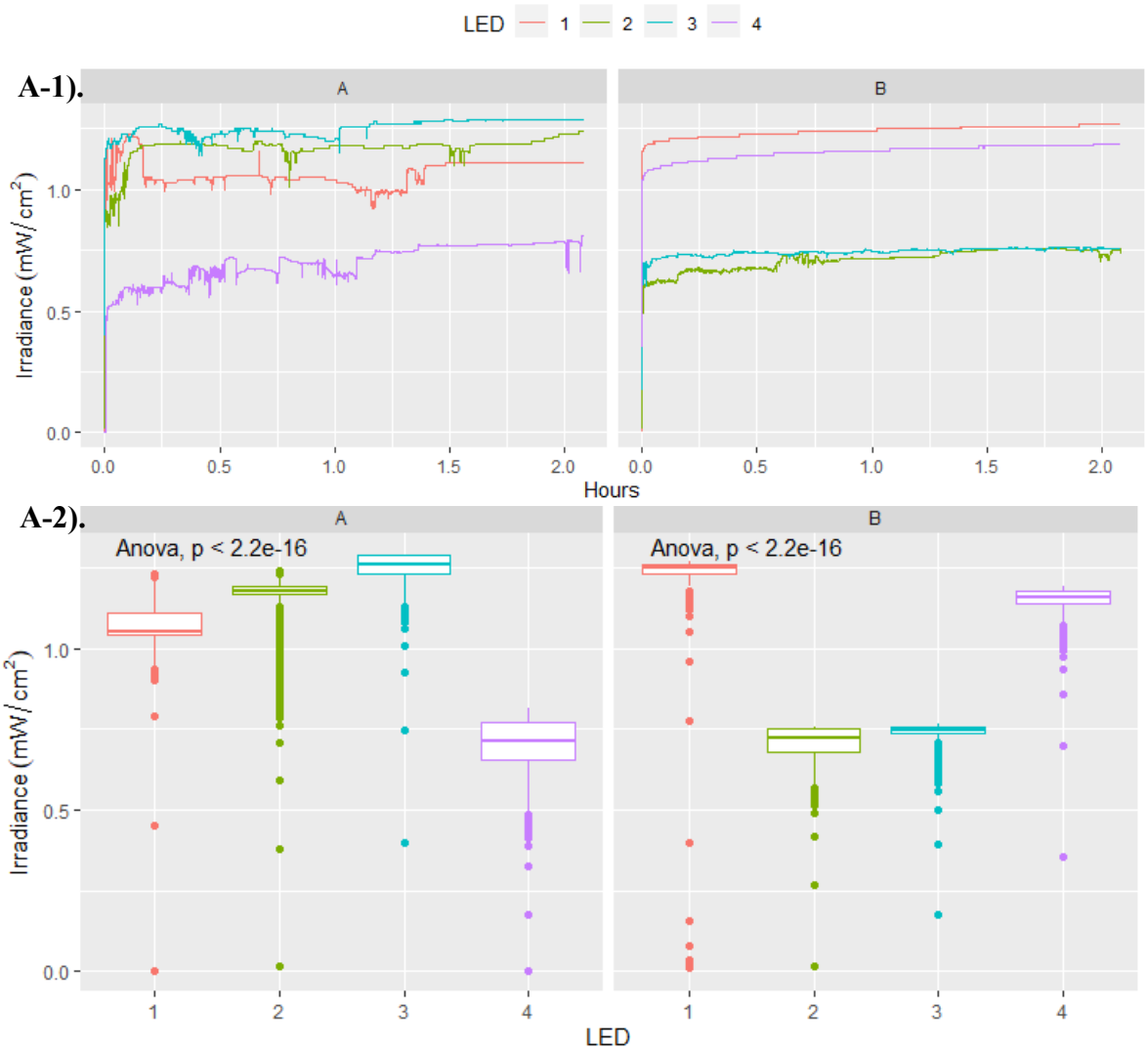

Figure 2.3. A-1). Irradiance output of Tiles A and B over a duration of 145 minutes. Readings taken directly over LEDs with 10 scans per second. A-2). Average irradiance output (N=87000) over the 145-minute experiment. Statistical differences were detected between LEDs and tiles via ANOVA and Wilcoxon pairwise test ($P < 0.05$).

significantly different outputs ($P < 0.05$) with Tile A having the highest overall output and Tile B the lowest (Figure 2.3.).

2.3.1.2 LED heat generation analysis.

Upon the experimental start of the temperature study, the initial temperatures were 15.7ºC which increased to a mean temperature of 16.9ºC and 17.5ºC for the supply water and all remaining conditions respectively. Temperatures took ~ 30 minutes to reach a steady state before increases slowed from the resting room temperature (Figure 2.4.). All temperatures

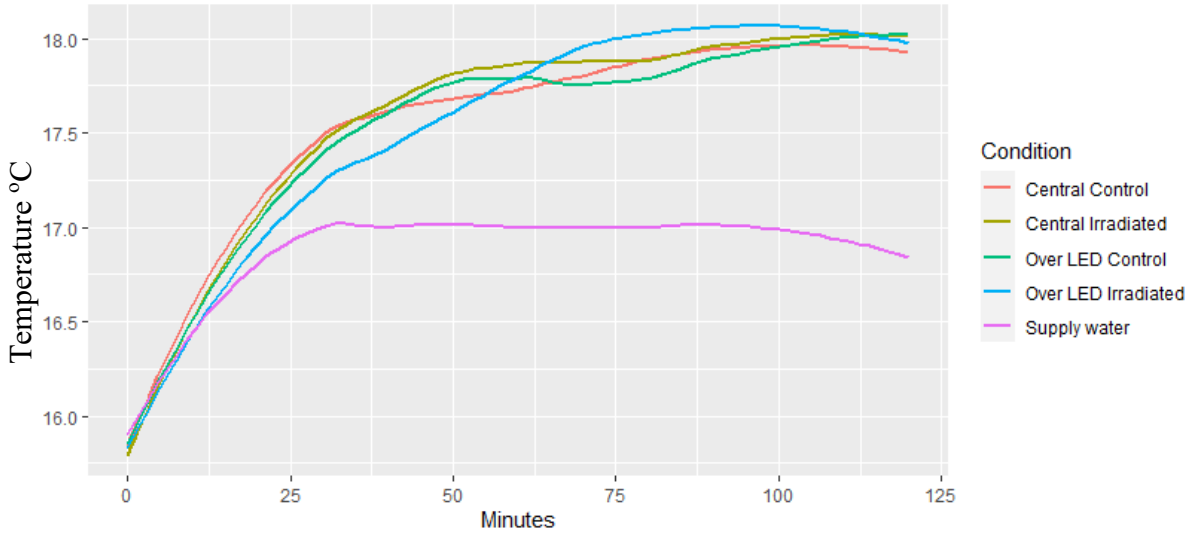

Figure 2.4. Water temperature increase over two hours. Readings taken in tile centre and over LEDs from irradiated, non-irradiated tiles and a supply water container. Statistical differences were not detected between irradiated and control tiles via ANOVA and Wilcoxon pairwise tests ($P > 0.05$), however, differences were detected between all tiles and the supply water ($P > 0.05$).

increased including the supply water, however, the supply water remained 1ºC lower than in the test experiments. A maximum rise of 2.4ºC was detected but was insignificant ($P > 0.05$) from all conditions except the supply of water. The experiments indicated a nominal change from each other throughout their operation.

2.3.1.3 Surface coverage of UV LEDs and UV irradiance levels.

Irradiance scans of the tiles indicated high and low regions of irradiance (Figure 2.5.). Directly over the LEDs had the highest irradiance with peaks of 120 µW/cm^2 recorded. The distal points between LEDs and at the tile's edges measurements were lowest and recorded at < 1µW/cm^2. LED output varied between LEDs with Tile B having the most variability and the lowest LED irradiance.

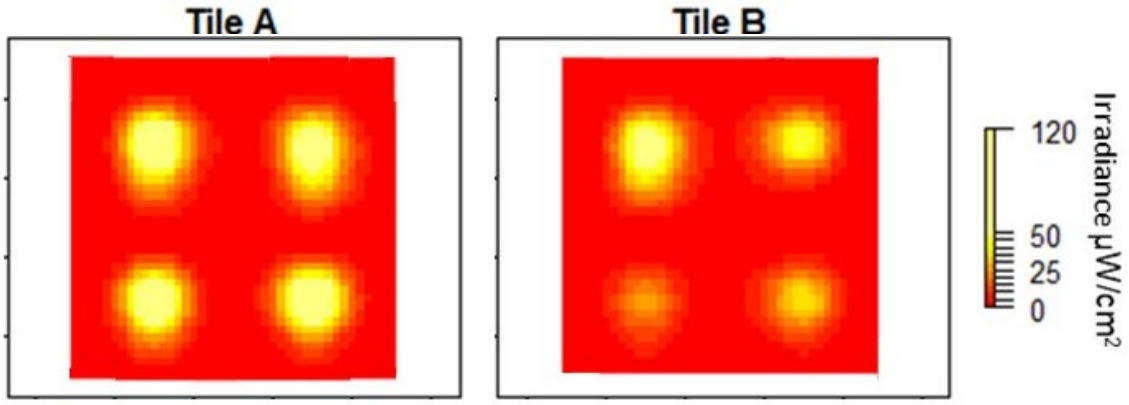

Figure 2.5. Tile scans of UV irradiance capacity from embedded 2x2 array. Readings taken at 1cm increments over the 7x7cm tile and interpolated within R. LEDs were labelled by arrangement from left to right and top down as LED 1-4.

The voltage experiments utilised an ILT 950 radiometer which provided specific wavelength details including where peaks occurred and at what capacity. Directly over the LEDs found that at 24 volts a peak irradiance was produced that ranged from 5.81 to 11.09 µW/cm^2 with an average of 7.989 µW/cm^2. Twenty-three volts had peak irradiances ranging from 3.24 to 6.48 µW/cm^2 with a mean of 4.58 µW/cm^2. Twenty-two volts had peak irradiances ranging from 1.58 to 3.42 µW/cm^2 with a mean of 2.24 µW/cm^2. Twenty-one volts had peak irradiances ranging from 0.6 to 1.34 µW/cm^2 with a mean of 0.89 µW/cm^2 (Figure 2.6.). Peak irradiance was higher on Tile B than that on Tile A at all voltages.

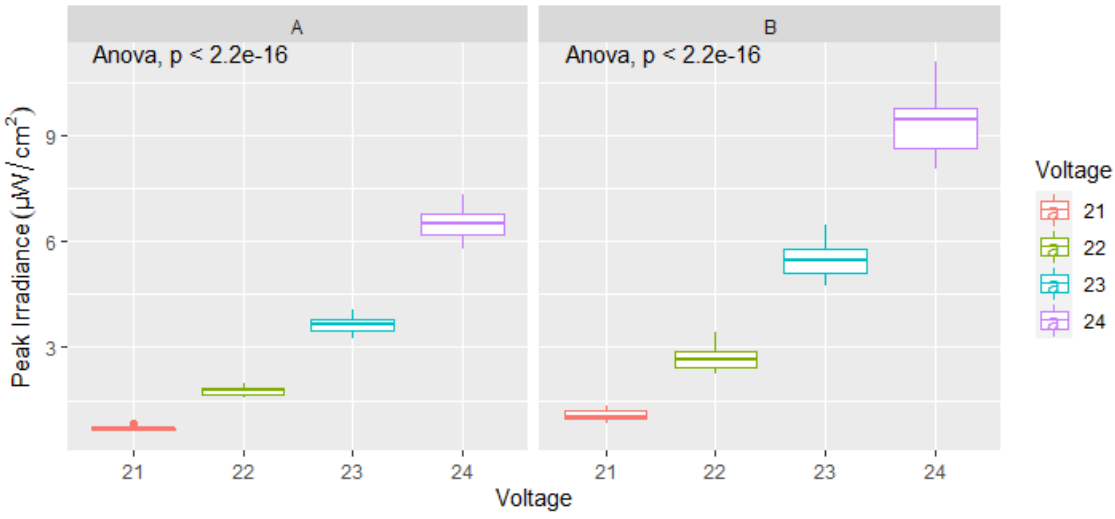

Figure 2.6. Average peak irradiance from all LEDs of Tile A and B at varying voltage supplies (21-24 volts). Statistical differences were detected between all voltages via ANOVA and Wilcoxon pairwise test (*P<0.05).*

2.3.2 Field scale tile assessment

2.3.2.1 UV transmission and irradiance loss through silicone

Before embedding the 350x350 mm surface indicated 100% coverage on most tiles, however, Tile H, LED 16 and Tile P LED 1 had lower irradiances than expected (Figure 2.7.). After LED

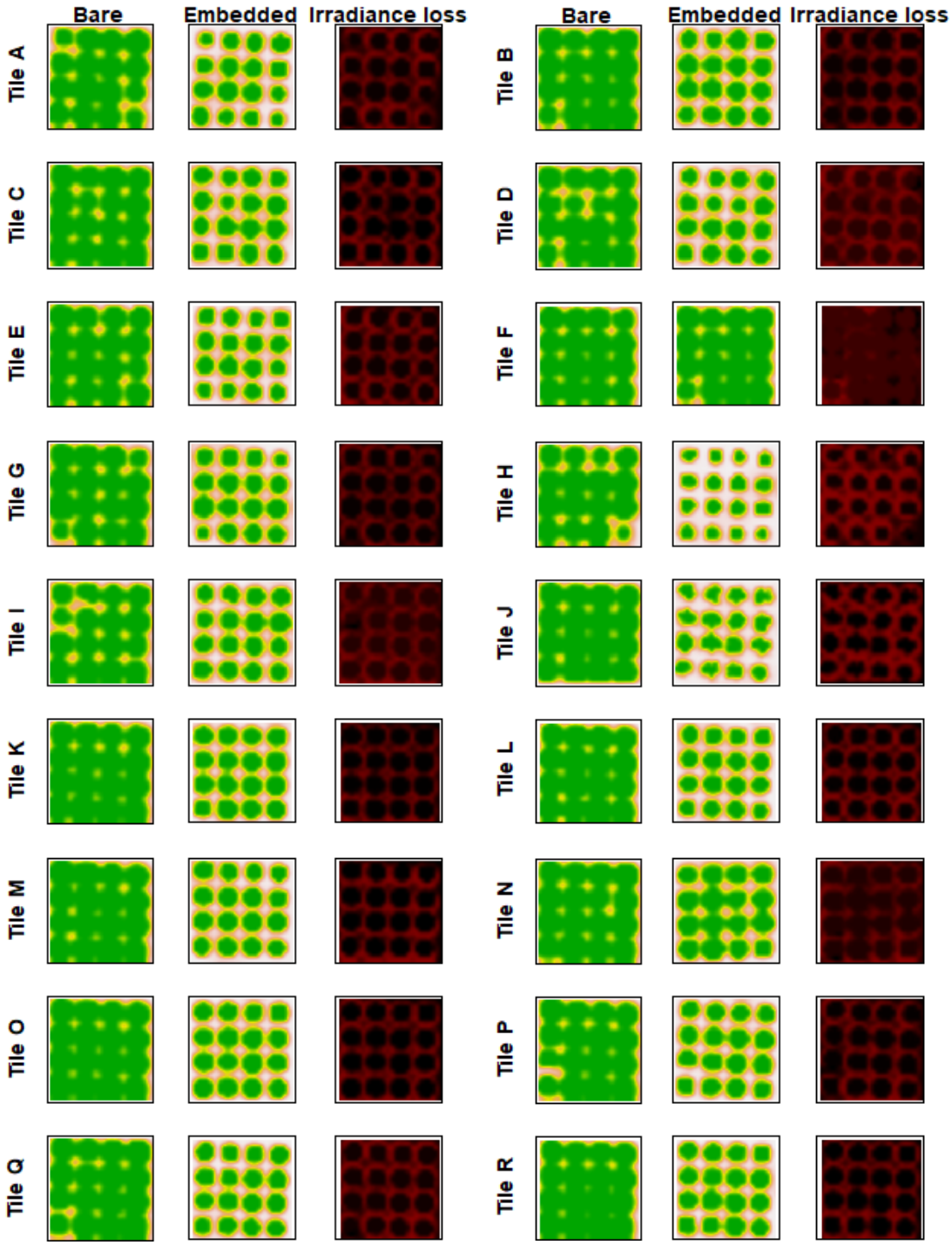

Figure 2.7. Irradiance scans of version 2 tiles. Readings taken over bare circuits and after embedding in silicone allowing the calculation of irradiance loss due to absorption and scattering. Green = high irradiance, White = low irradiance, Black = no irradiance loss, Red = high irradiance loss.

embedding the external edges and the distal points between LEDs had some irradiance loss. The mean drop in irradiances were between 1.105 and 2.269 mW/cm^2 which occurred on Tiles N and H respectively (Table 2.1). The tile edges and the distal points between LEDs had the largest irradiance reduction, whereas, directly over the LEDs had the smallest. Tile F had the highest reduction directly over the LEDs but not the most reduction overall. The mean reduction across all tiles by embedding in silicone was 40.5% with the highest and lowest reductions of 28 and 62.6% respectively.

Table 2.1. Mean irradiance of bare and embedded 4x4 tiles with calculated transmission loss.

	State	Irradiance (mW/cm^2)	Tile	State	Irradiance (mW/cm^2)
Tile A	Bare	3.620	**Tile B**	Bare	3.910
	Embedded	2.083		Embedded	2.483
	Loss	1.537		Loss	1.427
Tile C	Bare	3.910	**Tile D**	Bare	3.689
	Embedded	2.334		Embedded	2.212
	Loss	1.575		Loss	1.476
Tile E	Bare	3.873	**Tile F**	Bare	3.911
	Embedded	2.148		Embedded	2.594
	Loss	1.725		Loss	1.317
Tile G	Bare	3.748	**Tile H**	Bare	3.623
	Embedded	2.341		Embedded	1.354
	Loss	1.406		Loss	2.269
Tile I	Bare	3.620	**Tile J**	Bare	3.855
	Embedded	2.390		Embedded	1.817
	Loss	1.229		Loss	2.039
Tile K	Bare	3.972	**Tile L**	Bare	3.947
	Embedded	2.632		Embedded	2.206
	Loss	1.339		Loss	1.742
Tile M	Bare	3.964	**Tile N**	Bare	3.949
	Embedded	2.305		Embedded	2.844
	Loss	1.658		Loss	1.105
Tile O	Bare	3.994	**Tile P**	Bare	3.804
	Embedded	2.453		Embedded	2.342
	Loss	1.540		Loss	1.462
Tile Q	Bare	3.933	**Tile R**	Bare	3.971
	Embedded	2.292		Embedded	2.440
	Loss	1.641		Loss	1.531

Turbidity had a significant impact on irradiance transmission with higher turbidity having the least transmission distances. Turbidity of 4000 NTU had the worst transmission and was unable to be detected at ≥ 1cm. Turbidity of 1200 and 2000 NTU had transmission reduced by 90% within the first 1cm. Turbidity's of 108, 216, 360 and 720 NTU had transmission reduced below

90% within 2cm. The remaining turbidity was reduced by 90% within 5cm of transmission (Figure 2.8.). Only turbidity of 0.1, 1, 5 and 10 NTU were able to be detected at 14cm, however, their irradiance had reduced to below the reported effective antifouling level (1 µW/cm^2) (Piola *et al*., 2016). Reduction across all tiles by embedding in silicone was 40.5% with the highest and lowest reductions of 28 and 62.6% respectively.

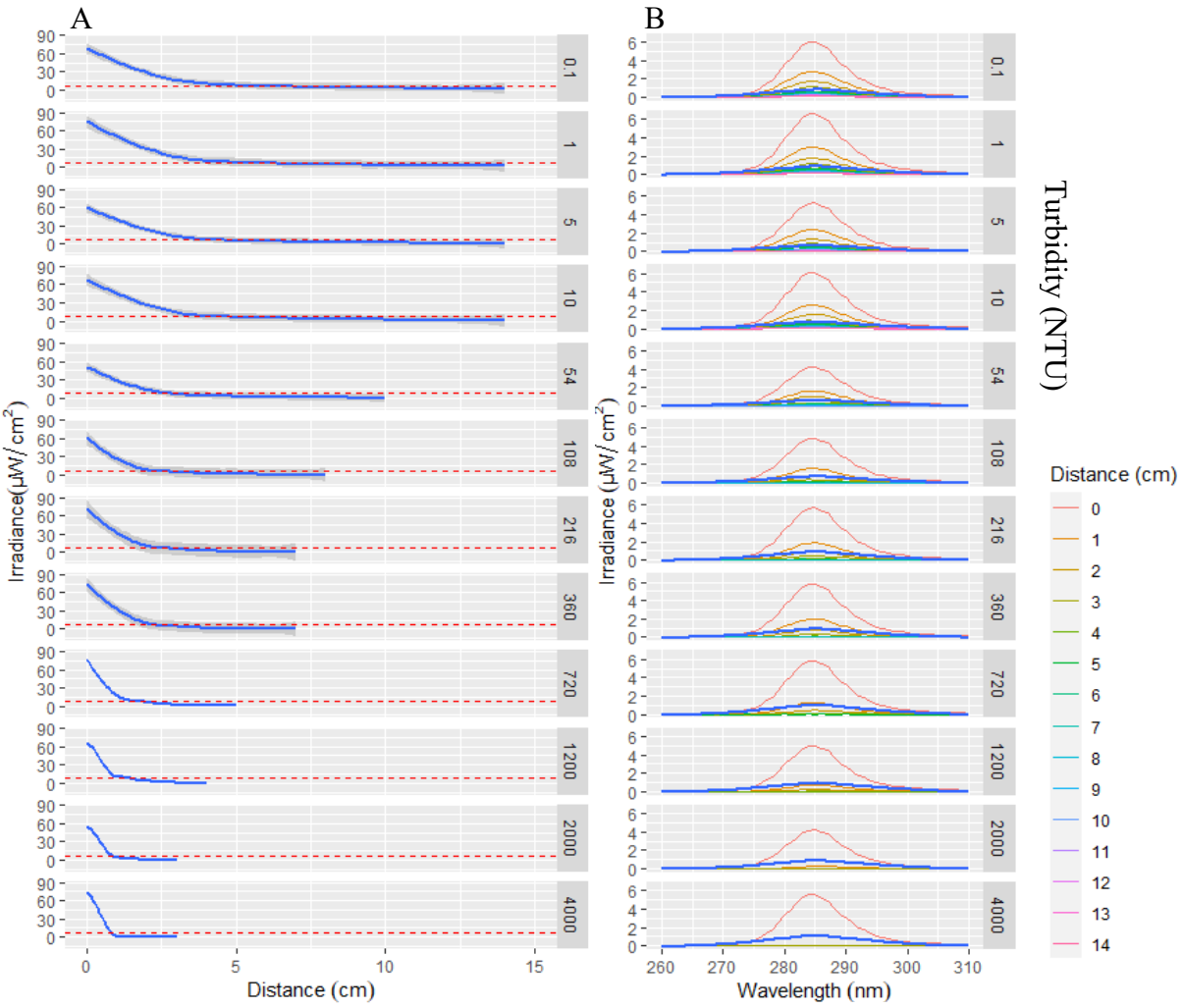

Figure 2.8. A) Sum of LED irradiance readings taken at variable distances (1-14cm) from the tiles surface within different turbid solutions (NTU). Red dashed line represents point in which irradiance was reduced by 90%. B) LED irradiance readings with wavelength (nm), from variable distances (1-14cm) from the tiles surface within different turbid solutions (NTU).

2.4 Discussion

2.4.1 Laboratory scale tile

The variation between LED output was significant and indicated that LED output was not stable upon initiation. Although within two minutes irradiance outputs across all LEDs on both tiles had reached a degree of stability and would produce reliable irradiances for experimentation.

Tile B indicated a smoother output with less variation than Tile A which could be explained by connection issues causing electronic peaks and troughs. However, as all LEDs were arranged in a single circuit, all LEDs would experience any flux in power.

The results of the heat exchange trials indicated that the heat generated from the initiated electrical components did not impact the surrounding media even at a low volume of 50mL. Experiments were conducted from midmorning into early afternoon and increases over the two hours may have represented the room temperature shift which was not measured. Barring the temperature increase over time the only significant change was between the trials and the supply of water. This difference can be explained by the trials only containing 50mL of ASW whereas the supply water contained 6L. As the body of water was 120 times larger than the trials, it took longer to heat. No change in heat exchange was indicated between control and powered systems which is promising as increases in surrounding waters could create non-desirable side effects.

LED irradiance reduction concerning voltage was evident with a single volt reduction nearly halving the irradiance output. All LEDs on both tiles responded similarly and provided irradiance rates for all LEDs at respective voltages. Controlling irradiance output by altering voltage allows the tiles to be versatile in their delivery method and adjustable for specific threshold needs. Peak wavelengths were higher on Tile B which was different to the warmup results which measured total UV output. Tile B has a marginally narrower wavelength coverage than that of Tile A, as Tile A had the higher total irradiance, but Tile B had the higher peak irradiance. Overall irradiances from both tiles were comparable and using the measured emittance, provided specific exposure fluences to which organisms would be exposed.

The 1cm incremental scan reveals that the surface coverage of the irradiance was sub-optimal and that dead zones were present. The LED coverage left a dead zone central to the tile that could be explained via the height of the surface from the LED source. LEDs give off irradiance in a cone with a set angle of dispersal, scattering by particles within the Lumisil® was predicted to amplify transmission further than the cone area. The angle of emittance was 120^{o} which was predicted to be amplified by internal scattering, so the tile's surface was only 12.5cm above the LED source. However, the silicone allowed more transmission than expected and less scattering resulting in a more concentrated beam directly above the LEDs. This resulted in the hotspots in Figure 2.3. and a variation in exposure across the tile's surface. The irradiance variation with surface location is undesirable as organisms may use the low irradiance spots as a refuge and still be able to foul the surface. To resolve the issue tile improvements would be required to use a translucent silicone with more particles to enable enhanced scattering which would reach more areas of the tile. However, this scattering may absorb some of the UV rays and reduce the

tile's operational capacity. A second option would be to adjust the silicone thickness following the emittance angle from the LED source to the surface to determine better coverage. This would require a thicker silicone which would increase mass but would ensure a broader coverage at a high irradiance rate.

2.4.2 Field scale tile

UV transmission through relatively clear water (0.1 NTU) indicated high reductions (> 90%) within 5cm and irradiance rates were negligible at 14cm from the tile surface. Higher NTU levels drastically reduced the transmission of light and saw linear drops with distance. The average turbidity of the North Sea ranges with coastal turbidity from 15-60 NTU and offshore turbidity averaging below 7 NTU (Vansteenbrugge *et al*., 2015). Under these conditions, the irradiance would penetrate to < 10cm in coastal environments and < 14cm when offshore. The Canadian River, Texas, has a mean turbidity that ranges from 22 to 264 NTU from December–February and can reach up to 4,770 NTU from June-August (Bonner, 2000). Under the most extreme situations, this would restrict the attenuation of the light to < 1cm from the surface. As an antifouling method, the restricted distance is preferable to reduce the impact on none target marine life. The LEDs are embedded within the silicone and thus the reduction in attenuation would not impact their performance as an antifoulant. The tile design is aiming to restrict settling organisms from colonising the surface of the tiles and not impact organisms in the surrounding water column. The maximum attenuation of 14cm indicates that organisms further than this distance would not be affected by the harmful rays and in highly turbid waters, organisms further than 1cm would be unharmed.

Embedding within the silicone had a higher transmission reduction than the reported 10% in the technical data sheets. This may be due to the wavelength of irradiance or the thickness of the silicone. The 10% reduction stated within the technical datasheet was associated with irradiance at 450nm through a 1 mm film. UV wavelength affects the transmittance within silicone as lower wavelengths transmit less than higher wavelengths (Lin *et al*., 2010). The LEDs utilised in the 4x4 tile version had a peak irradiance of 278nm which was 172nm lower than the results stipulated within the technical datasheet. The total silicone thickness was 18mm and the LED with starboard was 2mm plus an additional 0.5mm below to sufficiently seal the LED, this left from the point of emittance to the surface of the tile a silicone thickness of 15.5 mm. This is 15 times thicker than the conditions stipulated within the technical datasheet and combined with the variation in wavelength can explain the reduced transmission. Although the Lumisil® embedding significantly reduced the irradiance, the reduction was restricted to the distal points and the tile edging. Furthermore, the reduction did not go below the reported

effective antifouling level that is recommended in the literature (Piola *et al*., 2016). The coverage of the tile indicated sufficient coverage at irradiance rates that have been reported to prevent biofouling and were appropriate for further experimentation.

LED variation is evident with some LEDs underperforming immediately after tile construction (Tile H,16 and P,1). This could be problematic as reliability in LED supply is required. UVC LED supply is a new technology with initial production only beginning in 2000 (Muramoto *et al*., 2014). With new technology, issues are expected, as is constant progression to introduce better-performing supplies that can operate more efficiently at higher capacities for longer durations. LEDs are considered to be two generations behind visual light and currently, Phoseon Technology supplies UV disinfection and a supply of other UV products that operate at 275nm. Their products have displayed usage of 40-60,000 h whilst achieving an irradiance up to 80% of initial levels (L80). This reliability and duration are desirable as continuous irradiance would be required for continuous antifouling.

Far UVC use as an antimicrobial is becoming more preferential as organisms with larger cells aren't as affected and the germicidal effect can be as effective as the more common 264nm wavelengths (Yamano *et al*., 2020; Buonanno *et al*., 2020). The production of LEDs for far UVC emittance can be problematic as they require a higher concentration of aluminium during production which results in a shorter lifespan (Moe *et al*., 2018). In a 2020 study far UVC LEDs were enhanced that were able to achieve 3600 h of constant emission before having an L50 reduction (Yoshikawa *et al*., 2020). At the time, this was 1 log longer than any other recorded lifespan for a far LED source. Cathodoluminescent UVC light sources have indicated some promise with far UV light but miniaturisation of the product limits their lifespan with current L80s of ~ 500 h (Sharma & Demir, 2022). Recently a tuneable light source with a wavelength range from 200-770nm has indicated a 10,000 h lifespan (Ye *et al*., 2022). Although this is not an LED system, the ability to attune the light to a more efficient wavelength for specific organisms is a desirable advancement which could benefit future tile developments. Electronic components and light generation technology is progressing with more efficient sources and technical capabilities highlighting the future feasibility of utilizing UV light as an antifoulant.

2.5 Conclusion

The current study has displayed that manufacturing a UV-emitting tile and the introduction of UV as an antifoulant is achievable. Initial tile production required amendments to ensure full surface coverage and highlighted the requirement of thorough tile design. The silicone encapsulant provided a sealant which allowed UV transmission and protection of the electronic

components. LEDs supplied ample irradiance at and above predicted antifouling levels whilst maintaining a low power demand and not producing any temperature impact on the surrounding media. Alteration of the LED supply voltage allowed a tunability of the irradiance source to better meet desirable thresholds. UV transmission in surrounding media was limited and in high turbid environments, organisms ≥ 1cm from the tile's surface would not be impacted. The variation in LEDs indicates that future LED development would be beneficial and visible light technologies indicate a prosperous future for UV as a marine biofouling control.

Chapter 3. Importance of Duration, Duty-Cycling and Thresholds for the Implementation of Ultraviolet C in Marine Biofouling Control

An edited form of this chapter was published in February of 2022 in Frontiers in Marine Science as part of the special article, Impact and Management of Marine Biofouling.

Whitworth, P., Aldred, N., Reynolds, K. J., Plummer, J., Duke, P., & Clare, A. S. (2022). Importance of Duration, Duty-Cycling and Thresholds for the Implementation of Ultraviolet C in Marine Biofouling Control. Frontiers in Marine Science. **DOI:** https://doi.org/10.3389/fmars.2021.809011.

3.1 Introduction

Marine biofouling is an expansive industrial problem that is well-studied, with multiple reviews focusing on or around specific niches (Pritchard, 1988; Dobretsov *et al*., 2013). Methods to limit fouling on ships include biocidal treatment, interference with adhesion, settlement deterrence, and physical removal of foulers (Han *et al*., 2021; Liu *et al*., 2021; Pistone *et al*., 2021). Between these groups, many strategies have been developed, ranging from electrochlorination to biocidal products (Growcott *et al*., 2017), self-polishing and controlled depletion paints (Almeida *et al*., 2007), fouling-release coatings (Lejars *et al*., 2012), and the development of new experimental approaches (Li *et al*., 2020).

The inhibition of early-forming biofilms has been proposed as a means to counteract macrofouling, by interfering with the proposed successional development of a fouling community (Hadfield & Paul, 2001; Hadfield, 2011; Salta *et al*., 2013). Under this scenario, the biofouling process begins with the formation of a conditioning layer providing nutrients for subsequent adhering organisms (Wahl & Lafargue, 1990; Railkin, 2003; Grzegorczyk *et al*., 2018). Next, bacteria and diatoms use the nutrient-rich conditioning layer to produce an exopolymeric material resulting in a biofilm (Dang & Lovell, 2016a). Diatoms are associated with the early colonization of surfaces and are ubiquitous in their distribution (Hunsucker *et al*., 2014; Gómez-Ramírez *et al*., 2019). Diatomaceous biofilms can increase vessel hull friction by up to 70% based on the biofilm's thickness and percentage coverage; this can require increases in vessel power between 1.5 and 10.1% (Schultz *et al*., 2015). Biofilm formation is dependent on the physical and chemical conditions of the water, such as temperature and chemical input, and is vulnerable to unfavourable conditions (Cacabelos *et al*., 2020). Biofilms may then induce larval settlement and allow the formation of a macrofouling layer of juvenile barnacles, mussels, ascidians, polychaetes, and algal spores. While this process is generally considered to be successional (Scheer, 1943; Wahl, 1989; Bloecher *et al*., 2013; Chen *et al*., 2013), this is not

always the case and many fouling organisms, which are opportunistic by nature, exhibit settlement inhibition or ambivalence in the presence of a biofilm (Roberts *et al*., 1991; Clare *et al*., 1992; Hadfield & Paul, 2001; Callow & Callow, 2011; Salta *et al*., 2013; Piola *et al*., 2016). As bacteria and single-celled organisms, such as diatoms, are particularly susceptible to ultraviolet (UV) light, its use as an antifouling strategy has generated interest both for the prevention of biofilm formation and possible knock-on effects to macroscopic biofouling prevention.

Diatoms, *Navicula incerta* were chosen as a representative slime-forming species; a major challenge for contemporary non-biocidal fouling-release coatings (Schultz *et al*., 2015). The Genus *Navicula* comprise of over 1200 species which can be found globally (Falasco et al., 2009). *N.incerta* secrete an adhesive exopolymer which interacts with a surface and can create a strong adhesion. *N. incerta* have been used in multiple fouling related studies for removal assays in determination of effectivity of new AF coatings (Alles & Rosenhahn, 2015; Zargiel et al., 2011; Hunsucker & Swain, 2016; Gómez-Ramírez et al., 2019). As an initial coloniser of surfaces and making up constituents of biofilms worldwide *N. incerta* are a prime candidate for determining the potential of UV as a marine antifoulant.

UV irradiation is used for sterilization in many industries including water purification, sewage treatment, medical surface cleansing, food preservation, and in scientific laboratories for routine sterilization of equipment. The UV spectrum inactivates organisms most effectively at 254nm (UVC; Zelle, 1960). By isomerizing hydrogen bonds it forms a cyclobutane pyrimidine dimer (CPD) or 6-4 photoproduct (6-4 PP; Schreier *et al*., 2009). In algae, these lesions distort the structure of DNA, which fail a DNA assessment during photosystem II. This can lead to a failure in cell division and reproduction and can cause cell apoptosis (Szabó & Ohshima, 1997). The impediment to proliferation has the potential to halt biofilm formation and inhibit fouling by organisms that require a biofilm for settlement. Additionally, evidence suggests that macrofouling larvae are more susceptible to UV light than adult phases, indicating that settlement could be prevented and macrofouling inhibited with continuous exposure (Kuffner, 2001; Hunsucker *et al*., 2019).

The use of UV sterilization has become more prevalent as technology has progressed and the costs and scale of the light sources have reduced. Mono- and polychromatic halogen lamps provide a high irradiance capacity but, due to their size, remain unfeasible for many applications. UV light-emitting diodes (LEDs) have improved since the early 2000s and are now commercially available at a reasonable scale and cost (Bugbee, 2017). This has allowed for technological integration where UV use was not previously considered. However, the

specifics of duration for effective removal, duty cycling (pulsing) period requirements and level of irradiance rates for an effect have thus far not been explored.

Using the initial findings of Piola *et al*. (2016), this study aimed to determine the efficacy of UVB/C LED embedded tiles in inhibiting biofouling over varying exposure durations, duty cycle periods, and fluence rates to establish a range of thresholds for these factors. For our experiments, we used a laboratory model biofilm-forming diatom, *Navicula incerta*. To determine thresholds, the minimum dosages required to attain a significant reduction in growth and removal followed by a 1 log reduction in the density of exposed organisms was investigated. By comparing settlement and survival, a novel UVC based antifouling approach that is effective may be achievable.

3.2 Methods

3.2.1 Units and nomenclature

Throughout this manuscript, irradiances (a radiant flux which a surface receives per unit area - $\mu W/cm^2$) were measured using an ILT 950 spectroradiometer by taking a reading at the experimental surface. These measures were treated as the surface irradiance, which gave individual nm irradiances and total UVB/C spectral range irradiances. The term fluence (units J/cm^2) is used interchangeably with UV dose. Fluence/dose is the amount of irradiance the organisms were exposed to over a given time (in seconds). The quantum yield, and how much of the dose was absorbed by individual organisms, was not measured. The UV dose was determined by taking an irradiance reading at the experimental surface and multiplying it by the duration of exposure in seconds.

3.2.2 Methods and Materials

A total of four tiles (two irradiated and two control) were produced with a 2 x 2 array of UV (265-300nm) LEDs embedded 1cm beneath the surface of a 70 x 70 x 25 mm Lumisil® 400 (Wacker) silicone polymer (Figure 2.1). To degas the Lumisil® 400, it was cured at -0.1 MPa within a Medline Scientific™ Jeio Tech 665 L vacuum oven (OV-12) over 48 hours at 70 ^{o}C. This prevented bubble formation on the surface and allowed optimal internal cross-linking.

Supplier recommendations stipulated that LED power requirement was 24 V and 0.17 amps per LED to achieve an expected 10,000 hours of dependable performance. This was used as the standard operating power supply and only altered in specific experiments, as described below.

N. incerta strain UTEX B 2046 from the culture collection at the University of Texas in Austin, USA was cultured following Kardela *et al*. (2019), and were used for experiments on day 5 of

culture, at the peak of their exponential growth phase. Cells were agitated and suspended before experimentation, allowing the cell density to be calculated. The culture was then diluted with F/2 medium to give a 150,000 cells/mL culture. To the surface of the tiles, 20 mL of the 150,000 cells/mL culture was added and allowed 2 minutes to acclimate before irradiance was initiated. Tiles were split into irradiated and control and operated in replicates of five for durations of 2 hours, 1 day, 2 days, 3 days, 4 days, and 5 days. After the allotted exposure duration, tiles were transferred to fresh artificial seawater (ASW) made to 33 ppt using Tropic Marin® salts and placed on an orbital shaker for 5 minutes as a wash step. The wash step allowed any deceased and non-adhered *N. incerta* to be removed from the surface so that differences between viable cell densities could be determined.

Cells remaining adhered were photographed using an epifluorescence microscope (Leica DMi8 with Texas Red filter set, 570-600 EX and 604-644 EM). To control for possible uneven coverage, 30 fields of view were taken at randomly chosen locations (Callow & Callow, 2002), three of which were counted manually for comparison to subsequent automated counts. These were made using Image J software by converting images to 16-bit format, altering the threshold to isolate cells from the surface, and counting with a minimum pixel count of 35 and curvature of 0.2. All cell count survival and settlement data were then subjected to generalized linear modelling (GLM) and statistical analysis using R 4.0.0 (Bunn, 2013).

The method described above was used for the pulsing study, which was conducted after the completion of the initial study but varied with irradiance supplied in periods of 20 minutes according to the following duty cycles: 10:10, 5:15, 2.50:17.50, 1:19, and 0.50:19.50 (irradiated: no irradiance). Experiments were run for 2 days, based on findings from the diatom settlement study.

To determine thresholds for survival of diatoms, the irradiance was altered by controlling the voltage to the tiles. Diatom cultures and methodology otherwise followed the same protocol as above. Irradiance was measured using an ILT 950 spectroradiometer. Based on these findings, voltage experiments were conducted with increments from 18 V to 24 V. Settlement and survival of *N. incerta* were measured and statistically compared for all voltage increments. Smooth line plots were generated using a t-based approximation, and GLM, where the normal confidence interval is constructed on the link scale and then back-transformed to the response scale within the ggplot2 package using the geom_smooth function (Wickham *et al*., 2016).

3.3 Results

Kruskal-Wallis and Wilcoxon pairwise tests were used for statistical analysis of all data as data did not conform to assumptions of normality and equal variance after multiple transformation attempts.

3.3.1 Tile specifications

Tile irradiance was measured, using an ILT 950 spectroradiometer, at the water-tile interface directly over the LEDs and at the centre of each tile. The mean irradiance from all tiles was 108.23 µW/cm^2 with an average peak irradiance of 5.77 µW/cm^2 at 281nm, which did not vary significantly between the LEDs ($P > 0.05$), and had a wavelength range from 265-300nm (Figure 3.1). There was some substantial drop off in fluence based on the tile surface location

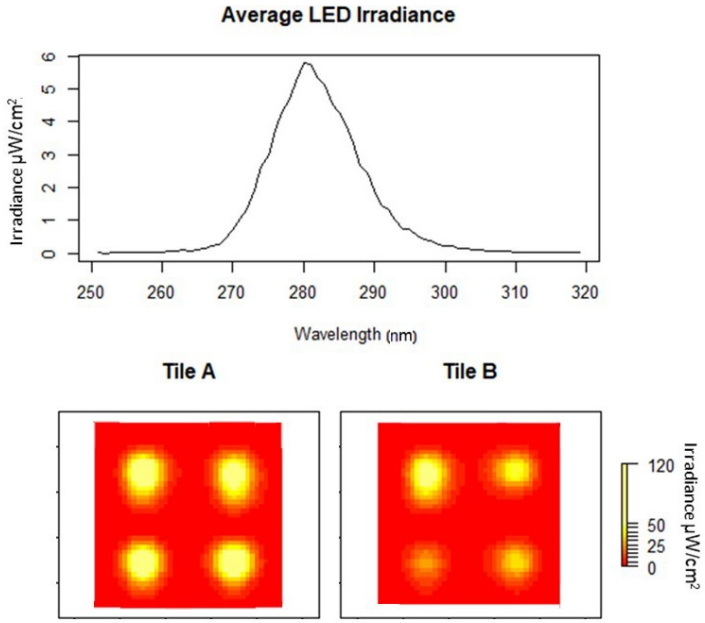

Figure 3.1. Average peak wavelength of eight LEDs embedded in two tiles at 24 volts (A,B). Heat maps of individual tile irradiances (yellow high and red low).

(Figure 3.1). These variations were taken into consideration in the design of experiments. The irradiances for LEDs used in this study were determined at 18 V (0.07 µW/cm^2), 19 V (0.88 µW/cm^2), 20 V (4.76 µW/cm^2), 21 V (15.32 µW/cm^2), 22 V (36.04 µW/cm^2), 23 V (64.34 µW/cm^2), and 24 V (108.23 µW/cm^2). These gave fluence values over 48 hours of 0.01, 0.15, 0.82, 2.65, 6.23, 11.12, and 18.70 J/cm^2, respectively (Figure 3.2). All rates and dose measurements were compiled and are supplied in Table 3.1.

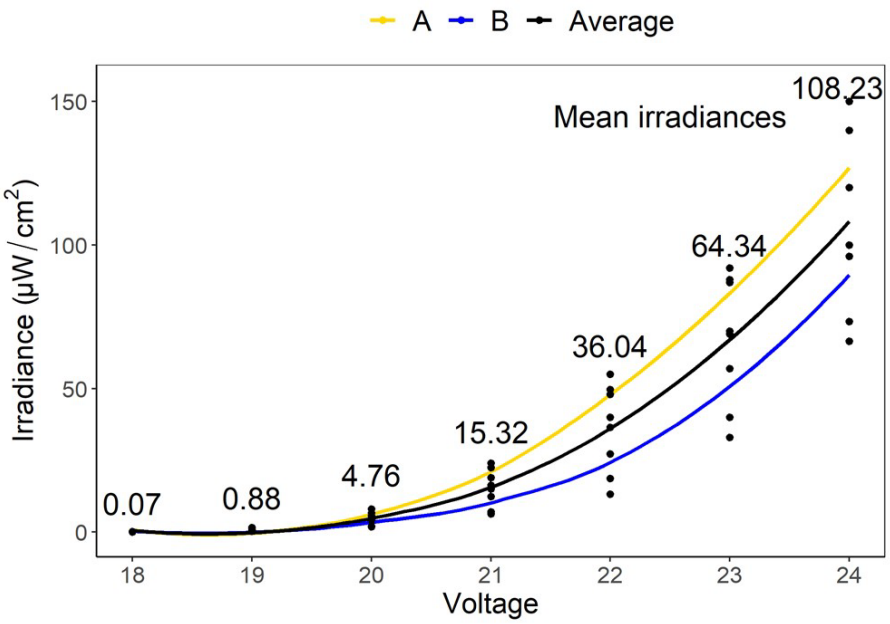

Figure 3.2. Mean irradiances of eight LEDs embedded in two tiles (A,B) at varying voltages (18–24 V). These gave fluence values over 48 h of 0.01, 0.15, 0.82, 2.65, 6.23, 11.12, and 18.70 J/cm^2, respectively.

Table 3.1. Cell abundances, survival, and removal percentage of *Navicula incerta* during ultraviolet irradiance at varying durations, duty cycles, intensities and fluences.

	Method	Experimental duration (s^{-1})	Exposure duration (s^{-1})	Fluence rate (µW/cm^2/s^{-1})	Fluence dose (J/cm^2)	Mean control abundance (Cells/mm^2)	SD	SE	Mean exposed abundance (Cells/mm^2)	SD	SE	% of mean control to initial	% of mean irradiated to initial	% of mean irradiated to inflated control
Duration	2 hours	7200	7200	108.23	0.78	209.5	105.1	9.6	136.8	107.1	9.8	0.0	65.3	65.3
	1 day	86400	86400	108.23	9.35	748.2	212.0	19.4	90.3	90.8	8.3	257.2	43.1	12.1
	2 days	172800	172800	108.23	18.70	790.9	400.4	36.6	14.3	18.4	1.7	277.5	6.8	1.8
	3 days	259200	259200	108.23	28.05	1364.7	285.0	26.0	34.8	46.4	4.2	551.5	16.6	2.5
	4 days	345600	345600	108.23	37.40	1257.4	279.8	25.5	2.9	10.5	1.0	500.2	1.4	0.2
	5 days	432000	432000	108.23	46.75	1100.3	376.9	34.4	3.6	8.9	0.8	425.2	1.7	0.3
Pulse	0.50:19.50	172800	4320	108.23	0.47	1211.4	276.5	25.2	260.2	335.8	30.7	478.3	124.2	21.5
	01:19	172800	8640	108.23	0.94	1734.9	492.1	44.9	249.1	213.8	19.5	728.2	118.9	14.4
	02.50:17.50	172800	21600	108.23	2.34	1647.1	383.3	35	88.4	80.9	7.4	686.2	42.2	5.4
	05:15	172800	43200	108.23	4.68	1072.4	280.4	25.6	106.4	62.9	5.7	411.9	50.8	9.9
	10:10	172800	86400	108.23	9.35	1096.4	270.3	24.7	69.6	82.7	7.5	423.4	33.2	6.3
Voltage	18 Volts	172800	172800	0.07	0.01	1010.9	293.5	26.8	806.6	263.9	24.1	382.6	385.1	79.8
	19 Volts	172800	172800	0.88	0.15	530.9	160.7	14.7	364.9	264.5	24.1	153.4	174.2	68.7
	20 Volts	172800	172800	4.76	0.82	737.5	226.4	20.7	227.0	195.7	17.9	252.1	108.4	30.8
	21 Volts	172800	172800	15.32	2.65	826.1	415.1	37.9	101.4	80.2	7.3	294.4	48.4	12.3
	22 Volts	172800	172800	36.04	6.23	818.4	258.0	23.6	63.0	64.7	5.9	290.7	30.1	7.7
	23 Volts	172800	172800	64.34	11.12	921.3	240.3	21.9	23.4	32.4	3.0	339.8	11.2	2.5
	24 Volts	172800	172800	108.23	18.70	804.1	371.8	33.9	16.3	24.7	2.3	283.9	7.8	2.0

3.3.2 Duration of exposure to irradiance

Exposure durations of 2 hours, 1 day, 2 days, 3 days, 4 days, and 5 days produced fluences of 0.78, 9.35, 18.70, 28.05, 37.40, and 46.75 J/cm^2, respectively (Table 3.1). For the controls, of the total 150,000 cells/mL added within solution, ~ 1 million (~ 209 ± 100 cells/mm^2) were able to settle and adhere within the first 2 hours (Figure 3.3). Not all diatoms land on the raphe

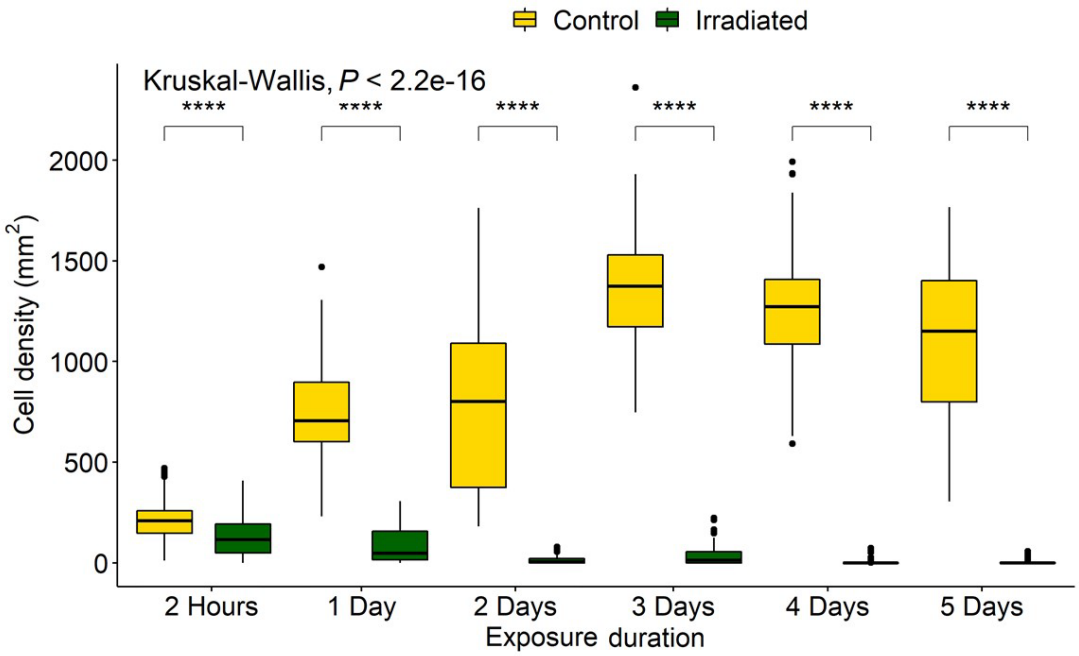

Figure 3.3. *Navicula incerta* densities after UV irradiance over varying periods. Durations of 2 h, 1, 2, 3, 4, and 5 days produced fluences of 0.78, 9.35, 18.70, 28.05, 37.40, and 46.75 J/cm^2, respectively. Kruskal-Wallis value displayed with Wilcoxon pairwise comparison arranged above groupings ($^{****}P < 0.0001$).

(which functions in adhesion and motility), and those that do not are able to reposition within 30-90 seconds for firm initial adhesion (Wetherbee *et al*., 1998). This indicates that the biofilm would sufficiently adhere within minutes, and that 2 hours allowed before counting was adequate as a measure of initial settlement. The diatoms remaining on the surface after 2 hours were referred to as initial input densities for comparison to control and irradiated treatment densities. Any irradiated treatment densities that were below this initial input level would be counted as a removal of cells, while higher levels would be counted as growth. The treatment controls represented the ability of the diatoms to proliferate with no UV treatment and indicated the population growth from the initial cell input. Comparing irradiated to both control and initial numbers enabled inhibition of reproduction and survival to be determined.

Control densities indicated population growth over time with increases of 257%, 277%, 551%, 500%, and 425% over the following 1 day, 2 days, 3 days, 4 days, and 5 days, respectively. Irradiated tiles showed a reduction of 35%, 57%, 93%, 83%, 99%, and 98%, respectively, compared to initial settlement. Compared to the growth that accrued on the controls, there were, respectively, 35%, 87%, 98%, 98%, 99%, and 99% fewer cells on the irradiated tiles (Figure 3.4). All doses resulted in a significant difference between the initial settlement, controls, and irradiated tiles (Figure 3.4).

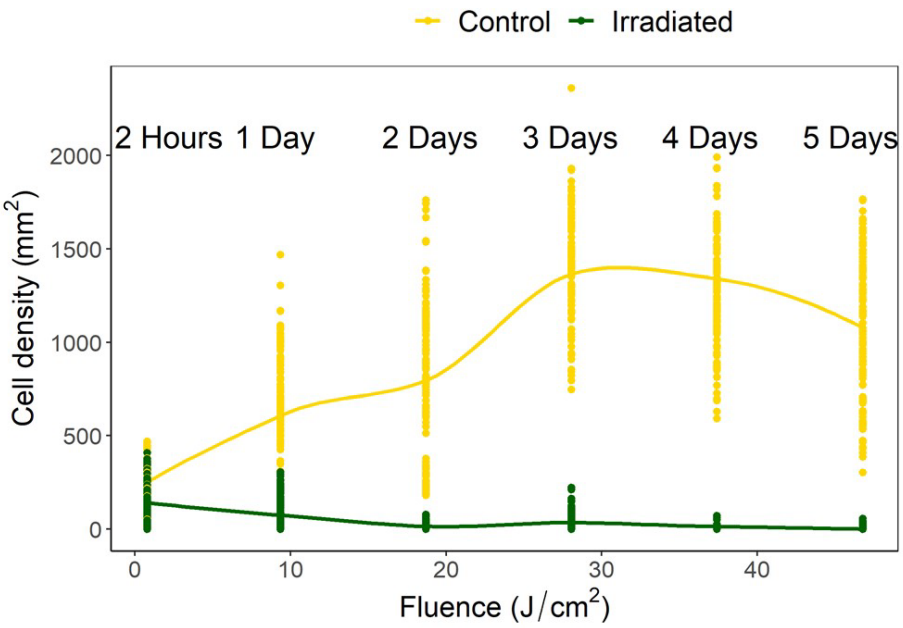

Figure 3.4. *Navicula incerta* abundance after UV irradiance over varying periods with respective fluences. Durations of 2 h, 1, 2, 3, 4, and 5 days produced fluences of 0.78, 9.35, 18.70, 28.05, 37.40, and 46.75 J/cm^2, respectively.

3.3.3 Effect of duty cycling

Interval experiments were run for 48 hours in periods of 20 minutes, allowing 144 duty cycles. Fluences were determined as 9.35, 4.68, 2.34, 0.94, and 0.47 J/cm^2 for each respective duty cycle of 10:10, 5:15, 2.50:17.50, 1:19, and 0.50:19.50 (irradiated: no irradiance).

The control treatments indicated a mean (± SD) diatom settlement of 1,352 ± 450 cells/mm^2, which was 989% higher than the initial cell input. Settlement differed significantly from the respective controls in all irradiance duty cycles $P < 0.05$ (Figure 3.5). Cell densities on irradiated tiles were reduced by 94%, 90%, 95%, 85%, and 78% of control tiles for the 10:10, 05:15, 02.50:17.50, 01:19, and 0.50:19.50 (irradiated: no irradiance) duty cycles, respectively. Duty cycles of 10:10, 05:15, and 02.50:17.50 had reductions of 67%, 49%, and 58%, respectively when irradiated tiles were compared to the initial settlement, whereas 01:19 and 0.50:19.50 had 19% and 24% growth, respectively. The point at which growth was inhibited, and reduction below initial input density observed, was between 0.94 and 2.34 J/cm^2 (Figure 3.6).

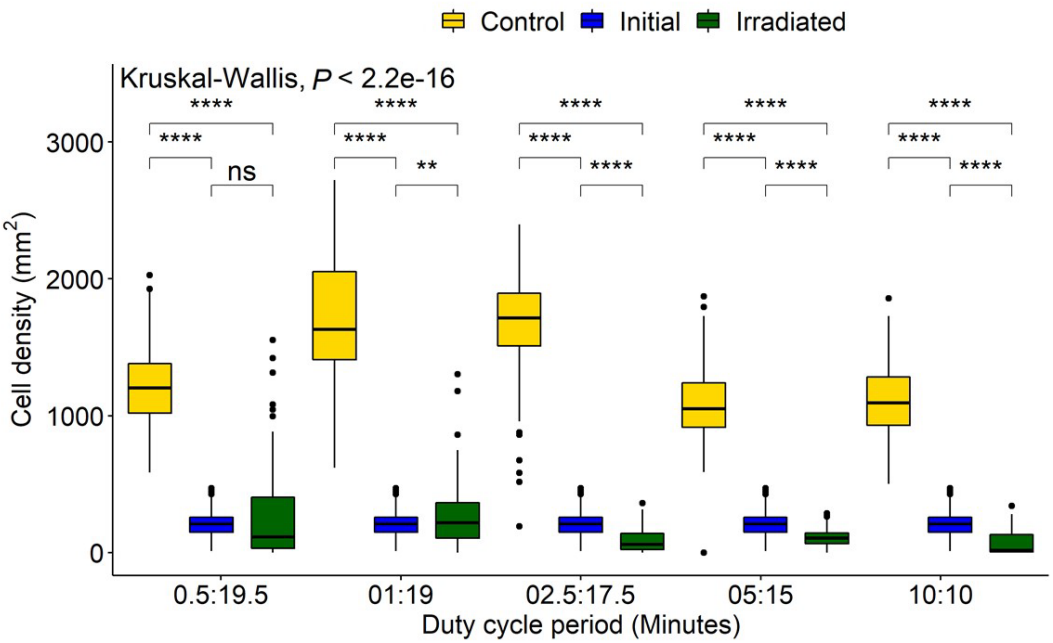

Figure 3.5. *Navicula incerta* abundance after UV irradiance over varying duty cycles. Duty cycling periods display minutes in which the UV light was turned on to minutes it was turned off (On:Off). Fluences were determined as 0.47, 0.94, 2.34, 4.68, and 9.35 J/cm^2 for each respective duty cycle 0.50:19.50, 1:19, 2.50:17.50, 5:15, and 10:10 (irradiated: no irradiance). Significant differences indicated via Wilcoxon pairwise comparison above groupings (ns, no significance, $^{**}P < 0.01$, $^{****}P < 0.0001$). Initial refers to cell density introduced at experiment start. Control refers to no UV supply. Irradiated refers to experiments with UV supply.

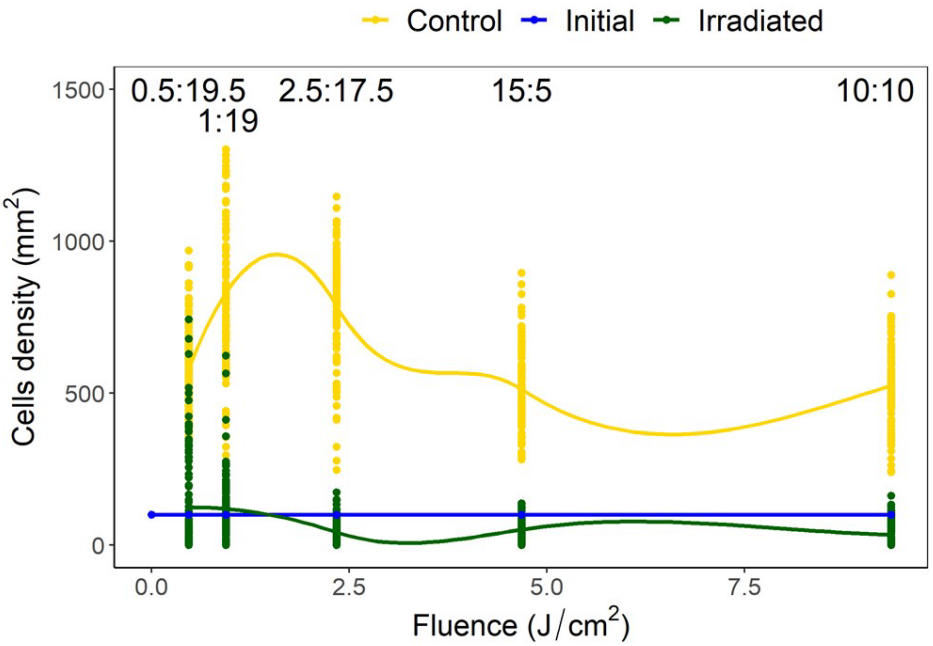

Figure 3.6. *Navicula incerta* density and range after UV irradiance over varying duty cycles with respective irradiance dosages. Duty cycling periods display minutes in which the UV light was turned on to minutes it was turned off (On:Off). Fluence dosages were determined as 0.47, 0.94, 2.34, 4.68, and 9.35 J/cm^2 for each respective duty cycle 0.50:19.50, 1:19, 2.50:17.50, 5:15, and 10:10 (irradiated: no irradiance). Irradiated and initial intercept point (between 0.94 and 2.34 J/cm^2) indicates the fluence required to reduce density below initial levels. Initial refers to cell density introduced at experiment start. Control refers to no UV supply. Irradiated refers to experiments with UV supply.

3.3.4 Effect of voltage changes

Voltage experiments were run to allow varying irradiance (Figure 3.7 and Table 3.1). All voltages indicated significant differences between control, initial, and irradiated samples (Figure 3.7). Low voltage irradiances resulted in diatom growth of 8%, 74%, and 285%, respectively compared to the initial density for 18, 19, and 20 V. Significant reductions of 52%, 70%, 89%, and 92% were also seen in the 21-, 22-, 23-, and 24-V treatments compared to the initial input. All voltages resulted in significantly lower densities (cell counts) than the growth controls, with one-volt increases from 18 to 24 V having 20%, 31%, 69%, 88%, 92%, 97.5%, and 98% lower densities, respectively. The intersect where the irradiated cell densities overlapped with the initial cell densities was between 20-21 V (Figure 3.8.). This was between

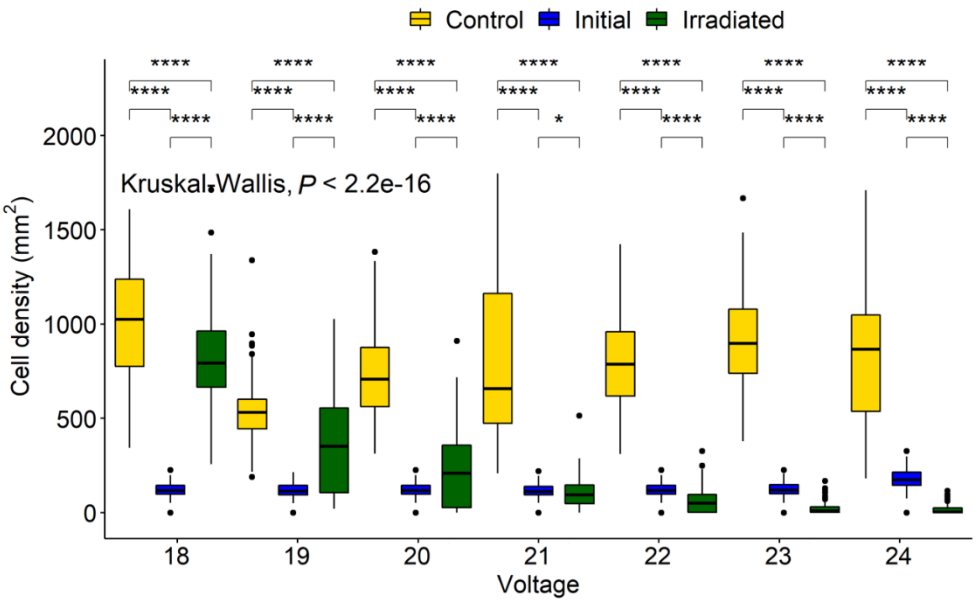

Figure 3.7. *Navicula incerta* abundance and range after UV irradiance over varying voltages. Kruskal-Wallis value displayed with Wilcoxon pairwise comparison ranged above groupings ($^{*}P < 0.05$, $^{****}P < 0.0001$). Initial refers to cell density introduced at experiment start. Control refers to no UV supply. Irradiated refers to experiments with UV supply.

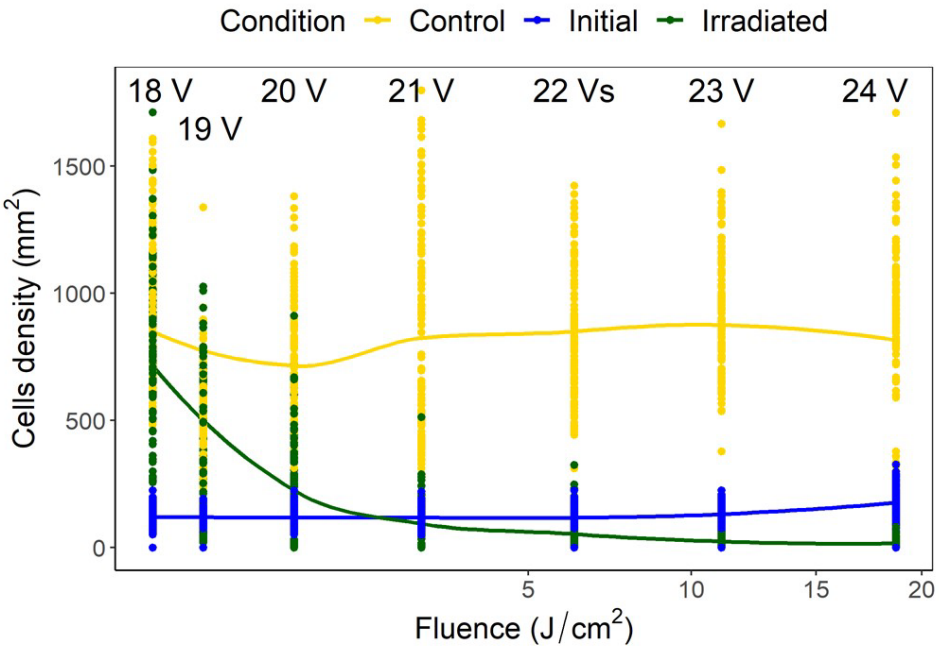

Figure 3.8. *Navicula incerta* cell densities and ranges at different voltages, with the corresponding fluence on the x axis. Predictive generalized linear modelling indicated the intercept between irradiated density and initial density to be between 20 and 21 volts (0.82–2.65 J/cm^2). Initial refers to cell density introduced at experiment start. Control refers to no UV supply. Irradiated refers to experiments with UV supply.

0.82 and 2.65 J/cm^2 and represents a threshold of fluence to halt growth and, above this level, to initiate removal (Figure 3.8).

3.3.5 Comparisons at high and low dosages

Fluence is reported to have the same biological effect regardless of the method of delivery (Bunsen & Roscoe, 1863). Therefore, the three methods discussed previously should have resulted in reproducible reductions in diatom cell counts, if doses were the same (Sommer *et al*., 1996, 1998). High and low fluence groups were identified based on doses across the three experimental procedures. A low fluence of 0.78-0.94 J/cm^2 included the 2 hours, 20 V, and 1:19 duty cycle samples, and a high fluence of 9.35-11.12 J/cm^2 included the 1 day, 23 V, and 10:10 duty cycle samples.

There were no significant differences in cell densities between the 20 V and the 1:19 duty cycle method, however, the 2-hour exposure was significantly more effective ($P < 0.05$). High fluence samples indicated that all treatment methods were significantly different from each other ($P < 0.05$), with 23 V having the highest removal and 1 day having the lowest removal (Figure 3.9).

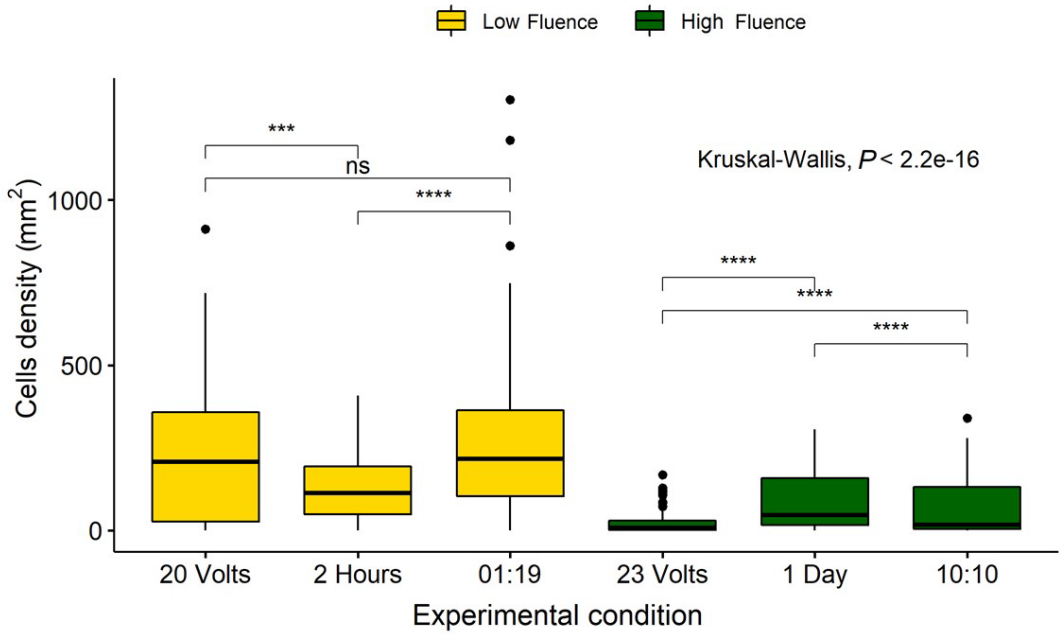

Figure 3.9. Comparison of *Navicula incerta* cell densities remaining on the surface after low and high irradiance exposures. Low fluence grouped based on fluence of 0.82, 0.78, and 0.94 J/cm^2 for 20 volts, 2 h, and a 01:19 duty cycle, respectively. High fluence grouped based on fluence of 11.12, 9.35, and 9.35 J/cm^2 for 23 volts, 1 day, and a 10:10 duty cycle, respectively. Kruskal-Wallis value displayed with Wilcoxon pairwise comparison arranged above groupings (ns, not significant, $^{***}P < 0.001$, $^{****}P < 0.0001$).

3.3.6 Determination of thresholds

The dose required to produce a 1 log reduction (lethal dose to achieve 90% cell reduction - LD_{90}) below initial densities was determined via GLM using predictive analysis based on the count data. Doses were compared separately by experiment and comprehensively by removing all control data, other than the initial settlement, and comparing irradiated data against the initial data. Only data that were below the initial density level were included as densities above this indicated growth and would produce predictions based on an inflated density. The duration experiment indicated that a fluence of 42 J/cm^2, with a range from 35-52 J/cm^2, would be required for a 90% reduction in diatom cell density (Figure 3.10). The pulsing data revealed increased cell densities in 0.5:19.5 and 01:19 duty cycles and these were thus removed from GLM. Modelling indicated that a fluence of 20 J/cm^2, with a range from 12-65 J/cm^2, would be required for 90% diatom removal. The voltage experiment indicated that cell numbers increased in the 18 to 20 V treatments which were, therefore, not included in the predictive analysis. The LD_{90} of the voltage experiments was a fluence of 21 J/cm^2 with a range of 17-28 J/cm^2. The comprehensive LD_{90} was predicted to be 25 J/cm^2 with a range from 19-36 J/cm^2. All four data sets produced different LD_{90}s and were indicative of variation between irradiance delivery method and effect. The LD_{90} was predicted to be between 20-42 J/cm^2, with an overall range of 12-65 J/cm^2.

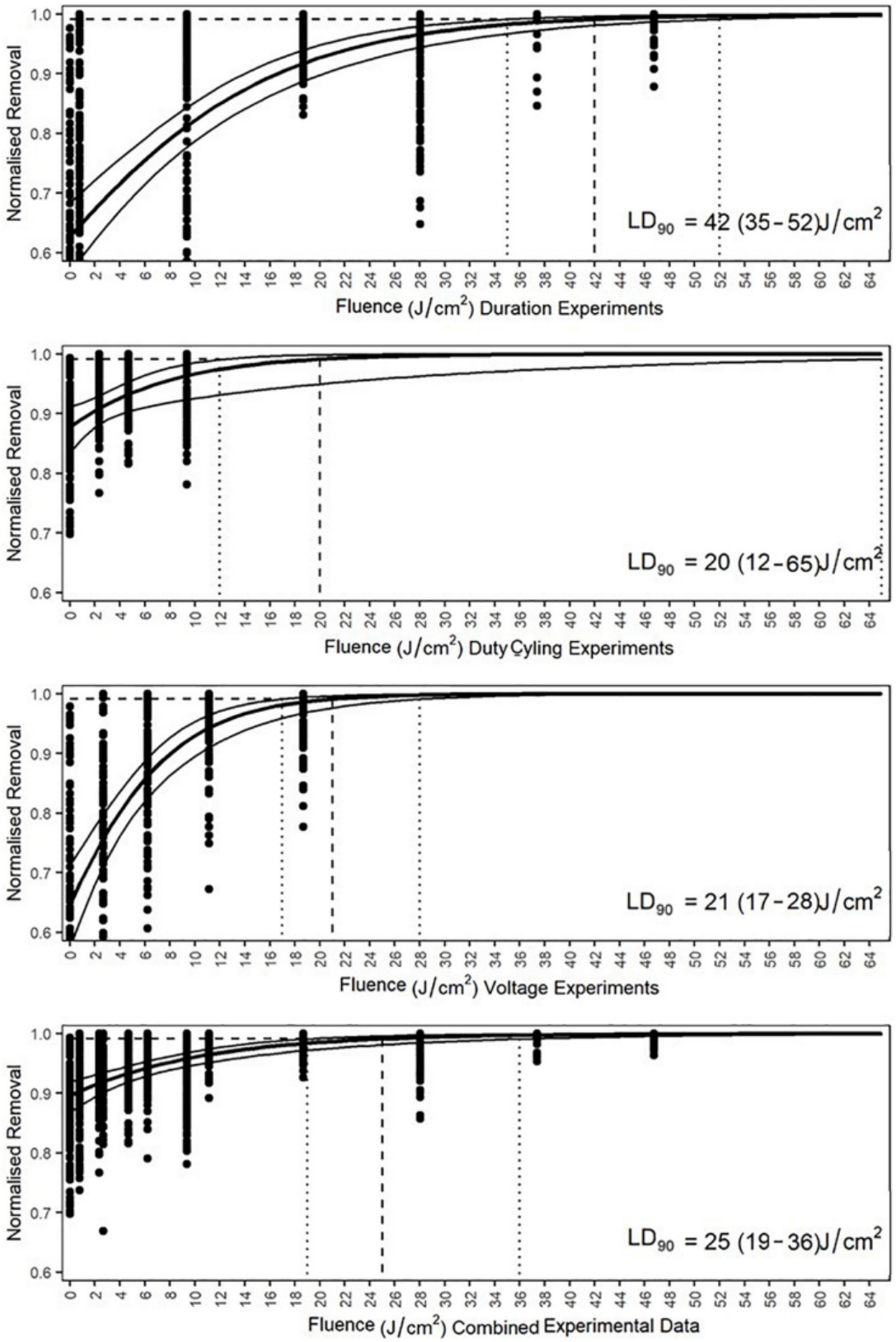

Figure 3.10. Generalized linear model predicted lethal fluences, expressed as LD_{90}, of each experiment and the combined data to obtain a 90% reduction in cell density of *Navicula incerta* below the initial cell density. Dashed lines intercept at the LD_{90}. The 95% confidence interval ranges are indicated by the vertical dotted lines with the values in parentheses.

3.4 Discussion

UV treatment is an effective form of sterilization used across diverse industries (Shaban *et al*., 1997; Tree *et al*., 1997; Bintsis *et al*., 2000; Shaw *et al*., 2008; Winward *et al*., 2008). The present results indicate the potential of UV treatment for control of biofouling of surfaces within the marine environment. In the experiments conducted in our study, all diatom (*Navicula incerta*) samples, even those exposed to low fluences (0.01, 0.47, and 0.78 J/cm^2), demonstrated a significant reduction in densities when compared to control counts. The suppression of growth at the lowest fluence (< 0.78 J/cm^2), combined with reduced cell densities above this level, highlights the efficacy of UV sterilization for biofouling control.

3.4.1 Effect of duration of irradiance

This study determined that diatom densities, compared to initial settlement, were impacted in all UV treatment durations. Cell densities in the controls (non-irradiated) increased above the initial settlement (after 2 hours) establishing the ability of *N. incerta* to grow within the experimental conditions. Cell densities above the initial input, but below the experimental control cell densities, suggested a negative impact of UV treatment on cell proliferation, but biofilm growth was not entirely prevented. Cell densities, which were similar to initial densities after irradiance, implied a stop to cell division and an equilibrium between the repair mechanisms and the exposure dosage. Finally, when cell counts were lower than the initial cell count, following irradiance at fluences from 0.78 to 46.75 J/cm^2, the implication is that cell division stopped, and repair mechanisms could not keep pace with the damage caused by UV exposure. By whatever mechanism, death and/or detachment, cells were lost from the surface.

The lowest fluences produced a reduction in cell densities, although a 1 log reduction compared to the initial settlement was only observed after 2 days of irradiance, equivalent to 18.70 J/cm^2 (Figures 3.3 & 3.4). After 4 days of irradiance, cell density was nearly 3 log lower than the control, suggesting that continuous irradiance was extremely effective, even at low fluence. This implied that fluence sufficient to negate growth and induce removal (i.e., above 18.7 J/cm^2), could be achieved to meet performance specifications required for antifouling approval by MIL-PRF-24647C and the European Chemical Agency (European Chemicals Agency, 2014; ECHA/EFSA, 2017). However, the methods required by the European Chemical Agency and MIL-PRF-24647C were mainly developed with chemical biocides in mind. There is currently no EU regulation under which an UV based antifouling method could be appropriately certified (ECHA/EFSA, 2017).

3.4.2 Effect of voltage

Voltage supply directly affected the irradiance of the LEDs with changes of a single voltage unit causing a reduction in irradiance (Figure 3.2). This had a substantial effect on the diatoms (Figures 3.7 & 3.8). Growth at the lowest voltages (18-20 V) was influenced by only small changes in voltage. Higher voltage supply (21-24 V) reduced cell density below the initial count, indicating a potential effective level for prevention of biofilm growth. This threshold is important for the optimized design of UVB/C LED systems for biofouling control, though additional target fouling species need to be tested. An effective antifouling level (the required irradiance for preventing the growth of organisms on a surface) has been predicted to be 1 $\mu W/cm^2$ for UV based antifouling systems (Piola *et al*., 2016). The fluence supplied to the tile surface in the current study had an average peak value which was 5.77 times higher than the predicted value at the recommended operating voltage (24 V), and a total UVB/C fluence that was 109 times greater. Based on spectroradiometer readings, 19 V (Figure 3.2) supplied the closest irradiance for comparison to the reported level. Piola *et al*. (2016) stated that the level could be even lower than 1 $\mu W/cm^2$ and, for the current study, the irradiance threshold for *N. incerta* was validated as below 0.7 $\mu W/cm^2$. Although, as indicated by the intercept point in Figure 3.8, to achieve a reduction below initial cell density, a fluence between 4.76-15.32 J/cm^2 (between 20 and 21 V) would be required. Determining whether this can translate into the natural environment is imperative, as cultured organisms are known to be less resilient than their wild-type counterparts (Falciatore *et al*., 2020). Dissolved organic matter within the water can also impede UV treatment efficacy (Georgiades *et al*., 2021). Moreover, diatoms are just one component of a complex biofouling community. The extracellular polymeric substances secreted by diatoms, and the silicate structures left behind by dead cells, could attract and protect further colonizers. Wild-type resilience and population interactions may cause the effective level to differ from that currently indicated.

3.4.3 Effect of duty cycling

Developing UV as an antifouling strategy will require the method to meet some design criteria, one of which is prolonged efficacy with minimal maintenance. The manufacturers' specifications for the half-life (irradiance output) of the LEDs used in this study was 10,000 hours (1.14 years), at constant irradiance. Visible light LEDs, on the other hand, can exceed 100,000 hours of use and UV LED life expectancy will likely improve as technology develops (Muramoto *et al*., 2014). Several years of fouling protection under various conditions will be required to make the integration of UV LEDs appealing to the shipping industry.

Duty cycles were compared to explore lengthening the longevity of the LEDs. Outcomes demonstrated that even the shortest duty cycle of 2.5% could inhibit biofilm growth. Control tiles of the 02.50:17.50 and 01:19 duty cycles had higher diatom densities than the other duty cycle controls ($P < 0.05$). This apparent anomaly may be explained by the use of a new stock of F/2 growth medium, or small variations in cell density at the start of the experiment. This higher density may have allowed some variation within the irradiated samples. Since the same stock was used for both control and irradiated exposures, however, the differences may be compared.

A 12.5% duty cycle would be required to prevent growth and effectively reduce fouling. At the lower 2.5% cycle, longevity of the LEDs could be increased to 45.6 years, whilst at 12.5% cycling, 9.2 years could be achieved. Duty cycling of 0.01 % (1 minute/week) has been reported by Richard *et al*. (2021) to have a significant impact, however, for full macrofouling prevention, a duty cycle of 0.69% (10 minutes per day) was required. Rates as low as these could see effective antifouling via UV lasting the entirety of a vessel's lifespan. Differences in the effectiveness of the duty cycling between this study and the study by Richard *et al*. (2021) could be due to the different light sources used. Richard *et al*. (2021) used a 25 W Aqua UVC (254nm) lamp rather than LEDs. This provided different irradiances than the current study and recorded an intensity of 1.31 $\mu W/cm^2$ at a peak wavelength of 254nm rather than the 281nm used herein. As biological impact is dose-dependent, a threshold would be advantageous in isolating specific duty cycles from individual light supplies.

3.4.4 Comparisons at high and low doses

Variation in dose and biological impact were comparable between the three methods of irradiance delivery used in the current study and provided effects of low and high fluence on cell density. Low fluence experiments included the 2-hour experiment, which resulted in lower cell densities than the other methods. The lower cell density in the 2-hour treatment, as opposed to 20 V and the 01:19 duty cycle, could be due to the fluence being below an effective inactivation level. This would enable the diatoms to proliferate during the 48-hour experiment. According to the Bunsen-Roscoe reciprocity law (Bunsen & Roscoe, 1863), the total photochemical dose absorbed by an organism will have the same effect regardless of varying irradiance and/or exposure durations. Supporting evidence was discussed by Sommer *et al*. (1998) who found that a microbiocidal dose of 400 J/m^2 was required for a 4-log bacterial reduction regardless of delivery intensity. Sommer *et al*. (1998) indicated that a low intensity and longer exposure duration was more effective at inactivation than short high irradiance on eukaryotic yeast cells. *Escherichia coli* and bacteriophages have displayed the opposite,

reducing more over shorter durations at higher intensities (Sommer *et al*., 1998; Werschkun *et al*., 2012). UV damage is not described as being time dependent and is associated with the overall dose. However, diatoms require time to complete biological processes such as division and growth. Therefore, the biological processes may have counteracted some of the damage and be accountable for the differences. The densities may have been relatable if the 2-hour experiment had the UV turned off and the diatoms left to grow for a further 46 hours.

The longer experimental duration could explain why the high exposure 23 V experiment, in high fluence samples, had a lower cell density than the 1 day and duty cycle doses. If the irradiance is above an effective threshold for a longer time, then there would be more time for the population to reduce in number. This could explain why the 23 V method was significantly more effective than its similar dosage counterparts (Figure 3.9). The variance between sample counts in the duty cycle and the 1-day method was large, whereas the 23 V experiment had minor variance. This may indicate greater resilience during the pulsed method and could also result from repair and recovery during LED downtime. With regard to the 1-day experiment, the shorter duration may have different effects on diatoms of different sizes, as described by van de Waal & Litchman, (2020). This could explain the variability within the counts and the deviation from the full exposure. The current results (Figure 3.9) contradict the Bunsen-Roscoe reciprocity law as similar irradiances produced significantly different effects. For *N. incerta* short, high irradiance treatments were more effective at inactivation than longer, lower intensity treatments which may indicate that biological factors can alter the overall outcome from a prolonged exposure.

It is important to consider that both high and low fluence had some variability and that the exact dose was not the same in all cases. The high doses, from the comprehensive analysis, had identical duty cycle and 1-day doses (9.35 J/cm^2), however, the 23 V dose was 1.77 J/cm^2 higher than these and could explain the lower cell density present within that treatment. Additionally, the low fluences were conducted with no two identical measures delivered, although they only varied by 0.16 J/cm^2 from highest to lowest. To clarify a fluence effect without variation, a repeat of the experiment with exact dose comparisons of the three different treatment methods would be necessary to determine if the small irradiance discrepancy was important.

The data in the current study suggest that the Bunsen-Roscoe law does not allow for interacting biological factors. Diatoms can self-repair photoactive lesions via excision repair mechanisms using photosynthetic light (de Tommasi *et al*., 2018). This enables them to excise the lesions from the DNA and combat the overall damage. A high intensity could overwhelm an organisms' repair mechanisms and a heavily outweighed system would be expected to inactivate quicker

than a neutrally balanced or minimally overcome system. Additionally, if there was no interacting repair mechanism, the organisms would still be limited due to their quantum yield (Braslavsky, 2007). Organisms can only absorb a certain number of photons in a set period before reaching their maximum quantum yield, after which photons that the organism is exposed to become surplus (Li *et al*., 2006, 2010). Like enzyme reactions, there would be a limit to the reactions that could take place at any given time.

3.4.5 Threshold analysis

The interaction between growth and density provides insight into a potential threshold of effect. To prevent growth, but not reduce below initial density, the threshold was determined to be between 0.01 and 0.78 J/cm^2. For densities to be reduced below the initial input levels, a threshold point between 0.78 and 2.65 J/cm^2 would be required. This is similar to the level reported by Piola *et al*. (2016). Using the densities and fluences from all three experiments and a combination of all the data, LD_{90}s were calculated, which suggest a predicted dose to reduce the initial input densities by 90% (Raikow *et al*., 2007). According to the Bunsen-Roscoe reciprocity law LD_{90} fluences should be the same regardless of methodology, however these were observed to vary in the current study. Cell density counts from pulsing (Table 3.1) indicated that supplied irradiance doses did not reduce initial levels below 90%, but duration and voltage methodologies both indicated that 18.7 J/cm^2 produced over 90% removal. The predicted LD_{90} for guaranteed effect ranged from 12-65 J/cm^2 depending on delivery method, and 25 J/cm^2 when averaged across all of the data. Experiments with diatoms were conducted using a high nutrient growth medium (F/2), these nutrient concentrations are not expected to be encountered in the natural environment. Biofilm growth would therefore be slower than observed in laboratory conditions that are optimized for growth. Accordingly, a lower dose may be required for wild type removal. However, as both controls and irradiated experiments used the same medium, the results within the study are comparable. An adaption for more accurate thresholds would require a comparison between this study and field experiments. The predicted threshold for 90% removal, based on all data, was 25 J/cm^2. However, this is likely to be a conservative estimate when the fluences and their respective cell densities are compared. Duration and voltage treatments had > 88% removal at 18.7 and 11.12 J/cm^2, respectively, which is considerably lower than the predicted value. The latter could have been impacted by the variability in densities and the pulsing not achieving 90% removal, which could explain why the threshold value was elevated. Adhering to an elevated fluence, similar to the conservative prediction, should result in effective antifouling prevention and removal but other factors that affect UV efficacy, not currently investigated, would need to be considered.

3.5 Conclusion

The effectiveness of UVB/C for antifouling has been confirmed using a technology (LEDs) that could plausibly be incorporated using a cladding system. The effective levels determined by duty cycling could allow longer lifespans of LED equipment, and longer intervals between repair or replacement. Lower voltages of delivery would lower LED strain and could also prolong longevity. By determining effective thresholds and doses, equipment can be developed to efficiently meet standards and protocols for the approval of UV B/C integration as an antifouling system. Exploration of ecosystem thresholds, under a range of field conditions (including non-target effects), is required to fine-tune this threshold level.

Chapter 4. Implications of Ultraviolet Light on Micro and Macrofouling Communities.

4.1 Introduction

During biofouling, bacteria and plankton, primarily diatoms, adhere to the surface and one another to create an extracellular matrix that is composed of polymeric substances forming a biofilm (Harder & Yee, 2009). The primary surface colonisers of biofouling are often single-celled which are susceptible to ultraviolet (UV) light exposure (Worrest *et al*., 1978; Karentz *et al*., 1991; Bothwell *et al*., 1993). The biofilm layer has been linked with the induction of settlement in larvae and algal spores of polychaetes, tunicates, barnacles and mussels (Richmond & Seed, 1991; Hadfield, 2011). These are among numerous species that utilise the biofilm to determine if a surface is suitable for colonisation (Richmond & Seed, 1991; Railkin, 2003; Dang & Lovell, 2016b). Some of these organisms are gregarious which can attract congeners and increase biofouling pressure (Dreanno *et al*., 2006; Burke, 1986; Toonen & Pawlik, 1996). Biofilm age can directly impact settlement. Wiekczorek *et al* (1995) produce experimental evidence of *Balanus amphitrite* being more likely to settle on older biofilms rather than newly formed ones. However, field studies have found that the settlement of *B. Amphitrite* decreases with biofilm age (Olivier *et al*., 2000). It has been hypothesised that preventing the growth of biofilm-forming microorganisms can interfere with subsequent settlement and prevent macrofouling (Chapman *et al*., 2010; Ponnusamy *et al*., 2009; le Norcy *et al*., 2017). UV exposure impacts a range of colonising organisms and may change biofilm community structure. The formation of a unique biofilm group could deter settlement cues allowing different dominant macrofouling communities to arise (Wieczorek & Todd, 1998; Hadfield, 2011; Flemming *et al*., 2009). This is controversial and some macrofoulers have displayed the ability to colonise a surface regardless of an initial biofilm presence (Roberts *et al*., 1991; Clare *et al*., 1992; Salta *et al*., 2013). Determining the impact caused by UV exposure on micro and macro communities provides insight into UVs potential ecological impact on biofouling organisms.

Introducing UV-emitting tiles into the marine environment is a recent concept and the interactions within the environment are unexplored. Water chemistry, environmental conditions or other factors can be altered which may impact community structure. UV treatment induces chemical reactions that produce reactive oxygen species (ROS) (Phukan *et al*., 2018). These ROS can interact with elements of the water causing chemical shifts. Elevated dissolved oxygen (DO) levels can interact with ROS, reducing the disinfection efficiency of UV and DO levels (Meunier *et al*., 2016). Low dissolved oxygen levels can promote the settlement of *Aurelia*

aurita planula larvae (Ishii *et al*., 2008). A range of other factors such as geographical location, water chemistry, environmental conditions, flow dynamics and biofilm composition can also interact with the recruitment of taxa (Cacabelos *et al*., 2020; Crimaldi *et al*., 2002; Dobretsov, 2009). Biofilms in membrane installations can develop faster at temperatures of 30ºC than at 10-20ºC (Farhat *et al*., 2016). Elevated temperatures can impose a faster rate of metamorphosis in barnacle larvae *Balanus trigonus*, however, high temperatures (~ 28ºC) and low salinity (< 26‰) can reduce cyprid attachment (Thiyagarajan *et al*., 2003). Low salinity treatment (~ 7‰) of panels deployed for 2 years in Plymouth, UK, was found to kill most biofouling species after 2 hours of submersion (De Castro *et al*., 2018). High flow velocities create more vortices in the water and generate higher sheer stress on settling organisms reducing recruitment (Faria *et al*., 2020; Alles & Rosenhahn, 2015). Taxa that colonise a surface can differ depending on seasonality and depend on geographical location (Wahl, 2020; Wahl & Lafargue, 1990; Hiebert *et al*., 2019). Depending on the change enacted, the altered chemical and/or physical conditions may be preferential or detrimental to biofouling taxa and cause variation in the community that colonises. Organism pressure is highly variable and antifoulants are required to encompass the recruitment adaptations of these organisms. Comparing a range of environmental and physical factors is paramount to determine whether UV has an impact on whether these can impact on the community structure.

Organisms such as tunicates, polychaetes and bryozoans for which there is evidence of UV tolerances to enable them to mitigate UV damage (Richard *et al*., 2021; Raikow *et al*., 2007; Hung *et al*., 2005). These tolerances differ, offering species-specific irradiance capacities that determine their resilience. If irradiance levels are below the specific capacity, it could enable resilient organisms to alter community structure. Wild-type organisms have greater genetic diversity which enables them to adapt to environmental conditions and cope more readily with changes than laboratory-cultured organisms (Montero *et al*., 2007). Organisms associated with in situ experiments do not always respond similarly to wild-type organisms (Habeebu *et al*., 2000; Huesemann *et al*., 2009; Bonhivers *et al*., 1998). To determine the effect of UV exposure on wild-type organisms' field deployed experiment and analysis is preferential.

Macrofouling communities are easy to visually distinguish at high taxonomic levels, however, identifying family and lower identities can be problematic. Determining the biofilm fauna is equally problematic and requires microscopy, which can be laborious and impractical for large surface and sample sizes. Amplicon methodologies have become more cost-efficient in recent years (Grant, 2022). Identifying both micro and macro fouling communities using metagenetic amplicon-based next-generation sequencing has been explored in several studies (Comeau *et*

al., 2019; Weber *et al*., 2009; Chen *et al*., 2013; de Vries *et al*., 2021; Angelova *et al*., 2019; Takada *et al*., 2018; Ammon *et al*., 2018; Chiellini *et al*., 2012). This approach enables detection that is highly accurate, time-efficient and cost-effective in identifying pro and eukaryotic communities (Grant, 2022). Unfortunately, due to the amplification required for next-generation sequencing, the abundance of reads can be misleading compared to conventional image analysis. Elucidating compositions at a high taxonomic level utilising both techniques can provide a detailed comparison of community structure.

The current study aimed to determine whether UV exposure to wild-type organisms in different flow regimes impacted the environmental conditions and/or the biofouling accumulation within niche areas. To achieve this, test systems, using simulated sea chests in a field-deployed experiment, were deployed in Hartlepool, UK and Melbourne, Australia, at high and low flow rate water supplies to irradiated and control chambers. To determine effectiveness against different recruiting organisms, control and irradiated polydimethylsiloxane and fluoropolymer fouling release surfaces were analysed for taxonomic differences at monthly intervals over 12 months (March 2021 – Feb 2022). By comparing community assemblages between different operational parameters, UV inhibition of biofouling was determined.

4.2 Methods

Field studies included test rigs (Figure 4.1) constructed and run at Hartlepool Marina 54.69N, -1.19 E and Melbourne 37.51 S, 144.53 E. Two test rigs were constructed at each location, one as a control and one for UV irradiated exposure. Each test rig included a fast and slow flow chamber and was comprised of glass-reinforced plastic one-piece tanks (45 litres - 560 x 410 x 340mm, SKU SC10, Hartlepool) and a custom-manufactured stainless-steel tank (120 litre – 450 x 1800 x 400mm, Melbourne). The Hartlepool chambers were coated internally in Intersleek® 1100SR which included an internal baffle system. The baffle design was attached to the chamber lid and used to deflect water ensuring organism dispersal and preventing a direct flow between input and output (Figure 4.1.). Water was supplied from the surrounding marina source using an Argonaut (AV200-3DN-S) seawater pump. Flow rates were monitored for each exposure directly before entering each test chamber using FlowVis flow meters (SKU: 4950m Hartlepool) and four Siemens SITRANS MagFlo flowmeters (Melbourne). Speeds were adjusted using flow control levers to account for a 9:1 flow division between fast:slow chambers. The control chambers each had two 350 x 350 x 7 mm Lumisol 903 silicone tiles (four total) attached internally in removable sheathes to allow access. Irradiated chambers had two 350 x 350 x 18 mm Lumisol 903 silicone tiles each (four total), attached internally in removable sheaths. Sixteen UVB/C LEDs were embedded in each tile and evenly spaced in a

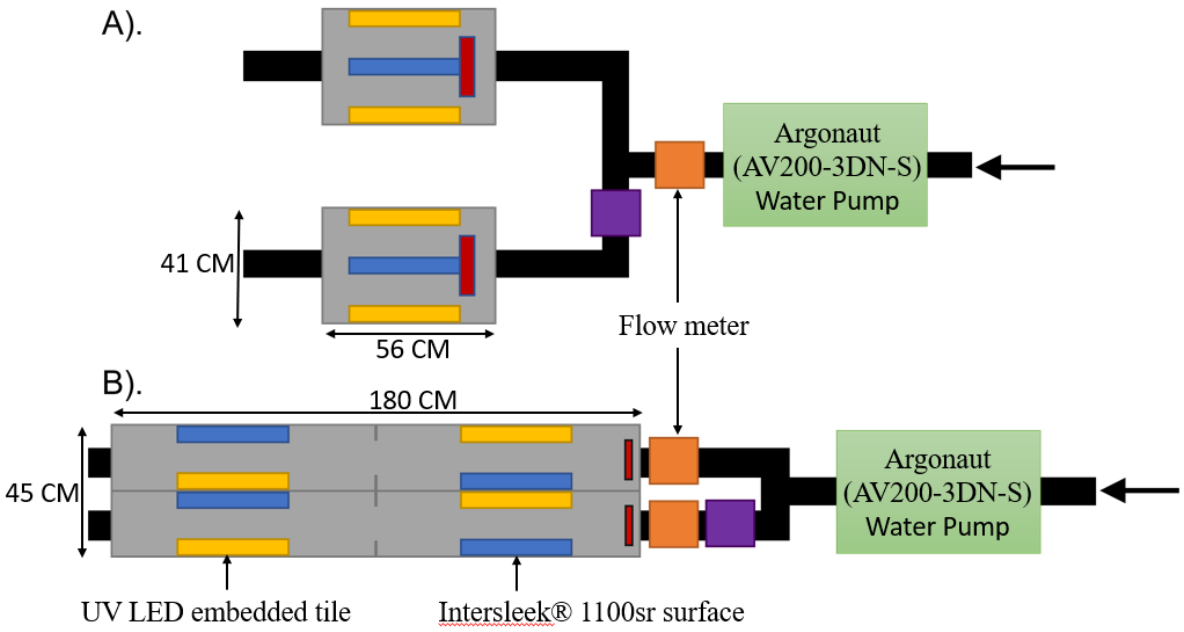

Figure 4.1. Test-rig schematic for A). Hartlepool and B). Melbourne. Each location had two test-rigs in operation, one with a UV irradiated tile and one with a blank tile as control. Chamber speed was distributed at a ratio of 9:1 for fast:slow chambers using flow control levers and based on the flow meter readings. Grey = experimental chamber, yellow = UV/ control tile, blue = Intersleek® 1100SR, red = baffle dispersal, orange = flow meter, purple = flow control, green = water pump, black = pipe work.

4x4 matrix to allow optimal coverage (section 2.4.1). Each chamber included two Intersleek® 1100SR surfaces positioned 11cm from tile surfaces. Intersleek® 1100SR surfaces were included as a standard fouling release (FR) coating to analyse if UV irradiance combined with a FR coating was beneficial.

At the start of the experiment and at monthly intervals UV irradiances were measured for each of the 16 LEDs on the four tiles at both locations (eight tiles and 128 LEDs total). Melbourne measurements were taken using a Solar Light IP60 radiometer (PMA2120) and at Hartlepool, an ILT 950 spectroradiometer and an SXL 55 radiometer were used. During the first 3 months of experimentation, both sites had radiometer issues with lower than expected readings. After June 2021 radiometers were acquired and calibrated providing accurate measurements.

Test rigs were deployed in February 2021. They were sampled after 2 weeks and then monthly thereafter for 12 months. For sampling, environmental conditions were recorded, the tiles were photographed for image analysis and swabs were taken for molecular analysis of community composition. Water flow and LED power were turned off whilst sampling was conducted. Environmental data for the chamber and source seawater was recorded using a Horiba U52G before 1L of water was collected for molecular analysis. Tiles were extracted within their

sheaths to be photographed before having 50 x 50mm of the community swabbed at random positions using TS/15-B hygiene sponge sampling kits (Hartlepool) and SurfACE™ Sponge-Stick (10006157) (Melbourne). The more substantial community required physical biomass removal and swabbing to achieve full 50 x 50mm sampling. Intersleek® and tile surfaces, from the four experimental chambers, were swabbed in replicate three times totalling 24 swabs and 16 photographs per sampling month.

The 1 L water samples were vacuum filtered onto sterile Whatman (10407713), MicroPlus-21 STL cellulose nitrate membranes. One-quarter of the membrane was sectioned and extracted for DNA using QIAGEN DNeasy biofilm Kits (product: 24000-50). Swab samples also had DNA extracted with 5 x 7 x 35 mm sections removed and analysed. The QIAGEN DNeasy biofilm standard operating procedure (SOP) provided was followed with three separate changes:

1. During step 5.B.2. the swabs were found to reabsorb the supernatant after centrifugation, this required an addition to the SOP to release the lysed DNA. The additional step consisted of removing the silicate membrane from sterile spin columns and placing the spin columns within a clean collection tube. The sponges were added to the spin column and centrifuged at 13,000 x g for 1 min. This allowed all lysed material to be spun down through the spin column into the collection tube below whilst the sponge remained in the upper spin column and did not reabsorb the lysed material.
2. Initial extractions gave poor NanoDrop results owing to high salt contamination. To resolve this, steps 12 and 13 were repeated and the solutions were used at -20ºC.
3. Finally, step 16 was split into two elutions of 50 µL rather than one 100µL elution. This gave higher DNA yields.

Purified DNA was frozen and stored until transfer for amplicon sequencing of 16S & 18S ribosomal RNA genes using an Illumina MiSeq platform. Hartlepool samples were sequenced at Northumbria's NU-OMICs facility, and the Melbourne samples underwent the same extraction process but were conducted by the Bioscience and Food Technology Laboratory at the Royal Melbourne Institute of Technology (RMIT). Library preparation and sequencing followed the Schloss wet lab protocol (Kozich *et al*., 2013) using Caporaso *et al*. (2018) primer sets for prokaryotic 16s amplification and Amaral-Zettler *et al*. (2018) primer sets for eukaryotic 18s amplification. The only variation within these protocols was the substitution of polymerase from the Invitrogen Platinum Taq kit which was changed to Kapa 2G robust which achieves better products. Amplified DNA was standardised for quantity and sequenced using an Illumina MiSeq (Kozich *et al*., 2013). Sequencing data were checked for quality, trimmed,

aligned, assessed for chimeric content, and filtered within Mothur (version 1.48). Each extraction had a blank extraction conducted, and any taxa identified in blank extractions were removed from sample comparisons. Alpha and beta diversity metrics were determined and compared within the ggplot2 package within R (version 4.2.0). Count data were compared between irradiated and control exposures for each month, on each surface and the two flow speeds.

Images of each surface and condition were taken at each sample collection throughout the deployment (Feb 2021 to Feb 2022). Images were cropped using ImageJ (version 1.53t), then uploaded and annotated for percentage coverage using the online software BIIGLE (Langenkämper *et al*., 2017). Background overlap was annotated on each image and removed from the total image pixel count for accurate coverage calculation (Figure 4.2). Hartlepool

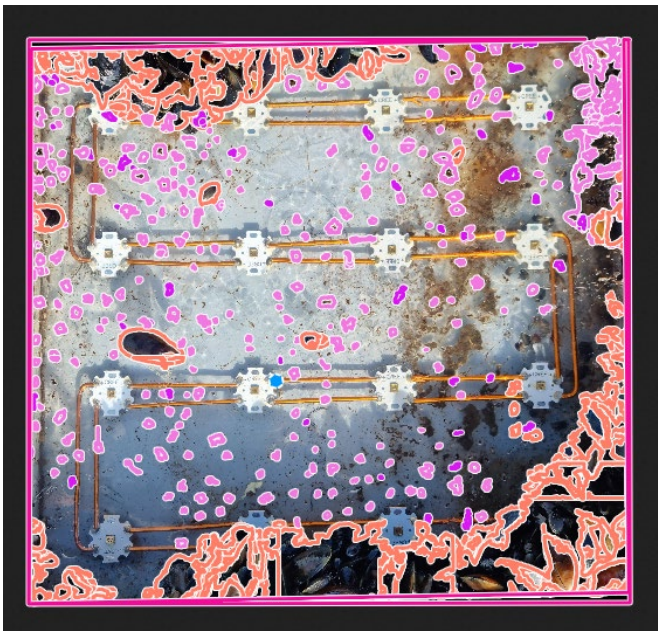

Figure 4.2. Surface analysis of deployed tiles conducted by highlighting taxa and determining individual percentage coverages. Highlights indicate taxa of mussels, amphipod nests and amphipods (pink, orange and blue respectively).

images had nine labels and the Melbourne images had 12 labels defined. The labels represented taxa with a visual surface presence, and they were defined to an accurate taxonomic level. Labels compromised of Amphipoda, Amphipod nests, Biofilm, Bryozoa, Hydrozoa, Bivalvia, Annelida, Tunicata and 'Unknown'. At Melbourne, Asteroidea and Porifera were also present. Images were individually annotated for all labels using BIIGLE's 'Lawnmower' feature at a magnification allowing 16 windows of annotation per image. Annotations were exported as an area coverage Excel document and pixel coverage was converted into percentage coverage. Percentage coverage was then plotted within R version 4.1.1 using the ggplot2 and ggpubr

packages (Wickham *et al*., 2016) (Figures 4.2, 4.3 & 4.6-4.9.). Data was checked for normal distribution and equal variance before being subject to relevant parametric or nonparametric testing within R. NMDDS data was analysed for statistical variation using Anosim and Adonis statistical comparisons within R.

4.3 Results

4.3.1 Statistical analysis

Environmental data conformed to normality and equal variance ($P < 0.05$) and was therefore subjected to parametric ANOVA and Wilcoxon pairwise testing. Count and surface coverage data did not conform to normality or equal variance ($P > 0.05$) so nonparametric Kruskal Wallace and MANN-Whitney pairwise comparisons were conducted.

4.3.2 Environmental data

The environmental data indicated seasonal changes in all metrics measured, however, small differences were found between experimental chambers. Hartlepool had a peak conductivity of 38 mS/cm in July and August with the lowest value (24 mS/cm) recorded in January. Dissolved oxygen (DO) was lowest in August/September at 7 and 9 mg/L for control and irradiated/raw chambers respectively. DO was highest at 12 mg/L in March for all conditions. The pH remained stable throughout the year, however, while sampling in October, the pH meter became damaged, and recordings were skewed to a lower pH thereafter and disregarded. Salinity peaked in September/ October at 27ppt and was lowest in March at 23ppt in all chambers. All flow and irradiance conditions had the highest temperature of 21ºC in July and August and the lowest of 4ºC from January-March with only the slow control chamber varying in March and reaching 8ºC. Turbidity remained below 10 NTU until October. The fast control then started to increase in turbidity up to ~ 200 NTU for December and February with a peak in January of 600 NTU. January had small fluctuations in the remaining chambers with highs of 55, 76 and 98 NTU for fast irradiated, slow irradiated and slow control respectively. At Melbourne, turbidity in all conditions remained at 0-5 NTU between March and August, after which the slow chambers increased up to 21 and 11 NTU for irradiated and control chambers, respectively. The fast control chambers peaked at 16 NTU in January 2022, whilst readings in all the other chambers remained low. In February and March 2022, more turbulent conditions were evident in all chambers. No significant differences between chambers were identified ($P > 0.05$) for temperature, which ranged from 10ºC in July 2021 to 25ºC in January 2022. Salinity, pH, DO,

and conductivity had no significant variation between chambers (Figure 4.3.).

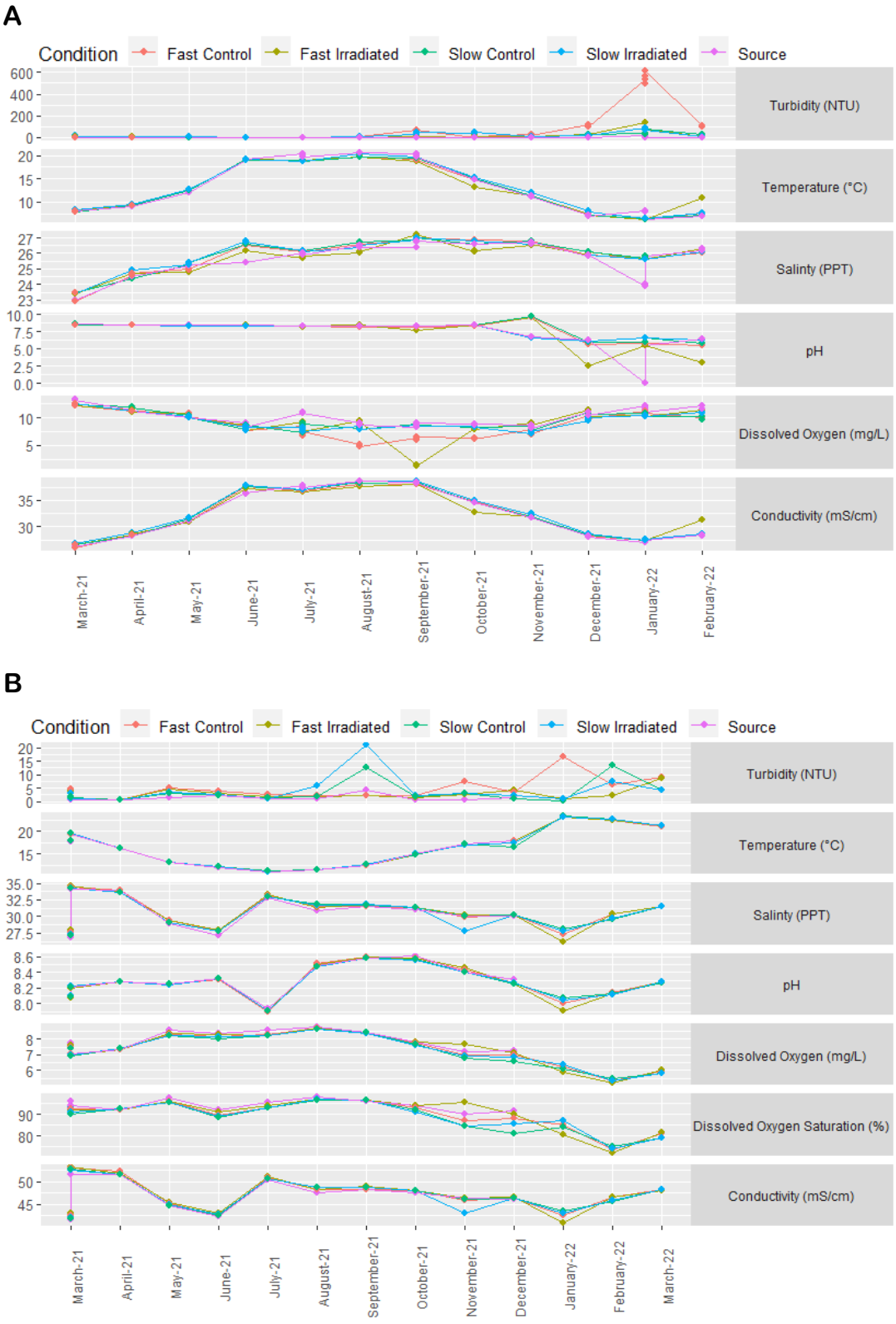

Figure 4.3. Environmental data from experimental chambers and source waters from March 2021- March 2022 in A. Hartlepool, UK and B. Melbourne, Au.

Water speed did not alter between exposures or across the duration of the experiments. Water flow rates were maintained at ~ 140:14 L/min with minimal change over the experimental period. A couple of declines were observed which after investigation, were found to be due to either: floating debris clogging the water intake or internal piping becoming fouled. Both incidents were immediately resolved, and after restart flow rates returned to the above speeds.

Hartlepool had irradiance levels accurately recorded in April 2021 and from June 2021 onwards. A gradual reduction in irradiance output was observed from all tiles, with tiles in fast flow degrading more than the tiles in slow flow. Tiles reduced in irradiance by 97%, 96%, 65% and 65% for fast left, fast right, slow left and slow right respectively. Of the 64 LEDs in Hartlepool, 35 had reduced to < 10% output (32 fast, 3 slow) and 16 gave off < 10μW/cm^2 (15 fast, 1 slow) at the end of the experiment.

Melbourne tiles in the fast chambers had their irradiance capacity reduced by 50% by 10 months of deployment, however, slow chambers were still operating at 50% after 12 months. At the end of the experiment, the overall tile irradiances in Melbourne had reduced by 75%, 63%, 49% and 50% for fast A, fast B, slow A, and slow B tiles respectively. Of the 64 LEDs operating over 12 months in Melbourne, 44 were reduced by > 50%, nine were reduced to < 10% (eight fast, one slow) and 11 were reduced to < 10 μW/cm^2 (8 fast, 3 slow).

4.3.3 Imaging community analysis

Image analysis results were compared between control and irradiated exposures, in both locations, for the community assemblage (all annotations), at each time point for fast and slow flow rates, on tile and Intersleek® surfaces. At both locations, irradiated surfaces were fouled less than the controls (Figures 4.4 & 4.5). Both locations had low initial settlement which increased colonisation from September onwards. The slow irradiated samples from Hartlepool had the lowest continuous biofouling presence with minimal coverage developing in December and January (Figure 4.6). Biofilm was better developed on the Hartlepool controls under slow flow compared to fast flow, however, the fast chambers had more macrofouling. In the fast flow chambers, the initial biofilm shifted to hydrozoans between May and June. The control Intersleek® then returned to predominately biofilm coverage between July and August. The control tile surface community also shifted from biofilm to hydrozoan dominated between May and June, however, they were thereafter dominated by bivalves from August. The irradiancechambers suppressed fouling throughout the study attracting significantly lower (P < 0.05) fouling than control surfaces.

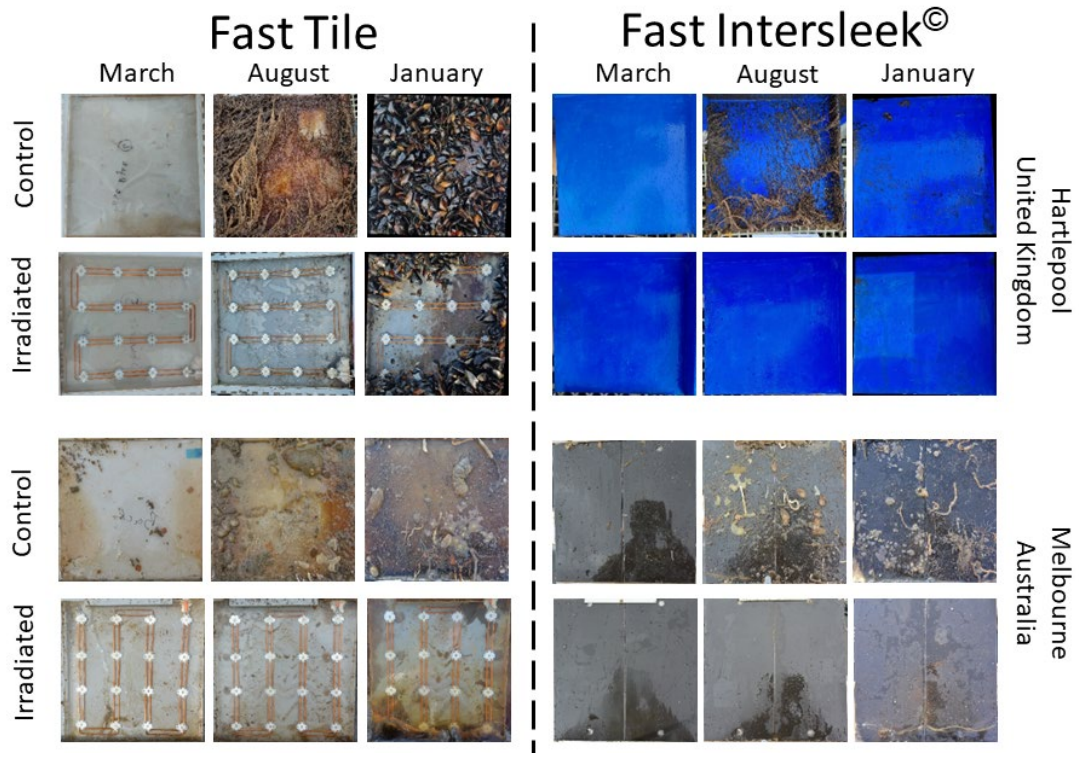

Figure 4.4. Imaging of biofouling after 1, 6 and 11-months from different surfaces in a fast flow experimental chamber.

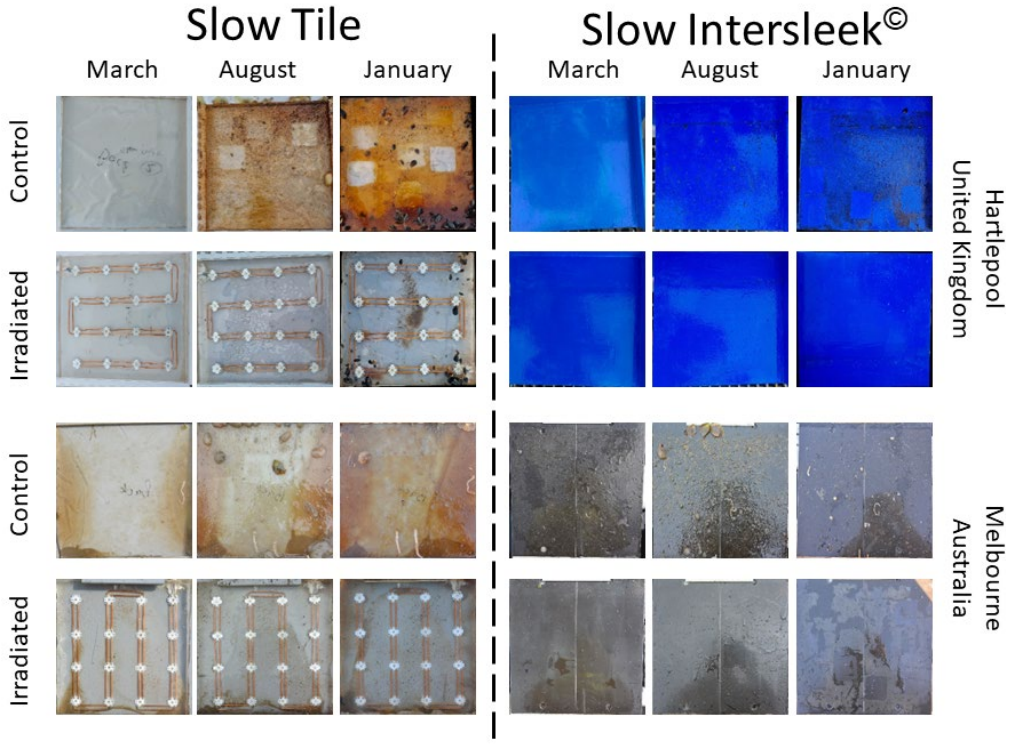

Figure 4.5. Imaging of biofouling after 1, 6 and 11-months from different surfaces in a slow flow experimental chamber.

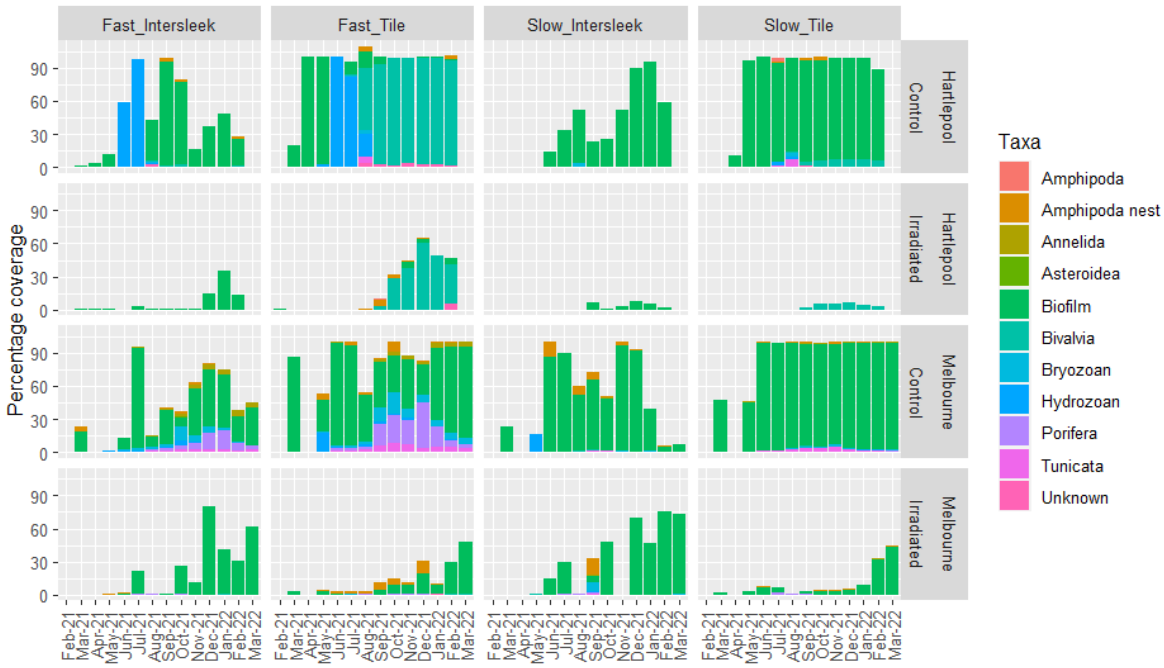

Figure 4.6. Taxonomic abundance expressed as percentage coverage in images of UV irradiated and control surfaces over a 12-month deployment in Hartlepool, UK and Melbourne, Au.

There was lower biomass coverage on irradiated surfaces compared to controls at both Hartlepool and Melbourne. Seasonal community shifts were, however, different at Melbourne compared to Hartlepool. Both surfaces in the fast flow chambers at Melbourne were initially dominated by biofilm, then sponges and finally bryozoans colonised between September and February. This shift in community structure to sponges and bryozoans did not occur on the surfaces in the slow flow chambers at Melbourne and instead remained dominated by biofilm from May onwards. Irradiated surfaces had less micro and macro fouling than the controls in both speed chambers. The community composition on the Intersleek® control surfaces was similar to the tile controls; however, a higher coverage was detected on the latter. All irradiated surfaces experienced gradual increases in biomass coverage over the last 6 months of the field exposure.

Kendall correlations were determined between image analysis surface coverage and environmental conditions (Figure 4.7). Total coverage and biofilm coverage were consistent in having opposite correlations to other taxa in most conditions. Hartlepool irradiated slow chambers had positive correlations with all taxa and pH. Irradiated slow taxa at Hartlepool had negative correlations with turbidity and salinity. Control slow chambers at Hartlepool had positive correlations with DO but negative correlations with turbidity. Most taxa in control fast

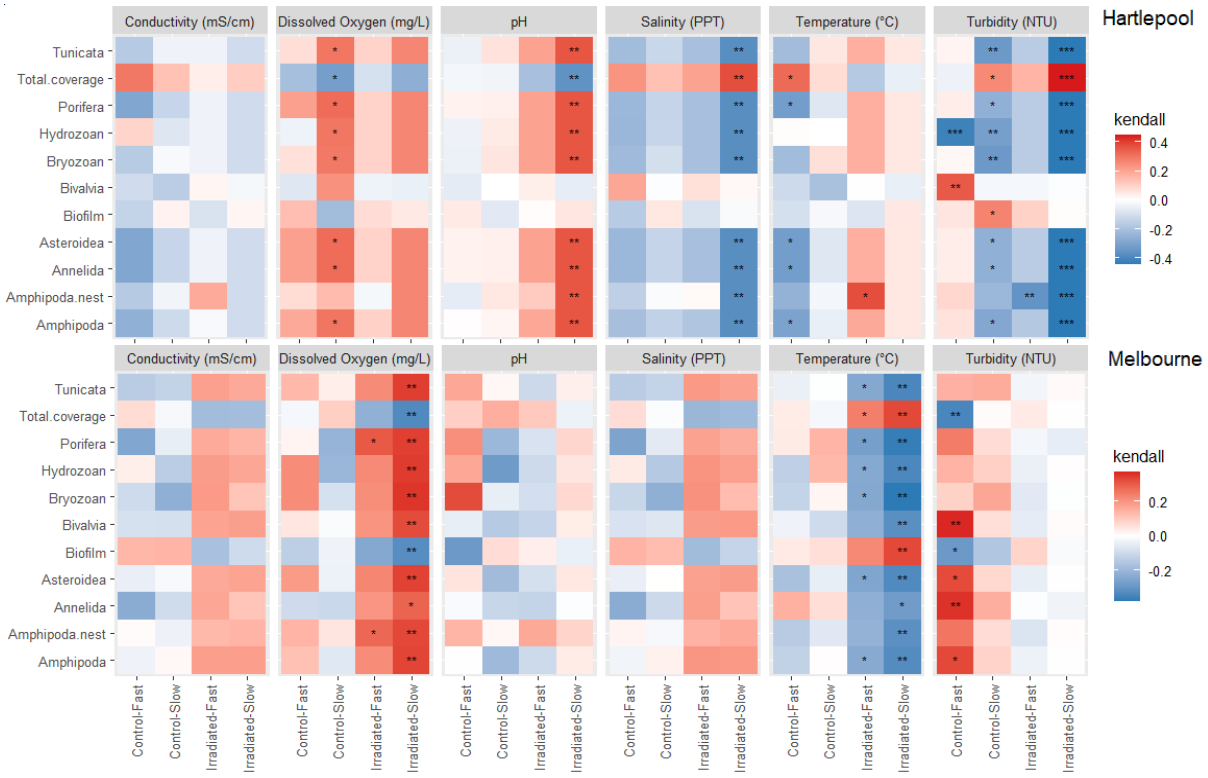

Figure 4.7. Positive and negative Kendall correlations between environmental conditions and taxa from four sampling conditions in Hartlepool and Melbourne. Red = Positive correlation, Blue = Negative correlation, statistically significant correlations indicated by * = $p < 0.05$, ** = $p < 0.01$, *** = $p < 0.001$.

chambers had a negative correlation with temperature. Melbourne irradiated slow chambers were strongly positively correlated with DO and taxa. Positive correlations were detected between control fast surface taxa and turbidity. The temperature was negatively correlated between fast and slow irradiated surfaces.

4.3.4 Metegenetic community analysis

Metagenetic 18s data produced a total of 8.5 million reads across all samples. After quality controls, chimaera detection and removal this was reduced to 4,775,605. A total of 61,972 operational taxonomic units (OTUs) were found and categorised within the 18S dataset. The sample mean was 13,013 counts with a range from 1-46,444 counts. Data were standardised by subsampling to the lowest count without sacrificing data, this was determined via rarefaction analysis to be 1,415 counts. Subsampling removed 13 samples below this threshold of which 7 were blank extractions. A total of 495,250 individual counts were left within 14,950 OTUs covering 76-99% of the community depending on the sample. There were 119 classes identified with over 90% of the abundance being represented by 10 classes (Figure 4.8). These enriched taxa were Eukaryota_unclassified, Bivalvia, Ascidiacea, Intramacronucleata, Diatomea, Arthropoda_unclassified, Dinophyceae, Maxillopoda, Scyphozoa, and Phaeophyceae, from

Figure 4.8. Proportional abundances of the top 31 Class identified using 18s rRNA metagenomic analysis. A). All data separated into experimental conditions over 12-months at Hartlepool, UK. B). All data separated into control and irradiated exposures over 12-months. Taxa not classifiable to Class level were labelled as the unclassified phylum.

most to least abundant respectively.

Eukaryotic community assemblages varied between irradiated and control exposures and displayed different community dynamics with various shifts over time (Figure 4.8). Control and irradiated samples were significantly different ($p < 0.05$) based on Adonis and Anosim PERMANOVA analysis (Figure 4.8.).

The seasonal community shifts in control chambers were different to those identified in irradiated chambers. Eukaryota_unclassified represented between 5-60% of the community but there was no difference between control and irradiated chambers (Figure 4.9).

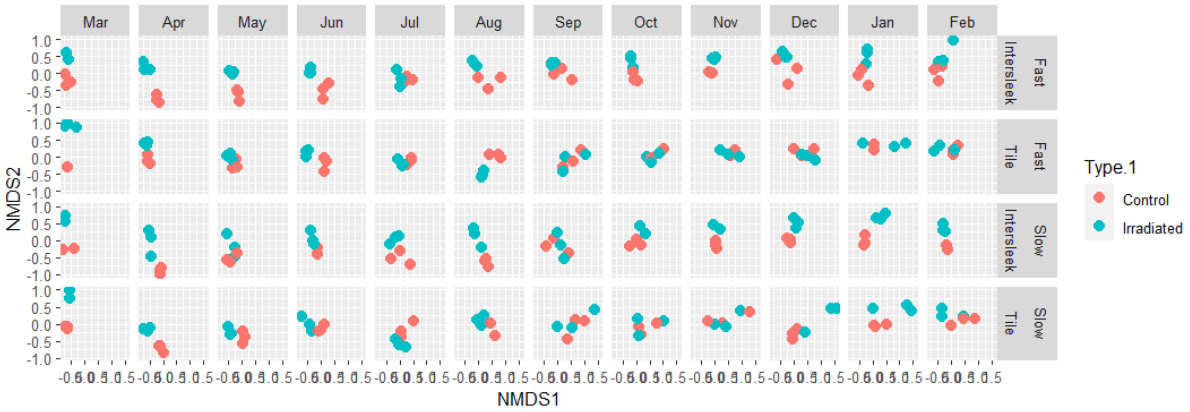

Figure 4.9. Bray Curtis dissimilarity index representing control and UV irradiated 18s eukaryotic communities. Non-metric multi-dimensional scale plot for each condition and surface over experimental duration. Points represent overall community assemblage, and distance between points symbolizes community disparity. The closer points are to one another the more similar their community assemblage is.

Arthropoda_unclassified and Maxillopoda had a higher proportional abundance in controls than in irradiated chambers. Bivalvia were detected in May in controls but not until July in irradiated chambers. Ascidiacea were detected in April in irradiated chambers but not until May/June in controls. Diatomea were more abundant in the irradiated chamber than in the control. Dinophycea and Tremellomycetes were only prominent in irradiated chambers.

Sobs, Chao and Ace diversity indices for all conditions indicated a rise in richness towards experimental completion. Initial richness suggested that irradiated samples were more diverse than controls, however, from October-February the controls had a higher richness. Water samples remained constant throughout and did not vary between control and irradiated exposures (Supplementary data 4.1).

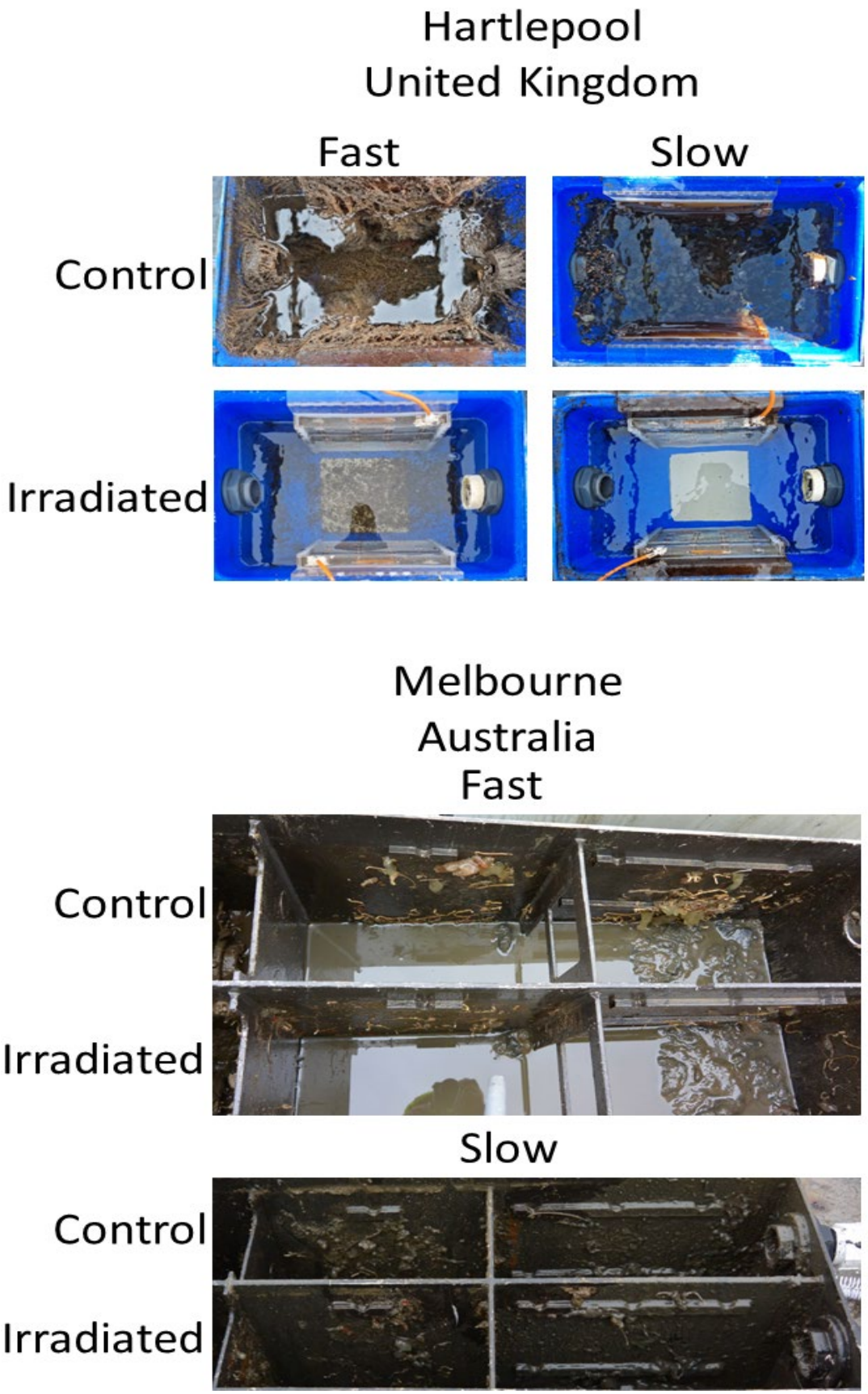

Figure 4.10. Biofouling in experimental chambers after deployment for 6-Months (UK) and 11 Months (Au).

4.4 Discussion

Field deployment across a broad range of conditions has shown the potential of UV irradiation to control biofouling across many taxa. Factors that can impact fouling recruitment were compared comprehensively under dynamic conditions, emulating those faced in the real world. Broad coverage of these factors is imperative for accurate projections of the effects of UV radiation on the fouling community.

4.4.1 Influence by environmental conditions

The use of UVC can have both direct and indirect effects on fouling communities. The direct effect is DNA damage, whereas indirect effects can alter water conditions which can have implications on larval settlement and the recruited population. The taxa that accumulate can affect environmental conditions, for example, hydroids can alter oxygen levels (Blöcher, 2013). Small changes in environmental conditions can influence the biofouling community composition (Rivero *et al*., 2013). Chemical availability, temperature, light levels and substrate texture are a few variables affecting biofilm and microbiota settlement and growth (Floerl *et al*., 2004; Mineur *et al*., 2012; Tait *et al*., 2016). By altering conditions, biofilm communities can be impacted, allowing a different range of taxa to accumulate (Lakretz *et al*., 2010, 2011; Whitworth *et al*., 2022). If UV alteration of water conditions were to occur due to UV inclusion, indirect effects could alter the successful colonising biota. Initial biofilm communities can be utilised by macrofoulers as an indicator of surface suitability (Railkin, 2003; Scheltema, 1974; Wieczorek & Todd, 1998). Although in the current study environmental conditions varied within the different chambers, no consistent change could be attributed to UV integration. Control and irradiated chambers maintained environmental readings relative to the source supply. It follows that the community changes detected were direct effects of the UV-LED exposure.

UV irradiance levels dropped substantially towards the end of the field experiments. Although all tiles showed falls in irradiance, not all LEDs degraded at the same rate. The suppliers predicted that irradiance levels would be reduced by half (L50) after 10,000 hours. The actual L50 observed was after 10-12 months or 7465-8880 hours. This discrepancy could explain the presence of fouling organisms on irradiated tiles in the final months of exposure. Nevertheless, biofouling was heavily reduced with a 40-90% variance compared to controls. The level of fouling on the irradiated tiles was proportional to the irradiance loss within specific chambers. Fast chambers experienced the largest UV reduction and the highest fouling, with the opposite observed for slow chambers. Extending the longevity of LEDs' life span is imperative to achieve continuous fouling control. Since the lifespan of light sources depends on the time the light is

powered on, optimising intermittent powering (on:off periods) for biofouling control is important to extend LED lifespans (Song *et al*., 2016, 2020). Duty cycling can be detrimental to traditional iridescent and halogen light sources (Tonzani, 2009), however, LEDs are not as susceptible. LED longevity can be extended via pulsing or irradiance output manipulation and still achieve effective fouling prevention (Hunsucker *et al*., 2019; Braga, 2018; Whitworth *et al*., 2022). Extended lifespans would have provided higher irradiance intensities towards the end of the project and may have prevented the taxa that were able to colonise towards the end of the project.

4.4.2 Imaging community analysis

Community assembly varied between irradiated and control exposures on the different surface types, chamber speeds and between geographical locations. Image analysis of the surface coverage allowed an insight into the most prevalent taxa. UV exposure can impact initial communities, and taxa resilient to UV will have a competitive advantage. The fouling that occurred on the surfaces in the slow chambers was mainly biofilm and soft fouling organisms, whereas the community in the fast chambers included hard macrofoulers. Based solely on percentage coverage, however, fast chambers had a similar level of fouling to slow chambers.

Although the slow chambers had similar surface coverage to the fast chambers, the communities identified were distinct. Initial community assemblages in fast chambers were composed of biofilms before shifting towards hydrozoans and then to bivalves, or back to biofilm depending on the surface. The conditioning layer and initial community composition can impact surface suitability for other organisms. This is a common transition within biofouling with initial biofilms forming before macrofouling dominance in terms of biomass (Bloecher *et al*., 2013). Surfaces may be slow to accumulate macrofoulers such as hydrozoans, bivalves and sponges due to the varying flow regime. Although surfaces under fast flow had similar percentage coverages to the corresponding surfaces in slow flow, the larger macrofouling organisms in the former would have a greater impact on drag. Image analysis only allowed a two-dimensional analysis of a three-dimensional community. Had biomass been measured, fast chambers would have far outweighed the slow chambers and may have allowed further insight into the factors affecting biofouling.

Community differences between fast and slow chambers may have been due to the nature of the flow. The organisms colonising the fast chambers were subjected to higher, more turbulent flows, which may select for strong adhesive traits at settlement and during growth. The flow difference of 140 L/min:14 L/min prompted fouling at an earlier stage in the fast chambers than in the slow chambers. Although the supply of potential recruits to the slow flow chambers

would have been lower, conditions may have favoured colonisation for some taxa. Larvae capable of attachment within fast-flow environments, often detach more frequently than organisms recruited in slower conditions (Mullineaux & Butman, 1991; Jonsson *et al*., 2004; Larsson & Jonsson, 2006). Faster flows create a more chaotic system which increases the number of turbulent eddies created and increases shear stress on organisms attempting to settle (Crimaldi *et al*., 2002; Eckman *et al*., 1990; Abelson & Denny, 1997). Increases in hydrodynamic stresses can negatively impact clam aggregation, for example, and rapid settlement methods are needed to adapt to turbulent conditions (Crimaldi *et al*., 2002). Additionally, rapid flow conditions can restrict larval exploration by some invertebrates (Walters *et al*., 1999; Pernet *et al*., 2003; Lindegarth *et al*., 2002). *Balanus amphitrite* larvae, however, have displayed a greater surface exploration within a flow than in still conditions (Walters *et al*., 1999). Higher flow can impact settlement, however the associated nutrient supply and increased biofouling pressure compared to slow chambers may have been a driver for the increased colonisation in the fast flow chambers. The greater macrofouling coverage in the fast flow chambers could also be associated with UV supply. UV irradiance in the fast flow chambers diminished more than that of the slow flow chambers, allowing more taxa to be recruited. If irradiance levels had remained comparable to the slow flow chambers, surfaces may have had similar communities and levels of fouling prevention. The communities in the controls also varied between fast and slow flow conditions suggesting that a combination of both factors were impacting community presence on the surfaces.

The colonisation of control and irradiated Intersleek® 1100SR surfaces was taxonomically different and surface coverage differences were apparent. Intersleek® 1100SR is a non-biocidal FR coating. FR coatings rely on shear forces to remove fouling organisms (Bus *et al*., 2020). The Intersleek® 1100SR surfaces remained free of hard macrofouling throughout the field exposure period and had a lower total fouling cover than the tile surfaces. This fouling mainly comprised biofilm. The low macrofouling cover on Intersleek® compared to tiles was anticipated for a commercial FR product. The Intersleek® surfaces were positioned at 12cm from the irradiation source. As UV was transmitted through water from the tile to the Intersleek® surface, photons would be absorbed and scattered by molecules and particles within the water (Sommer *et al*., 1997; Christensen & Linden, 2003). UV transmittance in turbidity of < 20 NTU is restricted to < 5cm (Figure 2.8.). However, the tile design incorporated minimal silicone height to achieve full surface coverage from the LED output and as LED output is in a cone, irradiance further from the surface would overlap. Irradiance overlap of multiple LEDs would be additive and provide higher irradiance outputs than the single LED source used in

section 2.3.2. The additive overlap likely accounts for the better than expected results given the transmission distance, and highlights the need to accurately determine irradiance transmission with distance from the source.

Environmental factors clearly affected the taxa present on the surfaces. Dissolved oxygen (DO), pH, salinity, temperature, and turbidity were all correlated, either negatively or positively, with certain taxa. In all conditions, biofilm and total coverage were linked, undergoing the same significant correlations. The biofilm/ total coverage correlations were inversely correlated to other correlations. The majority of the coverage being biofilm could explain this. As biofilm coverage reduced it was replaced by other fouling organisms creating an antagonistic correlation. The correlations between organisms and environmental conditions are not expected to be biofilm dependent but resulted from community transitions. The identified organism-environmental correlations other than biofilm/total coverage could be representative connections. Taxa coverage in the Hartlepool chambers with slow flow was negatively correlated with the turbidity of the water. More turbid waters contain higher dissolved organic matter (DOM), which is often used as a nutrient source for fouling organisms (Pierri *et al*., 2019; Trani *et al*., 2021; Charles *et al*., 1992). The higher presence of filter-feeding taxa such as bivalves, tunicates and tube worms would consume these nutrients and lower the DOM within the chambers. A positive correlation between pH and the number of taxa in the irradiated slow flow chamber may be an anomaly as these pH levels were taken with the faulty sensor. The false readings occurred after the sensor failed in August and coincided with peak growth. Negative correlations for salinity in the chambers could be attributed to the higher salinity upon setup. Salinity was highest in March 2021 when the tiles were introduced, and fouling pressure was comparatively low. The salinity in the marina varied substantially, which is likely attributable to precipitation and a partially closed system due to the loch gates. Fouling organisms in marinas are typically tolerant to changing conditions and can occupy locations with high salinity shifts (Morton, 1981; Nair *et al*., 1992; Mann & Harding, 2003; Astudillo *et al*., 2017; Lowe, 2002). At the start of the fouling season and towards the end of the field exposure, salinity was lower. Fouling coverage increased during the central portion of the field exposure and coincided with the salinity gradient.

In Melbourne, a negative correlation between the number of taxa and temperature was evident in irradiated chambers. Higher temperatures increase the metabolic rate of fouling organisms, which could leave them more susceptible to UV radiation leading to reduced survival (Lesser, 1997; Garcia-Corral *et al*., 2015; Icoglu Aksakal & Ciltas, 2018; Clarke & Fraser, 2004; Vernberg & Vernberg, 1972). A positive correlation in the Melbourne slow flow irradiated

chambers with taxa coverage could be due to denitrification. Microbial communities in low-flow environments can create increases in DO levels (Wang *et al*., 2018). High DO can impact EPS and membrane permeability and result in different microbial communities being present, which could, in turn, affect macrofouling (Skolimowski *et al*., 2010). Environmental conditions remained consistent between control and irradiated chambers demonstrating that UV was not altering the water conditions. Although community percentage coverages and environmental conditions were correlated (both +ve and -ve) in some chambers, this was not attributed to UV exposure, but to ecological water flow and different surfaces.

There were no hydrozoans, sponges or bryozoans on the irradiated surfaces, but bivalves were able to colonise from October 2021 to February 2022 at Hartlepool and polychaetes from September 2021 to March 2022 at Melbourne. Both periods were when the LED irradiance was waning with significant reductions across all LEDs. Biofouling increased gradually with the steady LED irradiance decline. The LEDs were in operation for 8880 hours and should have been able to retain 50% capacity for up to 10,000 hours. The observed L50 was considerably less than the manufacturer's claim. Fast flow chambers had the highest reductions in UV irradiance but were still sufficient to restrict fouling by 50-85% compared to controls for the tile and Intersleek® surfaces, respectively. Irradiance output was reduced more quickly in fast flow chambers compared to those in slow flow chambers which cannot be explained and requires investigation. LEDs were not exposed to the water and higher fouling would not impact the contained LEDs. Determining why the LED degradation was restricted to fast chambers needs to be investigated to ensure reliable irradiance can be supplied. Future Developments in LEDs may provide a solution.

One focus of this project was the protection of niche areas and presently surface type and chamber flow speed have been discussed. The chambers in which the experiments were conducted provided a degree of fouling prevention that was unexpected in the experimental design. The UV equipment was designed to have optimal coverage of only the tile surface and the structure of the chambers was not taken into consideration. The UV irradiance emitted, however, was scattered and transmitted within the chambers to achieve a near-fouling-free environment (Figure 4.10). Fouling was prevalent in areas shielded from UV exposure, such as behind the acrylic sheath containing the UV source and, in the supply and outflow pipe work. Acrylic and other compounds can absorb UV wavelengths at the LEDs output (Lowry *et al*., 2008) and these areas offered a sanctuary for organisms. Upon removal of the sheath, a defined area that matched the sheath shape was outlined. Investigating the effect of UV on pre-established biofouling would be an interesting advancement. The knowledge would be

beneficial in cases where the systems were required to be shut down for extended periods and fouling was allowed to accrue.

4.4.3 Metagenetic Amplicon Analysis

Unfortunately, due to time and computing constraints, Melbourne 16S and 18S and Hartlepool 16s data are still to be analysed. This restricted analysis to the 18s data from the Hartlepool site but provided insights that could be compared to the image analysis data. The metagenomic analysis provided an understanding of the community composition that was not detected from the imaging alone. Taxa were analysed to class level to allow associations with image analysis identifications. Distinct community compositions were detected, however, the 10 most abundant taxa comprised > 90% of the community. This represented the core community with a large overlap between conditions (Figures 4.8. & 4.9).

Unclassified eukaryotes were dominant at the class level; however, this was an accumulation of 9065 different unidentifiable OTUs. Unclassified eukaryotes represented > 60% of the OTUs subsampled and could not be aligned to a specific phylum or class. This is not ideal as the unidentified taxa may have been representatives of a key taxon. Underrepresented taxa may have had higher abundances and a greater impact on community assemblage variations. Updated 18s databases that improve taxa alignment are necessary to elucidate a deeper understanding of community dynamics. Nevertheless, the remaining enriched 18s taxa detected were similar to the taxa observed by image analysis. Irradiated surfaces had distinct community differences compared to the control surfaces over the duration of the experiment.

UV irradiation suppressed colonisation by some organisms, with the class ‘Bivalvia’ increasing in abundance two months later than under control conditions. Once established, abundance was similar to the controls, which contradicts the image analysis results. Bivalvia, a class of marine and freshwater molluscs, were most represented by the family Mytilidae. The Mytilidae are motile organisms that use filamentous secretions (byssus) as anchors to a surface and can use them for exploration of their environment (Seed & Richardson, 1999). The lack of Mytilidae in the image analysis suggests that they could not tolerate the UV exposure and sought a less detrimental location. Mytilidae were seen to colonise the back and side of the acrylic sheath holding the UV tiles in place. The acrylic sheaths provided a refuge from UV exposure and the Mytilidae presence here suggests suppression of macro fouling from the surfaces. The rise in abundance over the experimental period could be due to the UV shelters becoming overpopulated and increases in exploration for other habitable areas. Towards the end of the experiment, observation of the chambers revealed that the rise in bivalve coverage was from the periphery of the tile rather than in the tile centre. Byssal threads were visible on the

irradiated surfaces, which validates the genetic data regardless of organisms not being present. Changes in water chemistry may have also prevented mussel adhesive curing as the mechanism relies on redox conditions which may have been impacted by the constant UV irradiance (Waite, 2017). The detection on the irradiated surfaces is likely due to the remains of the byssus left over during habitat exploration.

Ascidiacea appeared two months earlier on irradiated surfaces than in the controls. This is the opposite of Bivalvia and potentially indicates the resilience of Ascidiacea to UV exposure. Ascidiacea are a subphylum of Tunicata that are filter feeders that can have algal symbionts for energy production. *Prochloron* sp is a symbiotic algal species of Ascidiacea that produce UV absorbing mycosporine-like amino acids (MAAs): mycosporine-glycine, palythine, shinorine, and porphyra-334 (Karentz, 2001). A broad range of Ascidiacea contain MAAs from their symbionts but are able to synthesise MAAs de novo (Shick *et al*., 2002; Hirose *et al*., 2004). Ascidiacea containing MAAs would be able to tolerate some level of irradiation and be more likely to colonise the substrate (Hirose *et al*., 2004). The initial absence in the control chambers could indicate that Ascidiacea were outcompeted by other taxa or required other taxa for settlement. More competitive organisms, found in controls, may have been suppressed in the UV chambers, whereas resilient species such as Ascidiacea were more prominent. Image analysis determined that Ascidiacea (Tunicata) were present from July only on the control surfaces. From February they were also identified on a single irradiated surface. The metagenomic analysis determined Ascidiacea presence at an earlier point than the image analysis and it occurred on all surfaces. Although Ascidiacea was detected on all surfaces with metagenetics, the absence of adults in image analysis alludes to UV impact. Ascidiacea larvae are highly diverse with some planktonic species developing a transparent tadpole morphology and others having non-motile morphologies that have lost the tail element (Swalla & Smith, 2008; Lemaire, 2011). Tunicata embryos are < 100µm in diameter and some larvacea are < 1mm in length (Gasparini & Ballarin, 2018). Microscopic, transparent larvae would be undetected during image analysis, explaining the differences between metagenetic and imaging methods. Larvae may have attempted to colonise the surfaces but the UV irradiance deterred their settlement by preventing metamorphosis or killing them.

Scyphozoa were found in both control and irradiated chambers periodically throughout field exposures. Scyphozoa are a class of the phylum Cnidaria that have a pelagic medusoid stage and can have a benthic polyp stage (Kingsford *et al*., 2000; Pitt & Kingsford, 2000). Cnidaria are also able to bioaccumulate MAAs as a protection against UV through the ingestion of algae (Klein *et al*., 2016; Carroll & Shick, 1996). The transparent planula larvae, which are generally

< 1.5 mm, may have attempted to colonise the surface and, similar to Ascidiacea, been undetected during image analysis (Isomura & Nishihira, 2001). Although Scyphozoa have indicated resilience and ability to survive under UV exposure, they were unable to thrive under continuous UV exposures (Klein *et al*., 2016). Continuous irradiance may have prevented planulae recruitment and affected their metamorphosis and growth into adult budding polyps.

A range of UV absorbing compounds are found in organisms such as bacteria, fungi, and algae (Shick & Dunlap, 2002; Hirose *et al*., 2004). Tremellomycetes are fungi known for their yeast states that can form hyphae, basidia, and basidiospores and are widespread through the marine environment as pathogens of marine mammals (Miller *et al*., 2002). Tremellomycetes were present in all irradiated samples at the start of the experiment and within the last 4 months, but not in any of the controls. Some species of Tremellomycetes can produce MAAs and some can produce UV absorbing mycosporine-glutamicol-glucoside (MGG) (Bellora *et al*., 2016; Chang *et al*., 2019; Sayed *et al*., 2020; Thomas, 2016). Tremellomycetes are found in the marine environment with yeasts rich in carotenoid pigments and are known to ferment sugars and can be a component of the biofilm (Jebaraj *et al*., 2012). Intramacronucleata were present on both control and irradiated surfaces throughout the experiment. Intramacronucleata is a subphylum of ciliates with some of the species capable of swimming freely and others being sessile components of biofilms (Lobban *et al*., 2007). Some ciliates can produce MAAs whilst others can form hypericin or hypericin-like pigments for protection against UVB damage (Buonanno *et al*., 2005; Miyake *et al*., 1990). Diatomea were found on all surfaces in both exposures but were more prominent in the irradiated chambers. Diatomea is a large group of microalgae that produce 20-25% of global primary production and are often dominant in biofilm formation (Ellegaard *et al*., 2016). Unique to this clade of marine algae is the silicate frustule that can reflect/absorb UV rays (Ellegaard *et al*., 2016).

These organisms were all constituents of the core community found within the experimental chambers. All of these microorganisms are associated in some form with UV resilience and can form biofilms (Dahms *et al*., 2004; Kirstein *et al*., 2018; Weber *et al*., 2009). They would constitute a portion of the biofilm category in image analysis, as microalgae and fungi are not identifiable without microscopic analysis. The higher presence of the varied microorganisms within the irradiated chambers is likely a combination of their UV absorbing compounds protecting them and the lack of adult filter feeders removing them from the environment. Control surfaces had high coverages of Bivalvia and Ascidiacea that feed on microalgae by filtering them from the surrounding water. Individual Mytilidae can filter water at a rate of > 700 ml/h which would only require 65 mytilids to filter the volume of water in the tanks(Pestana

et al., 2009). Counts were not taken of organisms during image analysis but there were more than this during the later stages of the experiment and sufficient to clear the water of planktonic organisms supplied to the slow flow chambers. The lack of suspension feeders and the ability to produce/accumulate UV absorbing compounds could explain the higher association of microalgae on UV-treated surfaces.

Maxillopoda is a diverse class of the phylum Arthropoda with jointed appendages and are small organisms with exoskeletons (Tiemeyer *et al*., 2009). Maxillopoda and Arthopoda_unclassified were present in all chambers throughout the experimentation according to metagenetic analysis. Image analysis assigned these as Amphipoda, as further identification was outside the scope of this study, and they only represented a small fraction of the community. The hard carapace that surrounds these organisms is composed of chitin, remicilin and other proteins that can block up to 80% of UVB (van den Broecke *et al*., 2012; Smith & Facts, 2019). These organisms are free-swimming but colonise surfaces by building nest structures (Barnard *et al*., 1988; Poore & Steinberg, 1999). The nests are in the form of tubes and are composed of benthic detritus, silt and silk, which some amphipods can produce (Barnard *et al*., 1991; Fernandez-Leborans *et al*., 2016). The nest protects amphipods inside from external predation; however, the nest bases are not enclosed, and UV can impact from underneath the tubes in the tile format used here. Nests would often become dislodged and leave a ring where they had once adhered. Higher abundances may have been identified in controls; however, the point of detection was when controls were dominated by Mytilidae, and they were outcompeted for surface access. High turnover and the free-swimming nature of these organisms could explain the higher presence in metagenetic analysis compared to imaging. Sampling of free-swimming arthropods from irradiated chambers could have enabled identification of CPD or 6-4 PP UV damage via enzyme-linked immunosorbent assays (ELISA). Further studies should consider the sampling of any free-swimming organisms as a non-target representative and analyse the UV damage incurred.

Metagenetics enabled taxa to be identified that were on the surfaces (or had been) but were undetectable through image analysis. Image analysis was only able to identify < 10% of the classes compared to metagenomic analysis. However, metagenomic data did not allow a reflective analysis of the total biomass present. Image analysis indicated a lower biomass coverage on irradiated surfaces compared to that of controls whereas metagenetics, by design, would represent these as equal. The combination of methods allowed clearer insight into the community dynamics that would have been provided by only one of these methods.

4.5 Conclusion

UV irradiance under field conditions prevented biofouling at two geographic locations. By integrating the tile system into the field, taxa that generate UV-resilient compounds were identified, however, they were not able to substantially colonise the surfaces. The reduced biomass on irradiated surfaces is positive for the potential of UV tile deployment as a biofouling control. UV exposure impacted the community composition and the time point at which some organisms were recruited. UV LEDs did not have indirect effects on environmental conditions as far as could be ascertained. Intersleek® 1100SR coated surfaces were not fouled at 12cm from the UV source, indicating an appropriate UV tile design and its transmission potential. Surface type, flow rate and geographical location all produced variations in community composition, however, UV exposure prevented these determined communities. A combination of image analysis and metagenetics was crucial to gain a more complete assessment of the nature of the biofouling. Suppression of biofouling growth was clear on all surfaces, but LED degradation allowed taxa to establish at the periphery of the surfaces towards the end of the experimental period. Improvements in LED performance and lifespan are required to achieve a long-term solution for niche area biofouling control.

Chapter 5. Ultraviolet-Induced Cyclobutane Pyrimidine Dimer Formation, Lesion Repair, and Mutagenesis of the Biofilm-Forming Diatom *Navicula incerta*.

5.1 Introduction

Diatoms are a main component of biofilms and are crucial to its development (Schultz *et al*., 2015; Dahms *et al*., 2004). Diatoms are single-celled, photosynthetic algae that contribute > 25% of global primary production (Lee *et al*., 2019; Zargiel *et al*., 2011; Hunsucker *et al*., 2014; Gómez-Ramírez *et al*., 2019). Centric diatoms are primarily planktonic, whereas pennate diatoms are benthic and attach to natural and artificial surfaces forming a biofilm (Cacabelos *et al*., 2020; Anil *et al*., 2006). When pennate diatoms contact a surface they glide across it (Wetherbee *et al*., 1998). If a surface is unsuitable they are able to detach, but if the surface is suitable they can initiate a secondary adhesion stage and produce proteins for long-term permanent adhesives (Cooksey & Wigglesworth-Cooksey, 1995; Hoagland *et al*., 1993; Anil *et al*., 2006). Adhered cells can then expend energy to reproduce, forming two new individuals from one parent frustule (Anil *et al*., 2006). As protein secretions for adhesion are energetically expensive (Wetherbee *et al*., 1998), exposing diatoms to unfavourable conditions such as ultraviolet light (UV) during initial adhesion can discourage secondary adhesion and restrict biofilm growth (Lebret *et al*., 2009).

UV is well-known for its ability to damage DNA. Direct UV exposure can result in lesion formation but secondary damage can occur when a chromophore is damaged in the presence of oxygen-creating reactive oxygen species (ROS) radicals (Sies & Stahl, 2004; Braga, 2018). Such radicals can cause breakages between nucleotide bases resulting in secondary lesion formation (Szeto *et al*., 2020). These lesions can be in the form of pyrimidine/purine photoproducts, single/double-strand breaks, apurine (AP)/ deamination sites or mispaired bases (Figure 5.1.) (Rastogi et al., 2010). The most common form of damage is when neighbouring pyrimidines bind together forming a cyclobutane pyrimidine dimer (CPD) or 6-4 photoproduct (6-4 PP) (de Tommasi *et al*., 2018; Cheigh *et al*., 2012). Lesions induce structural alteration of the DNA, which causes replication issues during transcription and DNA synthesis (Li *et al*., 2010) with negative effects on motility, photo-orientation, nutrient uptake, metabolic activity, enzyme production and ultimately cell apoptosis/death (Karentz *et al*., 1991; Jeffrey *et al*., 1999). The rate of lesion formation depends on the A/T content in an organism's DNA, and its UV tolerance.

An organism's tolerance to lesion formation is related to compounds within the cells and their repair mechanisms. Several mycosporine-like amino acids (MAAs), produced by a variety of

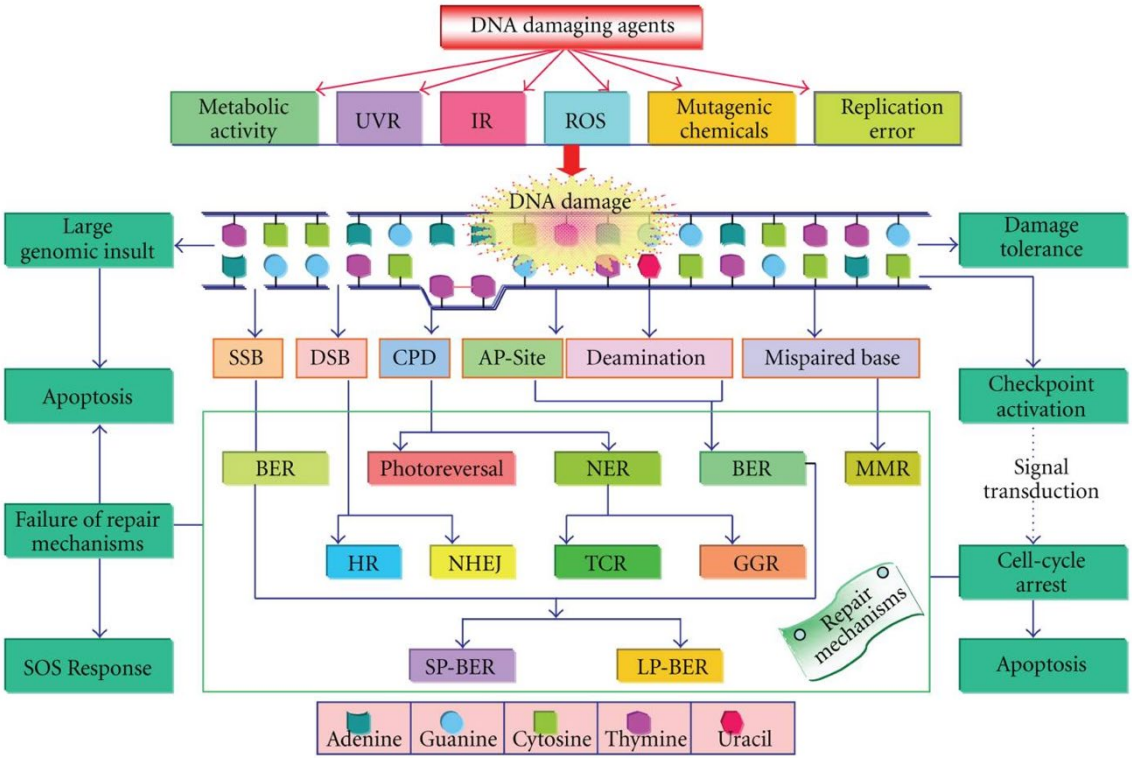

Figure 5.1. UV induced DNA damage, protection mechanisms and damage responses. UVR = ultraviolet radiation, IR = ionising radiation, ROS = reactive oxygen species, S/DSB = single/double strand break, CPD = cyclobutane pyrimidine dimer, AP = apurine, B/NER = base/nucleotide excision repair, MMR = mismatch repair, HR= homologous recombination, NHEJ = non-homologous end joining, TCR = transcription coupled repair, GGR = global genome repair, S/LP = short/long patch. After Rastogi *et al*. (2010).

diatoms, can absorb UV between 268 and 362nm (Ingalls *et al*., 2010). Putative genes for carotenoid biosynthesis identified in diatom genomes can protect from free radicals when accumulated in the cytoplasm (Bertrand, 2010; Bendich & Olson, 1989; Coesel *et al*., 2008). Both types of compound can absorb UV before it impacts DNA and reduce or negate any damage. Lesions that are still able to be produced can be restored by DNA repair mechanisms such as photoreactivation or excision repair (Zhang *et al*., 2017; Brych *et al*., 2016).

Photoreactivation uses photolyases, which are flavoproteins that can recognise and bind to DNA lesions (Brych *et al*., 2016). Photoactive light repair occurs when flavoproteins, such as the enzyme photolyase, bind with CPD lesions (Banaś *et al*., 2020). Photolyases utilise blue-green light ($\lambda = 300–500$nm) in a photoinduced cyclic electron transfer reaction (Britt, 1996) to cause photoreversal of the lesions to their normal undamaged form (Spampinato, 2017; Chinnapen & Sen, 2004; Kao *et al*., 2005; Sancar, 2003). In contrast, dark repair does not re-establish the lesions to the former state but removes one base (base excision repair, BER) or

excises an oligonucleotide at specific distances (5' and 3') from the damaged region (nucleotide excision repair, NER) (Schuch *et al*., 2017; Rastogi *et al*., 2010). Once a base lesion has been excised, exonucleases, a repair polymerase, and DNA ligase can restore the sequence. Endonucleases or lyases repair a range of DNA damage by cleaving out the damaged area and during this process, erroneous insertion of bases can occur (Mullenders *et al*., 1997). These nucleotide polymorphisms are mutations within the genome and can impact metabolic processes and ultimately the survival of the organism by altering protein functions and phenotypic changes.

The erroneous repair can produce variants in the form of single nucleotide polymorphisms (SNPs) (Mourya *et al*., 2022). SNPs occur when the genetic code of an organism is altered. If the DNA of an organism is mutated in this way, it can have unpredictable implications. SNPs can be formed by UV exposure via multiple routes. During photoreversal, nucleotides can be mis-repaired with a thymine (T)→ cytosine (C) transition and in rare cases TT→CC substitutions (Brash *et al*., 1991). This erroneous replacement of bases is a form of mutagenesis known as a UV signature (Ikehata & Ono, 2011). Cytosine is unstable in a CPD and often becomes deaminated to uracil (Burger *et al*., 2003; Peng & Shaw, 1996). CPDs containing uracil are the primary causative for UV-specific mutations as they can produce double-stranded breaks (Ikehata & Ono, 2011). Double-stranded breaks often lead to cell death, however, this is avoided via specialised translesion DNA synthesis (TLS) polymerases overcoming the replication block and restarting stalled DNA synthesis (Ikehata & Ono, 2011). DNA synthesis with TLS is error-prone and results in high rates of mutagenesis. Mutations can cause different responses which can be silent, missense, nonsense, frameshift or other mutations (Durland & Ahmadian-Moghadam, 2021). Genetic mutations are undesirable and understanding DNA damage, repair and mutagenic activity are of great importance.

This chapter investigated the magnitude of CPD formation in the model biofilm-producing diatom, *Navicula incerta*. The study evaluated the resilience and mutagenic implications of UV exposure by comparing different fluences of UV and analysing the effect on DNA. To achieve this, diatoms had CPD content assessed after variable UV fluences. Mutagenesis was analysed for the same exposures by de novo genome assembly and SNP mapping. Lesion repair was assessed by comparing the CPD abundance after initial exposure to abundances at different restorative intervals.

5.2 Methods

5.2.1 Experimental procedure

A 4x4 array of UV LEDs was embedded within a 350 x 350 x 18mm Lumisil® 903 silicone polymer tile (section 2.2.3). To form separate UV exposure compartments, single LEDs were isolated by affixing 62mm PVC pipes onto the surface of a Lumisil® 903 silicone tile directly over individual LEDs with opaque silicone sealant (Figure 5.2.). This allowed the UV light to

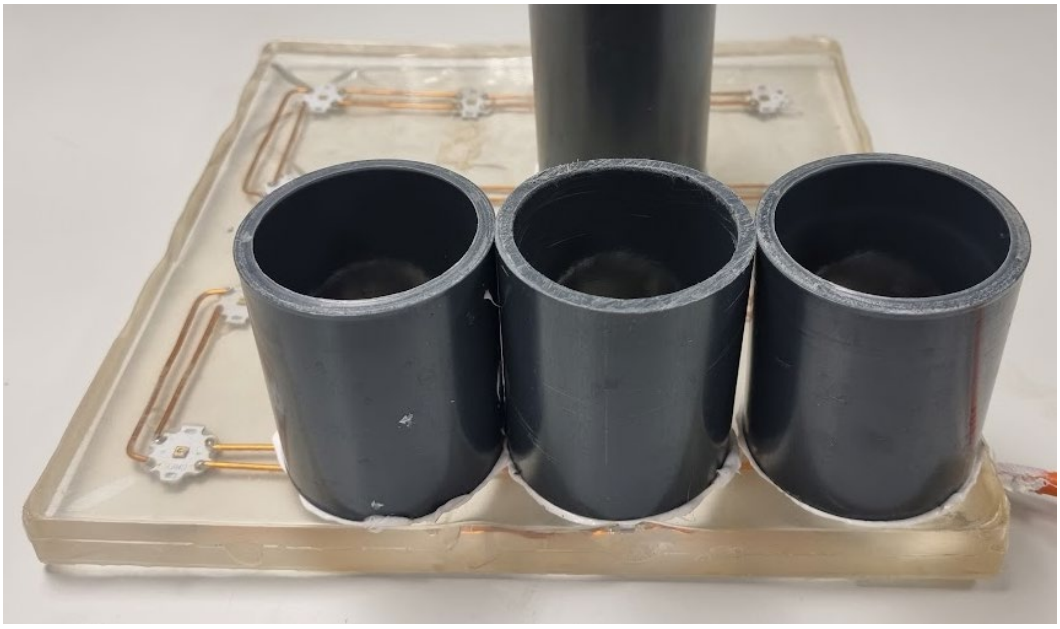

Figure 5.2. UV-emitting LEDs embedded in a Lumisil® 903 silicone polymer tile with three PVC pipes attached to create isolated experimental compartments.

be concentrated through the culture media and measured without influence from surrounding LEDs.

Diatom cultures were grown using the method described in section 3.2 and used on day 5 during their exponential growth phase. Diatoms were diluted to a cell density of 200,000/mm^2 and 25mL of the diluted culture was added to the PVC pipe. Irradiance was immediately initiated and a timer started. Exposures were conducted for 0 seconds (control), 30 seconds, 30 minutes, 60 minutes, 6 hours, 24 hours, and 48 hours. Irradiance readings were made using an SXL 55 radiometer on the surface of the tile before each experiment start and fluence was calculated over the exposure duration. After exposure, the culture was agitated using a sterilised sponge to resuspend adhered diatoms from the surface and 5mL aliquots were added to five 5mL clear Eppendorf tubes. One tube was immediately flash-frozen in liquid nitrogen and the remaining four were allowed repair intervals of 30 minutes, 60 minutes, 6 hours, and 24 hours under constant visible light, before being flash-frozen in liquid nitrogen and stored at -80ºC. Each exposure and repair interval was conducted in triplicate.

The frozen samples were thawed in batches of 24 for DNA extraction. Diatom suspensions were spun at 8000g, and the pellets were lysed with cell lysis buffer (0.5% SDS, 10 mM EDTA, 10 mM Tris HCl and a 100 mM NaCl) and 4µL of proteinase K, at 60ºC, in a Thermo mixer compact heat block for 45 minutes. DNA was extracted, cleaned and purified with phenol:chloroform:isoamyl alcohol (25:24:1) extractions and ethanol precipitation. All DNA was quality checked using 260:230nm and 260:280nm absorbance ratios using a NanoQuant microplate in a TECAN Spark plate reader and quantities were measured using a QUBIT fluorometer.

5.2.2 Mutation analysis

All exposure durations at time point zero of the repair intervals were analysed for mutagenic properties. This was achieved by creating a library and sequencing the DNA using an Illumina HiSeQ at 2x150bp at the Bristol Centre for Genomics. All fastq data files were checked for sequence quality before and after Illumina adapter trimming using Trimmomatic (version: 0.39). A de novo reference genome was produced from the unexposed diatoms using SPAdes (version: 3.13.0), which is a Python (version: 3.7.6) module. SPAdes was used at varying nucleotide substring lengths (Kmers) of 17, 41, 73, 93 and 123 to achieve the most complete genome assembly. Each scaffold and contig fasta file from each Kmer was analysed within QUAST (version: 5.0.2) to determine genome specifics (number of contigs formed, largest contig, total genome length, N50s, and GC content). All five genomes were evaluated for completeness using BUSCO (version: 5.1.2). The most complete genome was retained and advanced for variant mapping. Reads from each exposure duration were aligned to the de novo genome using Bowtie 2 (version: 2.4.2) to determine any variants in the form of single nucleotide polymorphisms (SNPs). Variants detected were then plotted using the ggplot2 package (version 3.3.6, (Wickham *et al*., 2016)) in R (version 4.2.0, (Bunn, 2013)) and compared to the zero exposure samples to determine any statistical significance.

5.2.3 CPD quantification

To quantify CPD formation, an OxiSelect™ UV-induced DNA damage ELISA combo kit (CPD / 6-4PP Quantitation) (Cat# STA-322-C) was used. DNA was diluted to 4 ng/µL and 50 µL of the diluted DNA was bound to the provided 96-well high DNA binding plate. The plate was incubated overnight at room temperature with the provided binding solution. After incubation, the remaining supernatant was removed, and the 96-well plate was cleaned with phosphate buffer saline (PBS) and assay diluent. The bound DNA was then probed using an anti-CPD antibody by incubating for 1 hour on an orbital shaker. All remaining primary antibody was then removed from the well plate and washed five times with the provided wash

buffer. A secondary antibody-HRP conjugate was added to bind to the primary antibody and incubated for 1 hour on an orbital shaker. Wells were emptied, washed and dried five times with the provided wash buffer. Fluorescence was initiated by the addition of an enzymatic substrate solution to each well and incubated on an orbital shaker for ~ 15 minutes until a clear colour change was visible. The enzyme reaction was stopped, once the colour had changed sufficiently, by the addition of the stop solution. The plate was then immediately measured for fluorescence using a Tecan SPARK plate reader at 450nm emission. Each assay consisted of a CPD standard, which was serially diluted to give concentrations of 100, 50, 25, 12.5, 6.25, 3.13, 1.56 and 0 ng/mL to create a calibration curve. Fluorescence values from the exposed samples were aligned to the calibration curve to quantify CPD formation.

All data were checked for normality and equal variance the subjected to relevant parametric or nonparametric testing to determine significant variation between variable groupings.

5.3 Results

5.3.1 CPD formation

Diatoms were exposed to an average irradiance of 70.62 $\mu W/cm^2$, which supplied fluences of 0.0021, 1.27, 2.54, 5.08, 15.25, 61.02, 122.04 J/cm^2 respectively for 30 seconds, 30 minutes, 60 minutes, 2 hours, 6 hours, 24 hours, and 48 hours. Diatoms had increasing CPD formation with longer exposure. A mean of 0, 0, 13, 54, 24 and 177 $\mu g/mL^{-1}$ of CPDs were found for 0, 30 seconds, 60 minutes, 2 hours, 6 hours, and 24 hours respectively (Figure 5.3A). However, the 30-min and 48-hour exposure samples, with no repair interval, did not provide sufficient DNA to standardise the volume required for the ELISA assay (50 µL at 4 ng/µL) and could not be quantified.

5.3.2 CPD repair

Repair intervals had various responses for the different exposures (Table 5.1). No CPDs were identified for the zero and 30-second exposures and their corresponding repair intervals. After 24-hour repair intervals, CPD abundances were 0, 0, 6, 11, 36, 43 and 75 ng/mL^{-1} for zero, 30 seconds, 30 minutes, 60 minutes, 2 hours, 6 hours 24 hours, and 48 hours of exposure, respectively. The corresponding recovery rates were 0, 0, 35, 92, 66, -80, 50, and 57% respectively. As no zero exposure CPD quantity was available for 30 minutes and 48 hours, the 30-min repair intervals were used for initial recovery rate comparisons. The 30-minute exposure had initial increases in CPD abundance for the 60-minute and 6-hour repair intervals but had

Table 5.1. Average cyclobutane pyrimidine dimers (CPDs) (N=3) and single nucleotide polymorphisms (SNPs) of *Navicula incerta* populations after UV treatment and repair.

Exposure	Repair interval	CPD (ng/ml)	% Loss	% Remaining	SNP content
No exposure	Zero	0.003726	0	100	17,242
	30 Minutes	0	100	0	
	60 Minutes	0	100	0	
	6 Hours	0	100	0	
	24 Hours	0	100	0	
30 Seconds	Zero	0	100	0	160,763
	30 Minutes	0	100	0	
	60 Minutes	0	100	0	
	6 Hours	0	100	0	
	24 Hours	0	100	0	
30 Minutes	Zero	NA	NA	NA	82,789
	30 Minutes	17.50038	0	100	
	60 Minutes	28.98256	-66	166	
	6 Hours	28.35133	-62	162	
	24 Hours	6.154676	65	35	
60 Minutes	Zero	12.93724	0	100	42,285
	30 Minutes	10.91943	16	84	
	60 Minutes	7.992694	38	62	
	6 Hours	3.704133	71	29	
	24 Hours	11.90612	8	92	
2 Hours	Zero	54.61267	0	100	18,168
	30 Minutes	51.57907	6	94	
	60 Minutes	34.67448	37	635	
	6 Hours	24.5193	55	45	
	24 Hours	36.58971	33	67	
6 Hours	Zero	24.42245	0	100	75,690
	30 Minutes	22.30614	9	91	
	60 Minutes	24.0068	2	98	
	6 Hours	43.08147	-76	176	
	24 Hours	43.99341	-80	180	
24 Hours	Zero	177.9056	0	100	15,258
	30 Minutes	175.2436	2	98	
	60 Minutes	163.6789	8	92	
	6 Hours	118.2665	34	66	
	24 Hours	90.31471	49	51	
48 Hours	Zero	NA	NA	NA	41,510
	30 Minutes	132.0508	0	100	
	60 Minutes	120.0896	9	91	
	6 Hours	151.8308	-15	115	
	24 Hours	75.90849	43	57	

its lowest CPD content after 24 hours. Both 60 minutes and 6 hours had positive correlations with repair interval and CPD abundance, the remaining exposures had neutral or strong negative correlations (Table 5.1 and Figure 5.2).

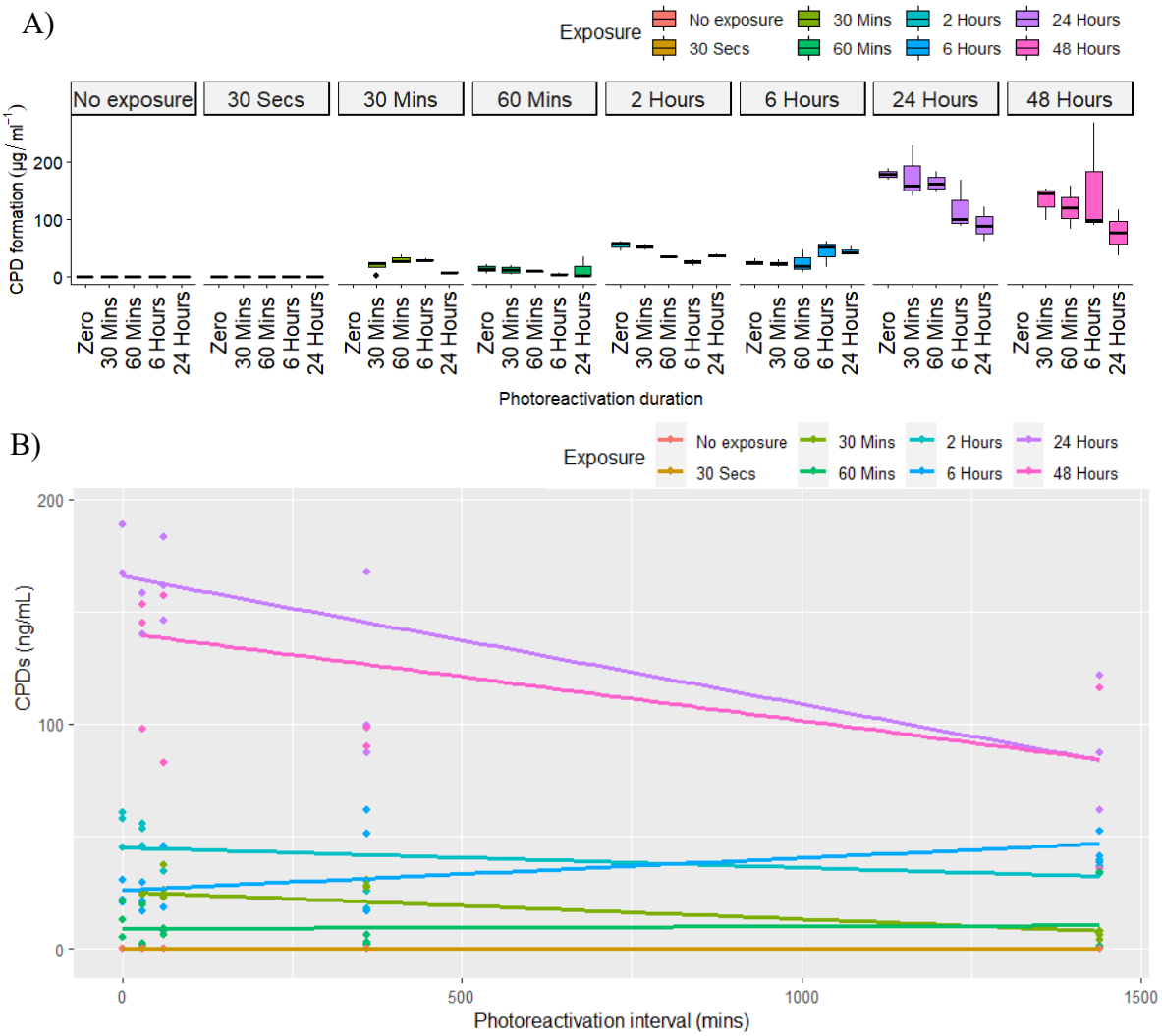

Figure 5.3. A). UV induced cyclobutane pyrimidine dimer concentrations, from *Navicula incerta,* over different exposure durations and repair intervals. B). Linear regressions of CPD concentrations for different exposure and repair periods.

Table 5.3. Regression statistics for CPD abundances during photoreactivation after eight different UV exposure periods. Coefficient indicates the correlation direction and intensity (positive number = positive correlation, negative number = negative correlation). Significance correlations displayed by . < 0.06, * < 0.05, ** < 0.01.

Exposure	Intercept	Coefficient	std.error	R^2	t statistic	p.value	Significance
No exposure	0.0014	0.0000	0.0000	0.04	-0.6256	0.5471	ns
30 Seconds	0.0000	0.0000	0.0000	NA	NA	NA	NA
30 Minutes	25.3169	-0.0120	0.0045	0.39	-2.6555	0.0224	*
60 Minutes	8.9668	0.0011	0.0048	<0.01	0.2187	0.8306	ns
2 Hours	45.0760	-0.0089	0.0061	0.16	-1.4525	0.1743	ns
6 Hours	26.1660	0.0143	0.0068	0.26	2.1148	0.0543	.
24 Hours	165.7825	-0.0569	0.0163	0.50	-3.4901	0.0045	**
48 Hours	140.6621	-0.0391	0.0371	0.12	-1.0548	0.0322	*

5.3.3 Genome assembly and Mutagenesis

De novo alignment of the reference genome comprised > 130 million nucleotides with a GC content of 45.86 %. Determining the quality of the de novo genome uses an assessment through benchmarking universal single-copy orthologs (BUSCO). The BUSCO package looks for complete BUSCOs (C), complete and single-copy BUSCOs (S), complete and duplicated BUSCOs (D), fragmented BUSCOs (F), missing BUSCOs (M), and total BUSCO groups searched (N). BUSCO scores for the various kmers (Table 5.3) determined K123 to be the most

Table 5.5. BUSCO assessment of different Kmers in genome assembly.

Kmer size	Complete and single-copy BUSCOs (C)	Complete and single-copy BUSCOs (S)	Complete and duplicated BUSCOs (D)	Fragmented BUSCOs (F)	Missing BUSCOs (M)	Total BUSCO groups searched (N)
K17	C:10%	S:0%,	D:0%,	F:5.3%,	M:85%,	N:100.
K41	C:83%	S:76%,	D:7.0%,	F:13%,	M:4%,	N:100.
K73	C:66%	S:52%,	D:14.0%,	F:17%,	M:17%,	N:100
K93	C:66%	S:47%,	D:19.0%,	F:16%,	M:18%,	N:100
K123	C:81.0%	S:34.0%,	D:47.0%,	F:11.0%,	M:8.0%,	N:100

complete genome and this was carried forward for SNP mapping. The selection was based on the high percentage (81%) of complete and single BUSCOs and higher duplicated BUSCOs than other Kmers. The genome contained a total of 49,115 contigs, the largest contig had 608,912 nucleotides and 5282 contigs were required to equal 50% of total nucleotides (N50). Sequencing data from the exposed DNA was mapped to the do novo genome to determine

mutagenesis. Nucleotide variants differing from the unexposed genome were assessed and averaged giving 17,242, 160,763, 82,789, 42,285, 18,168, 75,690, 15,258 and 41,510 variants, respectively, for exposures of zero, 30 seconds, 30 minutes, 60 minutes, 2 hours, 6 hours, 24 hours, and 48 hours (Figure 5.4 and Table 5.1).

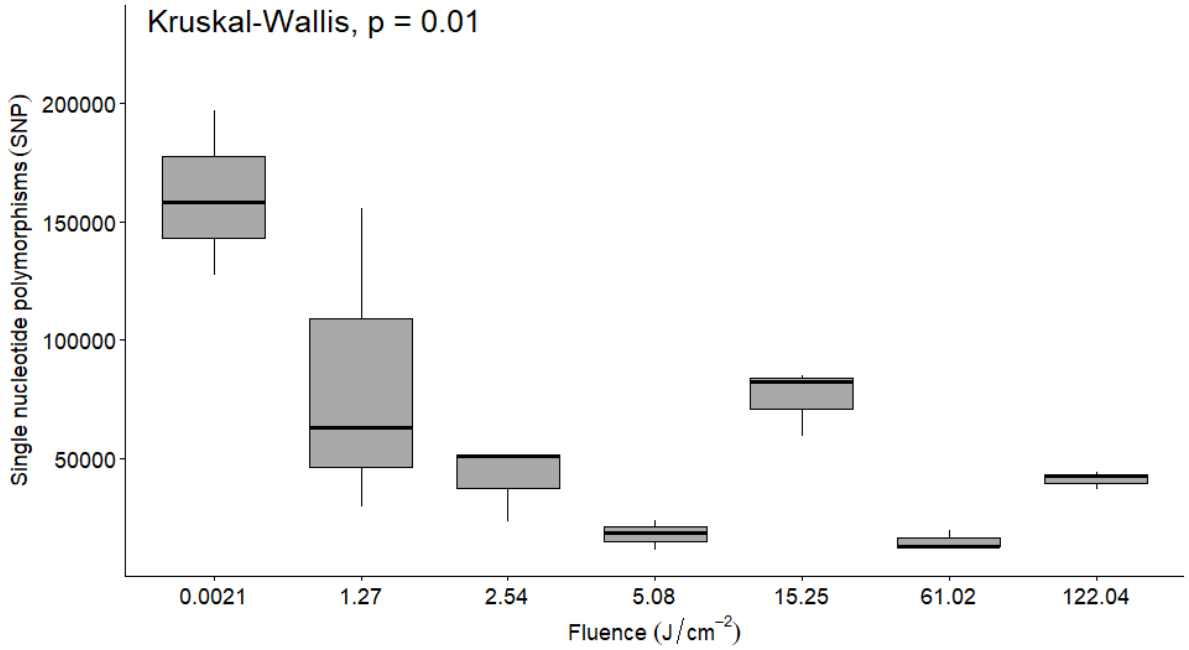

Figure 5.4. Mutation abundance at different UV fluences. Sequencing data from exposed samples mapped to de novo genome of control sequencing data from *Navicula incerta* to determine induced single nucleotide polymorphisms after different UV fluence exposures.

5.4 Discussion

5.4.1 CPD generation

When organisms are exposed to UV light, a 'contest' between UV damage and lesion repair commences (Schreier *et al*., 2009). Exposure to damaging UV rays that are over a harmful level causes CPD formation. Repair mechanisms can omit the damage if irradiance levels are below the repair rate. Prolonged exposure at elevated UV levels enables the accumulation of DNA damage to develop to a point where the cell cannot manage the damaged regions with wider biological implications (Buma *et al*., 2003). The current study found no CPD content for the lowest fluence of 0.0021 J/cm^2 but CPDs were detected at fluences of 1.27 J/cm^2 and above. This suggests a threshold for accumulative DNA damage in *N. incerta* to be between 0.0021 and 1.27 J/cm^2. Fluences over 1.27 J/cm^2 accumulated CPDs. The higher the fluence, the higher the CPD concentration. A more defined threshold could be determined between these fluences by the effect incremental fluence increases on CPD formation. At the lowest fluence, CPDs would have been forming as they can form within picoseconds (Li *et al*., 2010). Therefore, CPD

repair must have been restoring damage during exposure or in the short interval (< 1 minute) before being flash frozen.

5.4.2 CPD repair

After initial exposures, diatoms were allocated repair intervals where no UV was administered. This allowed a respite from the damaging rays and an opportunity for the diatoms to re-establish and repair. CPD repair was evident with reductions in abundances identified in low and high fluences. This demonstrates the resilience of diatoms to UV damage. Repair mechanisms may have been suppressed in 'high fluence-zero repair intervals. During longer repair intervals, the restorative mechanisms were able to activate and reduce CPD abundances. The highest fluences did not inactivate all diatoms as evidenced by CPD repair post-exposure.

Algae can induce metabolic processes such as oxidative stress responses upon inactivation but these are limited and would eventually halt (Darehshouri *et al*., 2008; Segev *et al*., 2016; Hong *et al*., 2008). Diatoms can enter a dormant state under unfavourable conditions where they minimise their metabolic activity but can become active again when conditions change (Ross & Hallock, 2019). *Odontella* spp. and *Grammatophora* spp. can remain dormant for up to 5 years and remain viable, while the dinoflagellate *Pentapharsodinium daleihave* remained dormant for up to a century (Anil *et al*., 2007; Ribeiro *et al*., 2011). However, the conditions under which *Odontella* spp. and *Grammatophora* spp. became dormant, were not damaging to the organism's genetic code. Environmental conditions (temperature shock, light and oxygen availability) can affect the duration of the dormancy period from which an organism can recover (Anil *et al*., 2006). Environmental conditions in the current study were nutrient rich providing optimum requirements for reactivation. Environmental conditions are highly dynamic, and extrapolating recovery rates and CPD damage to predict effects in field environments should be conducted with caution. To permanently inactivate *N. incerta*, UV exposure periods would have to be beyond the ones used here or would require continuous exposure.

Different organisms will have varying levels of response to similar UV exposures (Hannach & Sigleo, 1998). Marine cyanobacteria have displayed UVB (304nm) resistance with Bacilli more resistant than γ proteobacteria or Actinobacteria (Dzeha *et al*., 2019). *Sphingomonas* sp. strain *RB2256* displayed low CPD content after UVB exposures of 0.1 J/cm^2 indicating resistance, however, CPD abundance increased after a UVB exposure of 0.2 J/cm^2 (Joux *et al*., 1999). *Pseudomonas haloplanktis, Vibrio natriegens, Salmonella typhimurium* and *Deleya aquamarine* had ~ 400-700% more CPD content than *Sphingomonas* sp. after fluence of 0.1 J/cm^2 (Joux *et al*., 1999). This variation in organismal response is important to consider as other biofilm-forming diatoms may vary in UV resistance. Conducting a similar study on a variety

of different biofilm taxa or wild-type samples may identify different thresholds of CPD accumulation. CPDs are the most common damage induced and would be the major impacting factor, however, the development of other effects should be considered (Figure 5.1) (Rastogi *et al*., 2010). Damage and repair can be directly impacted by the UV intensity and visible light available for repair. Determining a fluence for long-term inactivation, in which *N. incerta* and similar biofilm-forming diatoms cannot recover, could prove beneficial in the prevention of biofilm formation.

The CPD repair results suggested that recovery rates were more rapid at higher UV exposures. Correlations predicted progressively increasing coefficients after higher fluences, indicating a faster level of repair (Table 5.2 and Figure 5.2). However, the 6-hour exposure treatment had a rise in CPD abundance over the repair intervals. This is unexpected as CPD formation has been recorded at ~ 1 picosecond after UV exposure (Schreier *et al*., 2007). Repair mechanisms should have reversed the lesions or excised them from the genome, lowering the CPD abundance. In most cases, CPD formation halts when irradiance stops. However, delayed CPD formation, termed dark CPD (dCPD), has been related to melanin concentration and currently has only been identified after UV exposure on the epidermis of humans and mice (Lawrence *et al*., 2022). Dark CPD formation has been associated with UVA chemiexcitation in melanocytes (Premi *et al*., 2015) and can occur for approximately three hours before CPD formation is offset by DNA repair (Yim *et al*., 2019; Premi *et al*., 2015). The lack of rising CPDs over repair intervals at the different exposures in the current study suggests that the 6-hour exposure may have been an anomaly. This could have been due to more DNA binding to the well plate and consequently more total CPDs present. Repetition of the experiment using a higher density of diatoms would allow a more accurate DNA quantitation and increases in replicate numbers, which could provide clearer insight into CPD abundances. The faster rate of repair detected in high fluences requires substantially more repair processes to be used. At high levels of UV exposure, both photoreactivation and excision repair pathways are required for the removal of lesions from the genome (Bray & West, 2005). Diatoms have several pathways to alleviate the damage caused by UV such as antioxidant systems, repair mechanisms, and the synthesis of MAAs, scytonemin, polyamines and carotenoids (Rastogi *et al*., 2020). Exposure to dangerous irradiances may have elicited a reaction in the diatom which recruited additional pathways to aid in defence against the high UV damage. The higher recovery enables protection from the high level of induced CPDs, however, lesion repair has been linked with other UV-induced damage such as mutagenesis (Ikenaga & Mabuchi, 1966).

5.4.3 Mutagenesis

Single nucleotide polymorphism mutations were detected in all samples including the zero exposure samples used to assemble the de novo genome. Mutation analysis was inversely related to CPD production with more mutations discovered at the lowest fluences. No CPD presence but high SNPs in the lowest fluences suggests that CPDs induced by the lowest fluence were fully repaired but a high rate of mutation occurred during CPD repair. A higher abundance of CPDs would require more repair, which allows more opportunity for mutations to occur. However, the highest CPD abundances were found in the highest fluences, which had the least mutagenesis. Mutagenesis requires the repair mechanisms to be actively restoring the lesions and incurring erroneous replacement of nucleotide bases (Durland & Ahmadian-Moghadam, 2021). The highest CPD formation and lowest SNP abundance in the 24-hour exposures suggest that CPDs were being formed but repair mechanisms may have been impeded by the UV damage. As with CPD abundance, a threshold for the inactivation of repair mechanisms can be inferred. At 0.0021 J/cm^2 recovery was high, as was mutagenesis. At 1.27 J/cm^2, mutations were still highly abundant, but a broad variation was seen indicating that repair by some diatoms was inhibited. At fluences of 2.54 J/cm^2 and above, the repair was minimal as SNP content was similar to the zero exposure SNP content. Low mutagenesis in the higher fluences could be due to metabolic suppression of the repair mechanisms. Blockage of transcription can impact processes needed for repair (Long *et al*., 2020; Berens & Molinier, 2020b). Wild carrot protoplasts have a suppression of excision repair at high fluences and repair mechanisms used are dependent on abundances of initial CPD formation (Howland, 1975). This suppression may prevent lesions from being reversed/cleaved and inhibit the mutagenic consequences.

SNP content was only determined for the zero repair interval samples from each exposure. Analysis of the individual ‘exposure repair interval’ samples for SNP content may have revealed higher mutagenic abundance, and this would be interesting to address in future studies. The increasing rate of repair with higher fluences utilises additional repair methods which allow greater opportunity for mutagenic impact. Comparing mutagenesis from recovery intervals may elucidate whether rapid or slow repair could be more erroneous. If rapid repair induced a heightened erroneous replacement of nucleotides over the ‘repair intervals' and cell arrest was minimal, then mutagenesis could have implications for protein synthesis/function (Durland & Ahmadian-Moghadam, 2021). Not all mutations are detrimental but organisms with these mutations could asexually reproduce and, as diatoms leave a complement of their genome in each of their two daughter cells (Mann, 1993), the mutations could be passed on to their progeny. Further study would benefit from analysing the ontogenetic transfer of mutations

vertically between generations to determine if UV-induced mutations from parents are transferred to offspring.

SNP detection was compared across the whole genome, but the affected genes were not determined. Annotating the genome identifies specific nucleotide sequences that have been characterised for specialized functions and labels them for that metabolic function (Bellora *et al*., 2016; Wang *et al*., 2019). Identifying locations with high SNP repetition in conjunction with the annotated genome can allow the determination of the regions most affected by UV exposure and highlight genes that are particularly susceptible to mutagenesis or UV damage (You *et al*., 2011). Identifying genes that are affected, such as those related to photolyase production or photosynthesis, would allow a greater understanding of the metabolic implications of UV exposure. Unfortunately, this was not explored within this project but may have allowed an insight into the negative correlation between repair and mutagenesis, which would be of interest in further studies.

5.5 Conclusion and future perspectives

The current study has investigated the impact of UV-induced CPD formation within *N. incerta*, as well as CPD repair rates over time and nucleotide mutation from varying fluences. UV-induced CPDs increased in abundance as fluences increased, however, mutations were inversely linked. A defined threshold of CPD formation is required for further determination of the UV level of effect, this includes the fluence required for permanent inhibition of *N. incerta* and other biofilm-forming taxa. Mutagenesis was more prominent at the lower fluences and progressively reduced with fluence increases. The metabolic regions of the genome that are heavily impacted by UV-induced mutagenesis were not explored but would be a target of interest for future studies. The vertical transfer of mutations between lineages should be investigated to determine whether the ontogenetic transfer of mutations impacts further generations. The examination of both CPD abundance and mutagenesis in combination suggested that repair mechanisms were inhibited at fluences > 2.54 J/cm^2 while UV was applied, which resulted in less mutagenesis. When UV irradiance was not administered during repair intervals, however, diatoms were able to re-engage their repair mechanisms and reduce CPD abundance. Overall, the findings of this study have given insight into the resilience of biofilm-forming diatoms to UV exposure.

Chapter 6. Antifouling Capabilities of an Ultraviolet Light Emitting Diode Embedded Silicone Tile System

6.1 Project Synthesis

The use of ultraviolet (UV) light is well established as an antimicrobial, with its use becoming more common in an expanding range of industries.(Song *et al*., 2016; Iervolino *et al*., 2020). Utilising the germicidal nature and implementing it within an aquatic environment is only achievable due to technological advancements. Since the first manufacture of UV LEDs in 2001, they have evolved exponentially in power, affordability and size, with promise of continual advancements (Muramoto *et al*., 2014). The development of UV LEDs indicates a versatility in light systems that can be incorporated into previously unconceptualized areas. The current study has explored one of these potential avenues that could revolutionise the marine antifouling industry and begin a new era of biofouling protection. Building upon past work (Piola *et al*., 2016; Zabihi *et al*., 2020; Bueley, 2014), UV as an antifoulant was developed into a system for effective delivery. The current study has shown that the integration of UV as an antifoulant has exceptional potential, with high rates of fouling prevention, on a broad assortment of biofouling organisms, which are brought together and discussed in this chapter.

Chapter 2 covered the development of a UV supply system in the form of a UV light-emitting diode (LED) embedded silicone polymer tile. The theory behind a tile design was to adhere the tile to a surface, and then the face of the tile would act as a secondary surface that was protected by the internal UV emitting components. Protection of the surface was the goal, rather than organisms in the water column. UV transmittance was measured for a single LED in Chapter 2 (Figure 2.2) and indicated that UV exposure should be below the reported effective antifouling level (REAL) when further than 5cm from the irradiance source. In Chapter 4, however, the Intersleek© 1100SR surface was 12cm from the UV emittance but a marked difference between irradiated and control was found. The ability to prevent fouling at this distance suggests that either the REAL is lower than currently reported or that the overlap of multiple LEDs may have had an additive effect giving a higher UV intensity. If the REAL is lower than predicted, then a further investigation, on wild-type fouling organisms, for thresholds of UV effect is required. For additive irradiance over distance, measurements at incremental distances from the tile's surface would be required to determine the output from the LED overlap. Either/both could be the causative and evaluating both would allow an understanding of how UV could impact non-target species in the surrounding water column. Depending on the situation in which the tile system was implemented, protection at a greater distance could be a positive or negative factor and must be considered before application.

Niche areas of ships such as sea chests, bow thrusters, inflow or outflow openings and internal seawater systems (Figure 1.4) could benefit from the extra transmission as they are enclosed systems that require protection of all regions within them. Niche areas covered in a system similar in design to that used herein, could not only prevent fouling accruing and causing blockages but also contribute to a wider area of impact. If vessels were fitted with a UV tile system during cruising to international locations, biofouling taxa that can be translocated within the niche areas may become inactivated preventing them from settling, reducing their retention and preventing their distribution. Non-indigenous species (NIS) can be detrimental towards an ecosystem, i.e invasive, and the control of their community can be difficult once they become established (Frey *et al*., 2014). Prevention of NIS using UV may not currently apply to all organisms due to the currently achievable output intensities. Chapter 5 found that *N. incerta* exposed to UV were able to reactivate during recovery intervals of < 24 hours. Additionally, the effective irradiance for UV prevention was identified in Chapter 2 to only transmit up to 14cm through the water depending on turbidity. If the target niche areas were fully encapsulated in UV tiles but the distance between tile surfaces was larger than 30cm or the turbidity was high, NIS could potentially find a refuge within and resist treatment. Tackling niche area biofouling with UV irradiance requires taking UV transmission and the size of the target area for protection into consideration to achieve optimum coverage. However, as technology improves and future UV LED intensities increase, treatment of larger more turbid areas may be achievable.

The LEDs used for UV supply required low energy to power them, however, the power demand would be sourced from the vessel or the equipment the system was applied to. Extra demand, even low requirement of power, on a vessel's equipment could be undesirable as it may raise costs through increased fuel consumption, extra pollution through increased emissions, and integration concerns if the hull required penetration for electrical access. Determining alternative power sources that do not impact the vessel and its equipment could make the prospect of UV integration more desirable. The ability to be powered by solar systems could be explored to determine its feasibility. The LEDs in the 4x4 tile (Chapter 2) had a demand of 6 volts and 0.018 amps, requiring ~ 0.1 wattage per LED for powering (1.73W total per tile). Most domestic solar voltaic systems have a 1-4 kW capacity per m^2 which would produce ~ 850-3400 kWh of electricity per year (Parida *et al*., 2011). This could power 24 tiles using 1 m^2 of solar panel at peak sun intensity. However, this would have high variability due to weather conditions, daylight hours, and power conversion efficiency. Solar-powered UV supply is already available for water purification systems and can provide clean water sources by

inactivating harmful bacteria (Salau *et al*., 2020). State-of-the-art solar power concentrating technologies are progressing beyond domestic conversion capacities which could improve efficiency and allow more electrical supply from smaller solar power surfaces (Islam *et al*., 2018). New technology cannot overcome weather and sun availability issues. If power failed and continuous supply failed, fouling would occur until repair was possible. Chapter 3 discussed how duty cycling can prevent fouling as long as the interval was not too long. Duty cycles were identified to prevent growth in all cycles trialled, but abundance reductions were only achieved for duty cycles of 2.5:17.5 mins and above. Analysing the powering capacities of photovoltaic systems on UV-emitting tiles is required to further explore this concept.

Equipment progression would not just benefit coverage and power supply but also deployment duration. In Chapter 4 the UV LEDs were used for a prolonged period of one year. All LEDs had a reduced irradiance intensity of > 50% within one year, whereas for others the irradiance reduction was < 10% of the original output. Protection for at least 3 years is required before vessels need their antifoulant of choice to be reapplied. For continual effective use of UV LEDs as an antifoulant, longevity of the system is key. Duty cycling was discussed in Chapter 3 for extending LED life. Intermittent exposure could allow an extended lifespan of light emitters; therefore, determination of effectiveness is required. However, duty cycling could have unknown effects over time. If organisms were to adhere and form a biofilm during LED down time, then perish on the surface when the LED was initiated, their cell structures such as silicate frustules may remain adhered to the surface (Gerdes *et al*., 1994). Silicate frustules have UV absorbing properties (de Tommasi *et al*., 2018) and if these remained adhered it could reduce the intensity being transmitted from the embedded light source. This could provide a progressively thickening layer and shield future fouling organisms over time. Some remains would decompose over time and shear forces in high hydrodynamic areas would remove fragments of the biofilm (Schultz *et al*., 2015) but in calm environments, the traces may impede the UV source. Chapter 3 evaluated duty cycling over 20 minute on:off cycles, duty cycle variations could be lengthened or shortened to obtain optimal delivery. Longer cycles may allow a denser biofilm to form during down time, whereas shorter cycles could prevent this layering and buildup of debris. Evaluating UV duty cycle treatment on different biofilm communities would allow an improved understanding as to whether or not a shielding layer could pile up or whether the remnants would be naturally cast off. The UV intensity used may also alter the effectiveness of each pulsing period.

The intensity of UV supply is the rate of irradiance provided and the fluence is the total irradiance supplied over a given time (Bueley *et al*., 2014; Keshavarzfathy *et al*., 2020). The

current study found in Chapter 3 that fluences of 0.01-0.82 J/cm^2 were required for the reduction of *Navicula incerta* growth and between 0.78-2.65 J/cm^2 was required for the reduction of diatoms below their input concentration. A lethal dose to achieve 90% removal (LD_{90}) was estimated to be 20-42 J/cm^2 depending on the method of UV exposure. Chapter 5 found that fluences between 0.0021-1.27 J/cm^2 would start to accumulate CPDs in *N. incerta* and fluences ≤1.27 J/cm^2 had high mutagenesis. Based on the lowest LD_{90} identified in Chapter 3, the system described in Chapter 5 would need to operate for 8 hours to remove 90% of the diatoms. However, the highest LD_{90} fluence would require 16.5 hours of exposure. This high variation was due to the method of delivery and puts into question the use of fluence as a measure. It is common in the literature to use fluence for determining the point at which UV affects an organism. This can be misleading as it describes the total irradiance that an organism is exposed to in seconds. A low intensity of 0.001 μW/cm^2 run for 2 years would provide a fluence of 63,080 μJ/cm^2 but the same fluence would be achieved with an intensity of 1 μW/cm^2 for 17.52 hrs. In the context of fluence, therefore, these treatments would be considered to enact similar responses. This is not representative when including interacting biological functions and, in certain circumstances, it would be more pertinent to discuss intensities rather than fluency. As DNA repair relies on biological functions, it is the intensity that would affect the damage rate and the organism's repair mechanisms. If an organism has a high rate of repair, a higher intensity would be required to outcompete the repair mechanisms and incur accumulative DNA damage. High irradiance intensity resistance has been identified for some bacteria, viruses and diatom species(Campana *et al*., 2008; Hargraves *et al*., 1993). High variation between the UV resistance of species and UV delivery methods having different inactivation responses, suggests that using fluence as a measure for inactivation is problematic. Using intensity instead of fluence may be more practical as the intensity can have weighted effects on an organism. If intensity levels are minimally elevated above the repair level and no accompanying adaption by an organism occurs, then there would be a slow accumulation of DNA damage. If a high intensity heavily outweighed the repair mechanism, it may cause faster DNA damage, inactivating the organisms more readily at a smaller overall fluence. If an intensity only slightly outweighed the repair mechanisms, the duration for inactivation would be sustained and be less efficient requiring a larger fluence. There would also be a balance in this as too high an intensity would reach a quantum yield, whereas all photons would not be absorbed and become surplus (Álvarez-Gómez *et al*., 2019). The hypothesized interaction for organisms' repair mechanisms is that there is a sigmoidal relationship between intensity and inactivation (Figure 6.1.). If the intensity is too low, repair mechanisms would be effective. After a threshold is reached the lesions produced would accumulate more rapidly with increasing intensity until an exponential

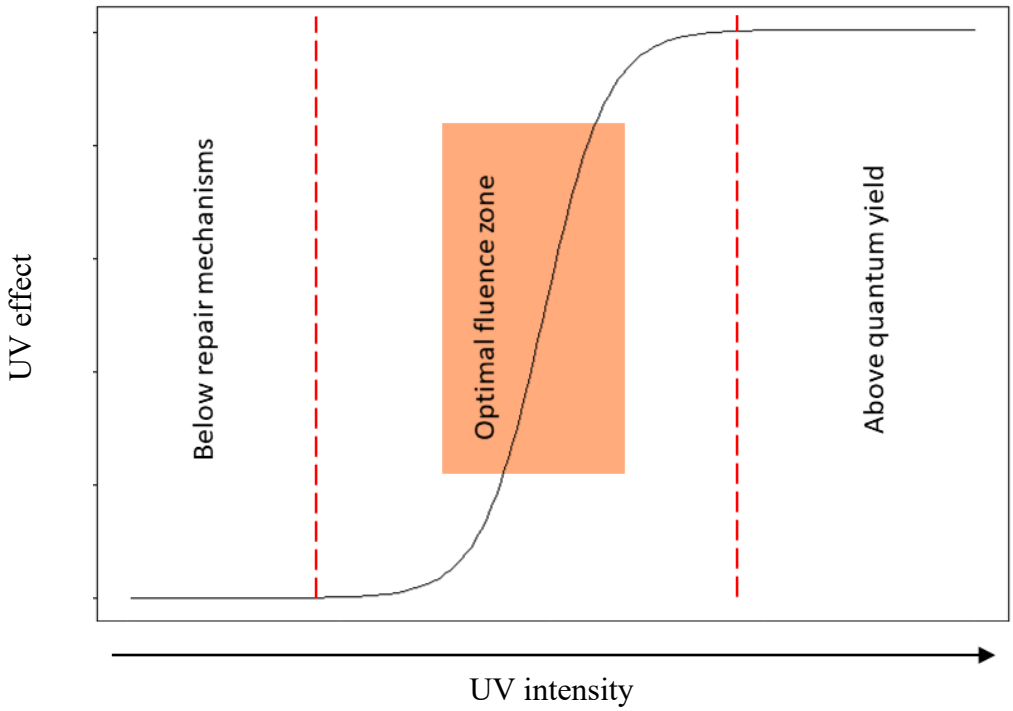

Figure 6.1. Proposed sigmoidal theory for UV induced inactivation of organisms with lesion repair mechanisms.

point was reached. Lesion would then begin to level off at an organism's photon absorption maximum (quantum yield). Going above this fluency would supply surplus irradiance, resulting in excess photons which would not affect the organism. The optimal inactivation intensity would be between these extremes. The sigmoidal curve for the reactions will shift for individual organisms based on the quantum yield and repair mechanisms in use. The effect of irradiance would be dependent on these factors and being overzealous with the irradiance intensity would only be detrimental to power consumption. If too low an irradiance power was provided, however, a specific species' threshold may sit above this irradiance, and it could prosper through a lack of competition. For *N. incerta* the threshold limit was explored in Chapters 3 and 5. This diatom may not be representative of other fouling organisms, however, or even wild *N. incerta*. Identifying this threshold for a single organism is achievable but when considering a range of organisms, all species would have to be analysed to determine the optimal intensity. Running intensity experiments on all biofouling species is not feasible as not all species can be cultured, not all species are known, and wild strains can often be more resilient to their cultured counterparts (Habeebu *et al*., 2000). A more achievable target would be to identify a communal intermediate area on a smaller range of organisms then identify any surviving organisms and adapt to the survivors until an optimal range was reached to inactivate most organisms. This is impractical in lab experiments, but field experimentation could allow a more concise evaluation of UVs impact on mixed wild communities.

A comprehensive field study was conducted in Chapter 4 which showed the effectiveness of UV within real-world circumstances over an extended period of 1 year. The taxa that were prevented from colonising surfaces ranged from tunicates to tube worms and this was achieved at two distinct geographical locations. The metagenetic analysis gave an insight into the microscopic biosphere that was undetectable in photographic analysis, indicating a need for mixed methods for thorough community assessment. Planktonic communities are the base of the food web and detrimental effects can cascade to higher trophic levels. These were not analysed in the current study and identifying implications on them should be determined in further studies. Identifying whether UV impacts the planktonic community is imperative for detecting if UV can impact organisms away from the surface as this may be desirable for locations, such as those downstream of sea chests.

6.2 Limitations and Future work

Throughout the current study, certain topics have been identified that require further investigation. Optimisation of LED longevity is required to allow a prolonged UV irradiance supply for maintaining biofouling prevention. By assessing irradiance emittance over time of newer LEDs and different treatment methods could enable longer lasting protection of surfaces. UV thresholds of effect were explored for *N.incerta*, but further investigation is required for other organisms as well as determining a threshold for biofilms consisting of wild mixed species. Exploring UV treatments over set durations on wild biofilm communities would be of great interest. Transmission of UV light through water at varying turbidity's was covered but identifying effect of the transmission potential of UV emittance on none target species needs further exploration. This could be conducted by sampling of organisms found in the water column near a UV source and assessing if DNA was impacted. The formation of CPD and SNPs were quantified alongside one another but exploring other lesions and exploring mutagenic implications on metabolic pathways is required. Assays are available and should be explored to quantify lesions e.g., 6-4PPs, and metabolic shifts. It would be valuable to examine long term damage to organism and to explore whether UV induced mutagenesis is transferred between lineages. By using an organism that has fast reproductivity such as *Daphnia sp*, adult organisms could be exposed and analysed, allowed to be reproduced and then offspring filtered and reanalysed. This could cover multiple generations and mutagenic transfer could be identified. Conducting studies into these suggested topics and other areas will improve and advance the future integration of UV as an antifoulant.

UV delivery and system modifications have been identified for future tile iterations. One limitation with this project was the thickness of the tiles used. Tiles were 18mm and 25mm

thick which would be costly, increase the weight and impact on buoyancy when applied. The LEDs used herein operated with the LEDs directing the UV irradiance upwards. LEDs on the market now are available to supply UV perpendicular to the source. This could allow UV to transmit through the tile horizontally and scatter up towards the surface, thereby covering a larger surface area than the supine format which had spot protection. The horizontal transmission would allow tiles to be thinner. Thinner tiles would reduce weight and cost of production and reduce buoyancy implications. Other technological advancements have been identified which can generate UV radiation from visible light. Through photonic crystal fibres incoming wavelengths are refracted and can be manipulated to a target wavelength (Palai *et al*., 2019). If the fibres could utilise natural sunlight and convert it to UVC this could enable fouling prevention that did not impede on equipment energy systems. Powering could also be done wirelessly by resonant inductive coupling which would obviate the need for penetrating the hull to supply power (Kuipers *et al*., 2015).

6.3 Novelty of the study

This project covered a range of aspects that were previously missing from literature or had not yet been explored. Studies have begun to explore the effect of UV on biofouling organisms, but that information has not been brought together to review what is known until now. This project brought together what is known of current UV technologies available and how it could be incorporated into a new industrial application.

The project introduced a novel approach to UV tile design. Including UV LEDs within a silicone polymer has been conducted before, but the LED layouts and silicone depths of the tiles within this study were unique. Incorporating the geometric distribution of the light emitted from LEDs to design and produce tiles ensured full surface coverage. Assessing the tile allowed the output power, temperature transfer and distance of transmission through water at varying turbidity's to be explored. These are invaluable findings that were previously unavailable and will be useful for further exploration of UVs use within the biofouling industry.

Biological implications of UV were explored to cover gaps within the literature. The UV levels used herein did not significantly impact upon the water chemistry which was an unexpected discovery. This is of great importance as indirect effects could be detrimental to implementation and render the system impractical. Determining thresholds in which UV effects on a model biofouling organism across different UV treatments has been explored within this thesis, which was previously lacking. The finding that delivery method impacts upon the survivability of an organism is newly discussed which contradicts some previous works. Assessing the production

of CPDs alongside mutagenic induced SNPs was explored for *N. incerta* for the first time within this project. Identifying the point at which this organism allows UV treatment of a biofilm to be finely tuned to prolong longevity of LEDs and improve on energy efficient biofouling control. The threshold for CPD/SNP formation and for metabolic inactivation was sorely lacking before now. Exploring this is an outstanding step towards further understanding the impact that UV could have on biofouling taxa.

6.4 Conclusion

Building upon conceptual efforts, this thesis has identified the scope for UV as an antifoulant. The use of UV for biofouling control is highly effective. Low energy required to power the system and long periods of reliable prevention would allow this technology to compete with current common antifouling methods. The extent of its use and current limitations have been mentioned with potential resolutions discussed to overcome constraints. Further work is required to optimise the methodology but even in its infancy, the prevention of a broad range of biofouling organisms was achieved for durations over 1 year. Adaptation and development of future designs are required and could allow UV integration as a widespread biofouling control method. The application of UV as an antifoulant is not limited to niche areas of marine vessels and could be designed and applied to meet desired targets for powerplant coolant intakes, submerged static artificial structures, aquaculture containment, oil rig platforms, scientific sensors etc. UV has shown to be highly effective in the prevention and reduction of marine biofouling and should be further implemented and become a common method of treatment within the antifouling industry.

References

Abelson, A. & Denny, M. (1997) 'Settlement of marine organisms in flow', *Annual Review of Ecology and Systematics*, pp. 317–339.

Ahmad, L., Khordehgah, N., Malinauskaite, J. & Jouhara, H. (2020) 'Recent advances and applications of solar photovoltaics and thermal technologies', *Energy*, 207p. 118254.

Alles, M. & Rosenhahn, A. (2015) 'Microfluidic detachment assay to probe the adhesion strength of diatoms', *Biofouling*, 31(5), pp. 469–480.

Almeida, E., Diamantino, T.C. & de Sousa, O. (2007) 'Marine paints: The particular case of antifouling paints', *Progress in Organic Coatings*, 59(1), pp. 2–20.

Álvarez-Gómez, F., Korbee, N. & Figueroa, F.L. (2019) 'Effects of UV radiation on photosynthesis, antioxidant Capacity and the accumulation of bioactive compounds in *Gracilariopsis longissima, Hydropuntia cornea* and *Halopithys incurva* (Rhodophyta)', *Journal of Phycology*, 55(6), pp. 1258–1273.

Alzieu, C. (2000) 'Impact of tributyltin on marine invertebrates', *Ecotoxicology*, 9(1), pp. 71–76.

Amaral-Zettler, L.A., Bauer, M., Berg-Lyons, D., Betley, J., Caporaso, J.G., Ducklow, W. & Walters, W.A. (2018) 'EMP 18S Illumina amplicon protocol', *Protocols. io*, pp. 1–8.

Ammon, U. von, Wood, S.A., Laroche, O., Zaiko, A., Tait, L., Lavery, S., Inglis, G.J. & Pochon, X. (2018) 'Combining morpho-taxonomy and metabarcoding enhances the detection of non-indigenous marine pests in biofouling communities', *Scientific Reports*, 8(1), pp. 1–11.

Ang, D.T.C. & Gan, S.N. (2012) 'Novel approach to convert non-self drying palm stearin alkyds into environmental friendly UV curable resins', *Progress in Organic Coatings*, 73(4), pp. 409–414.

Angelova, A.G., Ellis, G.A., Wijesekera, H.W. & Vora, G.J. (2019) 'Microbial composition and variability of natural marine planktonic and biofouling communities from the Bay of Bengal', *Frontiers in microbiology*, 10p. 2738.

Anil, A.C., Mitbavkar, S., D'Silva, M.S., Hegde, S., D'Costa, P.M., Meher, S.S. & Banerjee, D. (2007) 'Effect of ageing on survival of benthic diatom propagules', *Journal of Experimental Marine Biology and Ecology*, 343(1), pp. 37–43.

Anil, A.C., Patil, J.S., Mitbavkar, S., DeCosta, P.M., DeSilva, S., Hegde, S. & Naik, R. (2006) 'Role of diatoms in marine biofouling', *Recent Advances on Applied Aspects of Indian Marine Algae*, 1p. 351:365.

Anis, H.K., Curtis, G.L., Klika, A.K., Piuzzi, N.S., Otiso, J., Richter, S.S., Barsoum, W.K. & Higuera, C.A. (2020) 'In-room ultraviolet air filtration units reduce airborne particles during total joint arthroplasty', *Journal of Orthopaedic Research®*, 38(2), pp. 431–437.

Antelava, A., Constantinou, A., Bumajdad, A., Manos, G., Dewil, R. & Al-Salem, S.M. (2020) 'Identification of commercial oxo-biodegradable plastics: study of UV induced degradation in an effort to combat plastic waste accumulation', *Journal of Polymers and the Environment*, 28(9), pp. 2364–2376.

Astudillo, J.C., Bonebrake, T.C. & Leung, K.M.Y. (2017) 'The recently introduced bivalve *Xenostrobus securis* has higher thermal and salinity tolerance than the native *Brachidontes variabilis* and established *Mytilopsis sallei*', *Marine Pollution Bulletin*, 118(1–2), pp. 229–236.

Backer, L.C., Manassaram-Baptiste, D., LePrell, R. & Bolton, B. (2015) 'Cyanobacteria and algae blooms: review of health and environmental data from the harmful algal bloom-related illness surveillance system (HABISS) 2007–2011', *Toxins*, 7(4), pp. 1048–1064.

Banaś, A.K., Zgłobicki, P., Kowalska, E., Bażant, A., Dziga, D. & Strzałka, W. (2020) 'All you need is light. Photorepair of uv-induced pyrimidine dimers', *Genes*, 11(11), pp. 1–17.

Bannister, J., Sievers, M., Bush, F. & Bloecher, N. (2019) 'Biofouling in marine aquaculture: a review of recent research and developments', *Biofouling*, 35(6), pp. 631–648.

Barnard, J.L., Sandved, K. & Thomas, J.D. (1991) 'Tube-building behavior in *Grandidierella*, and two species of *Cerapus*', *Hydrobiologia*, 223(1)pp. 239–254.

Barnard, J.L., Thomas, J.D. & Sandved, K.B. (1988) 'Behavior of gammaridean Amphipoda: Corophium, *Grandidierella, Podocerus*, and *Gibberosus* (American Megaluropus) in Florida', *Crustaceana. Supplement*, pp. 234–244.

Barrado-Moreno, M.M., Beltrán-Heredia, J. & Martín-Gallardo, J. (2017) 'Degradation of microalgae from freshwater by UV radiation', *Journal of Industrial and Engineering Chemistry*, 48pp. 1–4.

Baum, B. & Deanin, R.D. (1973) 'Controlled UV degradation in plastics', *Polymer-Plastics Technology and Engineering*, (2(1)), p. 1:28.

Beall, G.H. & Duke, D.A. (1969) 'Transparent glass-ceramics', *Journal of Materials Science*, 4(4), pp. 340–352.

Beck, S.E., Wright, H.B., Hargy, T.M., Larason, T.C. & Linden, K.G. (2015) 'Action spectra for validation of pathogen disinfection in medium-pressure ultraviolet (UV) systems', *Water Research*, 70pp. 27–37.

Bellora, N., Moliné, M., David-Palma, M., Coelho, M.A., Hittinger, C.T., Sampaio, J.P., Gonçalves, P. & Libkind, D. (2016) 'Comparative genomics provides new insights into the diversity, physiology, and sexuality of the only industrially exploited tremellomycete: *Phaffia rhodozyma*', *BMC Genomics*, 17(1), pp. 1–16.

Beltrán, F.J., González, M. & González, J.F. (1997) 'Industrial wastewater advanced oxidation. Part 1. UV radiation in the presence and absence of hydrogen peroxide', *Water Research*, 31(10), pp. 2405–2414.

Bendich, A. & Olson, J.A. (1989) 'Biological actions of carotenoids', *Journal of Nutrition*, 119(3)(8), pp. 94–95.

Berens, P.J.T. & Molinier, J. (2020a) 'Formation and recognition of uv-induced dna damage within genome complexity', *International Journal of Molecular Sciences*, 21(18), pp. 1–23.

Berens, P.J.T. & Molinier, J. (2020b) 'Formation and recognition of uv-induced DNA damage within genome complexity', *International Journal of Molecular Sciences*, 21(18), pp. 1–23.

Bertrand, M. (2010) 'Carotenoid biosynthesis in diatoms', *Photosynthesis research*, 106(1), pp. 89–102.

Bintsis, T., Litopoulou-Tzanetaki, E. & Robinson, R.K. (2000) 'Existing and potential applications of ultraviolet light in the food industry - A critical review', *Journal of the Science of Food and Agriculture*, 80(6), pp. 637–645.

Blöcher, N. (2013) 'Biofouling in the Norwegian salmon farming industry', *Retrieved from http://www.diva-portal.org/smash/get/diva2:668287/FULLTEXT02.pdf*,

Bloecher, N., Olsen, Y. & Guenther, J. (2013) 'Variability of biofouling communities on fish cage nets: A 1-year field study at a Norwegian salmon farm', *Aquaculture*, 416–417pp. 302–309.

Boddy, P.J., Delaney, R.H., Lahti, J.N., Landry, E.F. & Restrick, R.C. (1976) 'Accelerated life testing of flexible printed circuits', *14th International Reliability Physics Symposium*, pp. 108–117.

Bolto, B.A. (1990) 'Magnetic particle technology for wastewater treatment', *Waste management*, 10(1), pp. 11–21.

Bonhivers, M., Carbrey, J.M., Gould, S.J. & Agre, P. (1998) 'Aquaporins in *Saccharomyces*: genetic and functional distinctions between laboratory and wild-type strains', *Journal of Biological Chemistry*, 273(42), pp. 27565–27572.

Bonner, T.H. (2000) *Life history and reproductive ecology of the Arkansas River shiner and peppered chub in the Canadian River, Texas and New Mexico*. Texas Tech University.

Bosselmann, K. (1996) *Environmental law and tributyltin in the environment In: de More ST (ed) Tributyltin: Case Study of an Environmenal Contaminant. Cambridge Environmental Chemistry Series 8*.

Bothwell, M.L., Sherbot, D., Roberge, A.C. & Daley, R.J. (1993) 'Influence of natural ultraviolet radiation on lotic periphytic diatom community growth, biomass accrual, and species composition: short-term versus long-term effects 1, 2', *Journal of Phycology*, 29(1), pp. 24–35.

Bourget, C.M. (2008) 'An introduction to light-emitting diodes', *Hortscience*, 43(7), pp. 1944–1946.

Brady Jr, R.F. & Singer, I.L. (2000) 'Mechanical factors favoring release from fouling release coatings', *Biofouling*, 15(1–3), pp. 73–81.

Braga, C.R. (2018) 'Lighting a path to biofouling prevention: investigating the effect of ultraviolet light on biofouling', *Photosynthetica*, 2(1), pp. 1–13.

Brash, D.E., Rudolph, J.A., Simon, J.A., Lin, A., McKenna, G.J., Baden, H.P., Halperin, A.J. & Ponten, J. (1991) 'A role for sunlight in skin cancer: UV-induced p53 mutations in squamous cell carcinoma.', *Proceedings of the National Academy of Sciences*, 88(22), pp. 10124–10128.

Braslavsky, S.E. (2007) 'Glossary of terms used in photochemistry 3rd edition: (IUPAC Recommendations 2006)', *Pure and Applied Chemistry*, 79(3), pp. 293–465.

Bray, C.M. & West, C.E. (2005) 'DNA repair mechanisms in plants: crucial sensors and

effectors for the maintenance of genome integrity', *New phytologist*, 168(3), pp. 511–528.

Britt, A.B. (1996) 'DNA damage and repair in plants', *Annual review of plant biology*, 47(1), pp. 75–100.

van den Broecke, L., Martens, K., Pieri, V. & Schön, I. (2012) 'Ostracod valves as efficient UV protection', *Journal of Limnology*, 71(1), pp. 119–124.

Brych, A., Mascarenhas, J., Jaeger, E., Charkiewicz, E., Pokorny, R., Bölker, M., Doehlemann, G. & Batschauer, A. (2016) 'White collar 1-induced photolyase expression contributes to UV-tolerance of *Ustilago maydis*', *Microbiologyopen*, 5(2), pp. 224–243.

Bueley, C. (2014) 'By : Chris Bueley , AML Oceanographic AML Oceanographic has developed a novel UV-based antifouling technology for use on virtually any submerged surface . The performance of the system in reducing fouling- induced measurement error on in-situ conductivity', *Ocean News & Technology*, pp. 10–12.

Bueley, C. (2016) 'UV irradiation: A new kind of antifoulant', *Ocean News and Technology.*, (Retrieved from https://www.oceannews.com/featured-stories/february-uv-irradiation-a-new-kind-of-antifoulant), .

Bueley, C., Olender, D. & Brocking, B. (2014) 'The (in) fluence of light', *Journal of Ocean Technology*, 9(4), pp. 48–67.

Bugbee, B. (2017) *Economics of LED lighting. In Light Emitting Diodes for agriculture: smart lighting*, in S Dutta Gupta (ed.) [Online]. Singapore: Springer Singapore. pp. 81–99.

Bukhari, Z., Hargy, T.M., Bolton, J.R., Dussert, B. & Clancy, J.L. (1999) 'Medium-pressure UV for oocyst inactivation', *Journal-American Water Works Association*, 91(3), pp. 86–94.

Buma, A.G.J., Boelen, P. & Jeffrey, W.H. (2003) 'UVR-induced DNA damage in aquatic organisms', *UV effects in aquatic organisms and ecosystems*, 1pp. 289–327.

Buma, A.G.J., Engelen, A.H. & Gieskes, W.W.C. (1997) 'Wavelength-dependent induction of thymine dimers and growth rate reduction in the marine diatom *Cyclotella sp*. exposed to ultraviolet radiation', *Marine Ecology Progress Series*, 153(1–3), pp. 91–97.

Bunn, A.M. (2013) 'R: A language and environment for statistical computing', *R Foundation for Statistical Computing*, 10(1), pp. 11–18.

Bunsen, R.W. & Roscoe, H.E. (1863) 'III. Photochemical researches.—Part V. On the

measurement of the chemical action of direct and diffuse sunlight', *Proceedings of the Royal Society of London*, (12), pp. 306–312.

Buonanno, F., Saltalamacchia, P. & Miyake, A. (2005) 'Defence function of pigmentocysts in the karyorelictid ciliate *Loxodes striatus*', *European Journal of Protistology*, 41(2), pp. 151–158.

Buonanno, M., Ponnaiya, B., Welch, D., Stanislauskas, M., Randers-Pehrson, G., Smilenov, L., Lowy, F.D., Owens, D.M. & Brenner, D.J. (2017) 'Germicidal efficacy and mammalian skin safety of 222-nm UV light', *Radiation research*, 187(4), pp. 493–501.

Buonanno, M., Randers-Pehrson, G., Bigelow, A.W., Trivedi, S., Lowy, F.D., Spotnitz, H.M., Hammer, S.M. & Brenner, D.J. (2013) '207-nm UV light-a promising tool for safe low-cost reduction of surgical site infections. I: in vitro studies', *PloS one*, 8(10), p. e76968.

Buonanno, M., Welch, D., Shuryak, I. & Brenner, D. (2020) 'Far-UVC light efficiently and safely inactivates airborne human coronaviruses', *Science Reports*, (10.1), pp. 1–8.

Burger, A., Fix, D., Liu, H., Hays, J. & Bockrath, R. (2003) 'In vivo deamination of cytosine-containing cyclobutane pyrimidine dimers in *E. coli*: a feasible part of UV-mutagenesis', *Mutation Research/Fundamental and Molecular Mechanisms of Mutagenesis*, 522(1–2), pp. 145–156.

Burke, R.D. (1986) 'Pheromones and the gregarious settlement of marine invertebrate larvae', *Bulletin of marine science*, 39(2), pp. 323–331.

Bus, T., Dale, M.L., Reynolds, K.J. & Bastiaansen, C.W.M. (2020) 'Thermoplastic, rubber-like marine antifouling coatings with micro-structures via mechanical embossing', *Biofouling*, 36(2), pp. 138–145.

Cacabelos, E., Ramalhosa, P., Canning-Clode, J., Troncoso, J.S., Olabarria, C., Delgado, C., Dobretsov, S. & Gestoso, I. (2020) 'The role of biofilms developed under different anthropogenic pressure on recruitment of macro-invertebrates', *International Journal of Molecular Sciences*, 21(6), pp. 1–28.

Callow, J.A. & Callow, M.E. (2011) 'Trends in the development of environmentally friendly fouling-resistant marine coatings', *Nature Communications*, 2(1), pp. 210–244.

Callow, M.E. (1993) 'A review of fouling in freshwaters', *Biofouling*, 7(4), pp. 313–327.

Callow, M.E. & Callow, J.A. (2002) 'Mariṅe biofouling: A sticky problem', *Biologist*, 49(1),

pp. 10–14.

Campana, G., Quartino, M.L., Yousif, A. & Wulff, A. (2008) 'Impacts of UV radiation and grazing on the structure of a subtidal benthic diatom assemblage in Antarctica', *Ber. Polarforsch. Meeresforsch*, 571pp. 302–310.

Capetillo, C. & Jesus, A. (2015) *Computational fluid dynamic modeling of in-duct UV air sterilisation systems.* [Online]. University of Leeds.

Caporaso, J.G., Ackermann, G., Apprill, A., Bauer, M., Berg-Lyons, D., Betley, J., Fierer, N., Fraser, L., Fuhrman, J.A. & Gilbert, J.A. (2018) 'EMP 16S Illumina amplicon protocol', *See http://www. earthmicrobiome. org/protocols-and-standards/16s*,

Carrasco, F., Pages, P., Pascual, S. & Colom, X. (2001) 'Artificial aging of high-density polyethylene by ultraviolet irradiation', *European polymer journal*, 37(7), pp. 1457–1464.

Carroll, A.K. & Shick, J.M. (1996) 'Dietary accumulation of UV-absorbing mycosporine-like amino acids (MAAs) by the green sea urchin (*Strongylocentrotus droebachiensis*)', *Marine Biology*, 124(4), pp. 561–569.

De Castro, M.C.T., Vance, T., Yunnie, A.L.E., Fileman, T.W. & Hall-Spencer, J.M. (2018) 'Low salinity as a biosecurity tool for minimizing biofouling on ship sea chests', *Ocean Science*, 14(4), pp. 661–667.

Chae, M.P., Rozen, W.M., McMenamin, P.G., Findlay, M.W., Spychal, R.T. & Hunter-Smith, D.J. (2015) 'Emerging applications of bedside 3D printing in plastic surgery', *Frontiers in surgery*, 2p. 25.

Chan, C.Y., Chan, H.S. & Wong, P.K. (2019) 'Integrated photocatalytic-biological treatment of triazine-containing pollutants', *Chemosphere*, 222pp. 371–380.

Chang, C.F., Lee, C.F. & Liu, S.M. (2019) '*Cystobasidium keelungensis* sp. nov., a novel mycosporine producing carotenogenic yeast isolated from the sea surface microlayer in Taiwan', *Archives of Microbiology*, 201(1), pp. 27–33.

Chapman, J., Weir, E. & Regan, F. (2010) 'Period four metal nanoparticles on the inhibition of biofouling', *Colloids and Surfaces B: Biointerfaces*, 78(2), pp. 208–216.

Charles, F., Grémare, A., Amouroux, J.-M. & Cahet, G. (1992) 'Filtration of the enteric bacteria *Escherichia coli* by two filter-feeding bivalves, *Venus verrucosa* and *Mytilus galloprovincialis*', *Marine Biology*, 113(1), pp. 117–124.

Cheigh, C.I., Park, M.H., Chung, M.S., Shin, J.K. & Park, Y.S. (2012) 'Comparison of intense pulsed light- and ultraviolet (UVC)-induced cell damage in *Listeria monocytogenes* and *Escherichia coli* O157:H7', *Food Control*, 25(2), pp. 654–659.

Chen, C.L., Maki, J.S., Rittschof, D. & Teo, S.L.M. (2013) 'Early marine bacterial biofilm on a copper-based antifouling paint', *International Biodeterioration and Biodegradation*, 83pp. 71–76.

Chen, E. & Bridgeman, T. (2017) 'The reduction of *Chlorella vulgaris* concentrations through UV-C radiation treatments: A nature-based solution (NBS)', *Environmental Research*, 156(January), pp. 183–189.

Cheng, N. & Moe, P. (2020) 'Inactivation of enveloped viruses (Coronavirus , H5N1 Virus) and disinfection of the air with Legionella-X100 via ultraviolet germicidal irradiation (UVGI)', *Academia.edu*, (1), pp. 1–18.

Cheng, X., Shi, H., Adams, C.D., Timmons, T. & Ma, Y. (2009) 'Effects of oxidative and physical treatments on inactivation of *Cylindrospermopsis raciborskii* and removal of cylindrospermopsin', *Water science and technology*, 60(3), pp. 689–697.

Chiellini, C., Iannelli, R., Modeo, L., Bianchi, V. & Petroni, G. (2012) 'Biofouling of reverse osmosis membranes used in river water purification for drinking purposes: analysis of microbial populations', *Biofouling*, 28(9), pp. 969–984.

Chiellini, E. & Corti, A. (2016) 'Oxo-biodegradable plastics: who they are and to what they serve—present status and future perspectives', *Polyolefin compounds and materials*, pp. 341–354.

Chinnapen, D.J.-F. & Sen, D. (2004) 'A deoxyribozyme that harnesses light to repair thymine dimers in DNA', *Proceedings of the National Academy of Sciences*, 101(1), pp. 65–69.

Christensen, J. & Linden, K.G. (2003) 'How particles affect UV light in the UV disinfection of unfiltered drinking water', *Journal-American Water Works Association*, 95(4), pp. 179–189.

Clare, A.S. & Aldred, N. (2009) 'Surface colonisation by marine organisms and its impact on antifouling research', *Advances in Marine Antifouling Coatings and Technologies*, pp. 46–79.

Clare, A.S., Rittschof, D., Gerhart, D.J. & Maki, J.S. (1992) 'Molecular approaches to nontoxic antifouling', *Invertebrate Reproduction \& Development*, 22(1–3), pp. 67–76.

Clarke, A. & Fraser, K.P.P. (2004) 'Why does metabolism scale with temperature?', *Functional ecology*, 18(2), pp. 243–251.

Cnossen, I., Sanz-Forcada, J., Favata, F., Witasse, O., Zegers, T. & Arnold, N.F. (2007) 'Habitat of early life: Solar X-ray and UV radiation at Earth's surface 4–3.5 billion years ago', *Journal of Geophysical Research: Planets*, 112p. 2008.

Coesel, S., Oborník, M., Varela, J., Falciatore, A. & Bowler, C. (2008) 'Evolutionary origins and functions of the carotenoid biosynthetic pathway in marine diatoms', *PloS one*, 3(8), p. e2896.

Comeau, A.M., Lagunas, M.G., Scarcella, K., Varela, D.E. & Lovejoy, C. (2019) 'Nitrate consumers in arctic marine eukaryotic communities: Comparative diversities of 18S rRNA, 18S rRNA genes, and nitrate reductase genes', *Applied and environmental microbiology*, 85(14), .

Components, R. (2022) *High Power COB LED*. [Online] [online]. Available from: https://uk.rs-online.com/ (Accessed 25 May 2022).

Cooksey, K.E. & Wigglesworth-Cooksey, B. (1995) 'Adhesion of bacteria and diatoms to surfaces in the sea: a review', *Aquatic microbial ecology*, 9(1), pp. 87–96.

Coutts, A.D.M. & Dodgshun, T.J. (2007) 'The nature and extent of organisms in vessel sea-chests: A protected mechanism for marine bioinvasions', *Marine Pollution Bulletin*, 54(7), pp. 875–886.

Coutts, A.D.M., Moore, K.M. & Hewitt, C.L. (2003) 'Ships' sea-chests: An overlooked transfer mechanism for non-indigenous marine species?', *Marine Pollution Bulletin*, 46(11), pp. 1510–1513.

Coutts, A.D.M. & Taylor, M.D. (2004) 'A preliminary investigation of biosecurity risks associated with biofouling on merchant vessels in New Zealand', *New Zealand Journal of Marine and Freshwater Research*, 38(2), pp. 215–229.

Craik, S.A., Weldon, D., Finch, G.R., Bolton, J.R. & Belosevic, M. (2001) 'Inactivation of *Cryptosporidium parvum* oocysts using medium-and low-pressure ultraviolet radiation', *Water research*, 35(6), pp. 1387–1398.

Crimaldi, J.P., Thompson, J.K., Rosman, J.H., Lowe, R.J. & Koseff, J.R. (2002) 'Hydrodynamics of larval settlement: the influence of turbulent stress events at potential recruitment sites', *Limnology and Oceanography*, 47(4), pp. 1137–1151.

Curiel, D., Rismondo, A., Marzocchi, M. & Scattolin, M. (1999) 'Benthic communities on hard substrata of Venice urban area; Comunita'bentoniche di substrato duro del centro storico venenziano', *Acqua-Aria*,

Dahms, H.-U., Dobretsov, S. & Qian, P.-Y. (2004) 'The effect of bacterial and diatom biofilms on the settlement of the bryozoan Bugula neritina', *Journal of Experimental Marine Biology and Ecology*, 313(1), pp. 191–209.

Dai, T., Vrahas, M.S., Murray, C.K. & Hamblin, M.R. (2012) 'Ultraviolet C irradiation: an alternative antimicrobial approach to localized infections?', *Expert review of anti-infective therapy*, 10(2), pp. 185–195.

Dang, H. & Lovell, C.R. (2016a) 'Microbial surface colonization and biofilm development in marine environments', *Microbiology and Molecular Biology Reviews*, 80(1), pp. 91–138.

Dang, H. & Lovell, C.R. (2016b) 'Microbial Surface Colonization and Biofilm Development in Marine Environments', *Microbiology and Molecular Biology Reviews*, 80(1), pp. 91–138.

Darehshouri, A., Affenzeller, M. & Lütz-Meindl, U. (2008) 'Cell death in the unicellular green alga *Micrasterias* upon H2O2 induction', *Plant biology (Stuttgart, Germany)*, 10(6), p. 732.

DeGroot Jr, J. V, Norris, A., Glover, S.O. & Clapp, T. V (2004) 'Highly transparent silicone materials', *Linear and Nonlinear Optics of Organic Materials IV*, 5517pp. 116–123.

Dobretsov, S. (2009) 'Expected effect of climate change on fouling communities and its impact on antifouling research', *Advances in Marine Antifouling Coatings and Technologies*, (x), pp. 222–239.

Dobretsov, S., Abed, R.M.M. & Teplitski, M. (2013) 'Mini-review: Inhibition of biofouling by marine microorganisms', *Biofouling*, 29(4), pp. 423–441.

Dreanno, C., Matsumura, K., Dohmae, N., Takio, K., Hirota, H., Kirby, R.R. & Clare, A.S. (2006) 'An α2-macroglobulin-like protein is the cue to gregarious settlement of the barnacle *Balanus amphitrite*', *Proceedings of the National Academy of Sciences*, 103(39), pp. 14396–14401.

Durland, J. & Ahmadian-Moghadam, H. (2021) 'Genetics, Mutagenesis', in *StatPearls [Internet]*. [Online]. StatPearls Publishing.

Dzeha, T., Nyiro, C., Kardasopoulos, D., Mburu, D., Mwafaida, J., Hall, M.J. & Burgess, J.G. (2019) 'UV Resistance of bacteria from the Kenyan Marine cyanobacterium *Moorea producens*', *MicrobiologyOpen*, 8(4), p. e00697.

Eadie, E., Hiwar, W., Fletcher, L., Tidswell, E., O'Mahoney, P., Buonanno, M., Welch, D., Adamson, C.S., Brenner, D.J. & Noakes, C. (2022) 'Far-UVC (222 nm) efficiently inactivates an airborne pathogen in a room-sized chamber', *Scientific reports*, 12(1), pp. 1–9.

ECHA/EFSA (2017) *Guidance on the Biocidal Products Regulation: Volume IV Environment - Assessment and Evaluation (Parts B + C)*. Vol. 16.

Eckman, J.E., Savidge, W.B. & Gross, T.F. (1990) 'Relationship between duration of cyprid attachment and drag forces associated with detachment of *Balanus amphitrite* cyprids', *Marine Biology*, 107(1), pp. 111–118.

Ellegaard, M., Lenau, T., Lundholm, N., Maibohm, C., Friis, S.M.M., Rottwitt, K. & Su, Y. (2016) 'The fascinating diatom frustule—can it play a role for attenuation of UV radiation?', *Journal of Applied Phycology*, 28(6), pp. 3295–3306.

Encinas, S., Belmadoui, N., Climent, M.J., Gil, S. & Miranda, M.A. (2004) 'Photosensitization of thymine nucleobase by benzophenone derivatives as models for photoinduced DNA damage: Paterno-Büchi vs energy and electron transfer processes', *Chemical Research in Toxicology*, 17(7), pp. 857–862.

Eswara, A.R. & Ramakrishnarao, M. (2013) 'Solar energy in food processing - A critical appraisal', *Journal of Food Science and Technology*, 50(2), pp. 209–227.

European Chemicals Agency (2014) *Transitional Guidance on the Biocidal Products Regulation - Transitional Guidance on mixture toxicity assessment for biocidal products for the environment*, p. 45.

Evans, S.M., Birchenough, A.C. & Brancato, M.S. (2000) 'The TBT ban: out of the frying pan into the fire?', *Marine pollution bulletin*, 40(3), pp. 204–211.

Falasco, E., Blanco Lanza, S., Bona, F., Gomá Martínez, J., Hlúbiková, D., Novais, M.H., Hoffmann, L. & Ector, L. (2009) *Taxonomy, morphology and distribution of the Sellaphora stroemii complex (Bacillariophyceae)*,

Falciatore, A., Jaubert, M., Bouly, J.P., Bailleul, B. & Mock, T. (2020) 'Diatom molecular research comes of age: Model species for studying phytoplankton biology and

diversity[open]'. Plant Cell 32 (3) p.pp. 547–572.

Farhat, N.M., Vrouwenvelder, J.S., Van Loosdrecht, M.C.M., Bucs, S.S. & Staal, M. (2016) 'Effect of water temperature on biofouling development in reverse osmosis membrane systems', *Water research*, 103pp. 149–159.

Faria, S.I., Teixeira-Santos, R., Romeu, M.J., Morais, J., Vasconcelos, V. & Mergulhão, F.J. (2020) 'The relative importance of shear forces and surface hydrophobicity on biofilm formation by coccoid cyanobacteria', *Polymers*, 12(3), .

Farnell (2011) *Standard LED*. [Online] [online]. Available from: https://uk.farnell.com/ (Accessed 4 May 2020).

Fernandes, J.A., Santos, L., Vance, T., Fileman, T., Smith, D., Bishop, J.D.D., Viard, F., Queirós, A.M., Merino, G., Buisman, E. & Austen, M.C. (2016) 'Costs and benefits to European shipping of ballast-water and hull-fouling treatment: Impacts of native and non-indigenous species', *Marine Policy*, 64pp. 148–155.

Fernandez-Leborans, G., Fernandez-Gonzalez, V., Sanchez-Jerez, P. & Roura, A. (2016) 'Epibiontic associations between apostomid ciliates *Conidophrys* spp. and amphipods associated with fish farms fouling in the western Mediterranean Sea', *Helgoland Marine Research*, 70(1), pp. 1–11.

Finlay, J.A., Callow, M.E., Ista, L.K., Lopez, G.P. & Callow, J.A. (2002) 'The influence of surface wettability on the adhesion strength of settled spores of the green alga *Enteromorpha* and the diatom *Amphora*', *Integrative and Comparative Biology*, 42(6), pp. 1116–1122.

Flemming, H.-C., Murthy, P.S., Venkatesan, R. & Cooksey, K. (2009) *Marine and industrial biofouling*. Vol. 333. Springer.

Fletcher, L.M., Forrest, B.M. & Bell, J.J. (2013) 'Impacts of the invasive ascidian *Didemnum vexillum* on green-lipped mussel *Perna canaliculus* aquaculture in New Zealand', *Aquaculture Environment Interactions*, 4(1), pp. 17–30.

Floerl, O., Pool, T.K. & Inglis, G.J. (2004) 'Positive interactions between nonindigenous species facilitate transport by human vectors', *Ecological Applications*, 14(6), pp. 1724–1736.

Forster, R.M. (1997) 'Wavelength dependence of photoinhibition in the green alga *Chlorella vulgaris*', *Photosynthetica*, 33pp. 541–542.

Frey, M.A., Simard, N., Robichaud, D.D., Martin, J.L. & Therriault, T.W. (2014) 'Fouling around: Vessel sea-chests as a vector for the introduction and spread of aquatic invasive species', *Management of Biological Invasions*, 5(1), pp. 21–30.

Friedberg, E.C., Walker, G.C., Siede, W. & Wood, R.D. (2005) *DNA repair and mutagenesis*. American Society for Microbiology Press.

Garcia-Corral, L.S., Martinez-Ayala, J., Duarte, C.M. & Agusti, S. (2015) 'Experimental assessment of cumulative temperature and UV-B radiation effects on Mediterranean plankton metabolism', *Frontiers in Marine Science*, 2p. 48.

Gasparini, F. & Ballarin, L. (2018) 'Reproduction in tunicates', in Michael K. Skinner (ed.) *Encyclopedia of Reproduction (Second Edition)*. Second [Online]. Elsevier. pp. 546–553.

Georgiades, E. & Kluza, D. (2020) 'Conduct of land-based biofouling surveys for domestic vessels', *Biosecurity Science and Risk Assessment Directorate*,

Georgiades, E., Kluza, D., Bates, T., Lubarsky, K., Brunton, J., Growcott, A., Smith, T., McDonald, S., Gould, B., Parker, N. & Bell, A. (2020) 'Regulating vessel biofouling to support New Zealand's marine biosecurity system – A blue print for evidence-based decision making', *Frontiers in Marine Science*, 7(June), pp. 1–15.

Georgiades, E., Scianni, C., Davidson, I., Tamburri, M.N., First, M.R., Ruiz, G., Ellard, K., Deveney, M. & Kluza, D. (2021) 'The role of vessel biofouling in the translocation of marine pathogens: Management considerations and challenges', *Frontiers in Marine Science*, 8(April), .

Gerchman, Y., Mamane, H., Friedman, N. & Mandelboim, M. (2020) 'UV-LED disinfection of Coronavirus: Wavelength effect', *Journal of Photochemistry and Photobiology B: Biology*, 212p. 112044.

Gerdes, G., Dunajtschik-Piewak, K., Riege, H., Taher, A.G., Krumbein, W.E. & Reineck, H. (1994) 'Structural diversity of biogenic carbonate particles in microbial mats', *Sedimentology*, 41(6), pp. 1273–1294.

Gómez-Ramírez, A.L., Enriquez-Ocaña, L.F., Miranda-Baeza, A., Cordero Esquivel, B., López-Elías, J.A. & Martínez-Córdova, L.R. (2019) 'Biofilm-forming capacity of two benthic microalgae, *Navicula incerta* and *Navicula* sp., on three substrates (*Naviculales: Naviculaceae*)', *Revista de Biología Tropical*, 67(3), pp. 599–607.

Grant, K.R. (2022) 'Next-generation amplicon sequencing: A cost-effective method for

exploring microbial biodiversity', in *Molecular Genetics and Genomics Tools in Biodiversity Conservation*. [Online]. Springer. pp. 203–236.

Griffith, K., Mowat, S., Holt, R.H.F., Ramsay, K., Bishop, J.D.D., Lambert, G. & Jenkins, S.R. (2009) 'First records in Great Britain of the invasive colonial ascidian *Didemnum vexillum* Kott, 2002', *Aquatic Invasions*, 4(4), pp. 581–590.

Grigalavicius, M., Moan, J., Dahlback, A. & Juzeniene, A. (2016) 'Daily, seasonal, and latitudinal variations in solar ultraviolet A and B radiation in relation to vitamin D production and risk for skin cancer.', *International journal of dermatology*, 55(1), pp. e23-8.

Growcott, A., Kluza, D. & Georgiades, E. (2017) 'Review: In-water systems to reactively manage biofouling in sea chests and internal pipework', *Marine Technology Society Journal*, 51(2), pp. 89–104.

Growcott, A., Kluza, D., Georgiades, E. & Science, B. (2019) *Technical advice : Evaluation of in-water systems to reactively treat or remove biofouling within vessel internal niche areas*. Vol. 4.

Grzegorczyk, M., Pogorzelski, S.J., Pospiech, A. & Boniewicz-Szmyt, K. (2018) 'Monitoring of marine biofilm formation dynamics at submerged solid surfaces with multitechnique sensors.', *Frontiers in Marine Science*, 5p. 363.

Habeebu, S.S., Liu, J., Liu, Y. & Klaassen, C.D. (2000) 'Metallothionein-null mice are more susceptible than wild-type mice to chronic CdCl2-induced bone injury', *Toxicological sciences*, 56(1), pp. 211–219.

Häder, D.-P., Kumar, H.D., Smith, R.C. & Worrest, R. (2007) 'Effects of solar UV radiation on aquatic ecosystems and interactions with climate change', *Photochemical & photobiological sciences*, 6(3), pp. 267–285.

Häder, D.-P. & Sinha, R.P. (2005) 'Solar ultraviolet radiation-induced DNA damage in aquatic organisms: potential environmental impact', *Mutation Research/Fundamental and Molecular Mechanisms of Mutagenesis*, 571(1–2), pp. 221–233.

Häder, D.P., Kumar, H.D., Smith, R.C. & Worrest, R.C. (2007) 'Effects of solar UV radiation on aquatic ecosystems and interactions with climate change', *Photochemical and Photobiological Sciences*, 6(3), pp. 267–285.

Hadfield, M. & Paul, V. (2001) 'Natural chemical cues for settlement and metamorphosis of

marine-invertebrate larvae', *Marine chemical ecologyology*, (February 2015), pp. 431–461.

Hadfield, M.G. (2011) 'Biofilms and marine invertebrate larvae: What bacteria produce that larvae use to choose settlement sites', *Annual Review of Marine Science*, 3pp. 453–470.

Hagen, A., Chisling, M., House, K., Katz, T., Abelseth, L., Fraser, I., Bradley, S., Kirsch, R., Morris, J. & Giles, J.W. (2021) '3D printing for medical applications: Current state of the art and perspectives during the COVID-19 crisis', *Surgeries*, 2(3), pp. 244–259.

Haiser, K., Fingerhut, B.P., Heil, K., Glas, A., Herzog, T.T., Pilles, B.M., Schreier, W.J., Zinth, W., Devivie-Riedle, R. & Carell, T. (2012) 'Mechanism of UV-induced formation of Dewar lesions in DNA', *Angewandte Chemie - International Edition*, 51(2), pp. 408–411.

Hallegraeff, G.M. (2003) 'Harmful algal blooms: a global overview', *Manual on harmful marine microalgae*, 33pp. 1–22.

Hallegraeff, G.M., Anderson, D.M., Belin, C., Bottein, M.-Y.D., Bresnan, E., Chinain, M., Enevoldsen, H., Iwataki, M., Karlson, B. & McKenzie, C.H. (2021) 'Perceived global increase in algal blooms is attributable to intensified monitoring and emerging bloom impacts', *Communications Earth & Environment*, 2(1), pp. 1–10.

Han, X., Wu, J., Zhang, X., Shi, J., Wei, J., Yang, Y., Wu, B. & Feng, Y. (2021) 'Special issue on advanced corrosion-resistance materials and emerging applications. The progress on antifouling organic coating: From biocide to biomimetic surface', *Journal of Materials Science and Technology*, 61(September 2008), pp. 46–62.

Hannach, G. & Sigleo, A.C. (1998) 'Photoinduction of UV-absorbing compounds in six species of marine phytoplankton', *Marine Ecology Progress Series*, 174pp. 207–222.

Harder, T. & Yee, L.H. (2009) 'Bacterial adhesion and marine fouling', *Advances in Marine Antifouling Coatings and Technologies*, pp. 113–131.

Hargraves, P.E., Zhang, J., Wang, R. & Shimizu, Y. (1993) 'Growth characteristics of the diatoms *Pseudonitzschia pungens* and *P. fraudulenta* exposed to ultraviolet radiation', *Hydrobiologia*, 269(1), pp. 207–212.

Harm, W., Harm, H., Rupert, C.S., Banaś, A.K., Zgłobicki, P., Kowalska, E., Bażant, A., Dziga, D., Strzałka, W., Klymiuk, I., Bambach, I., Patra, V., Trajanoski, S., Wolf, P., Rittschof, D., Chai, C., Lay, S., Teo, M., Maki, J.S., et al. (2020) 'Marine Biofouling', *Genes*, 21(1), pp. 1–17.

Hashlamon, A., Mohammad, A.W. & Ahmad, A. (2017) 'The effect of wastewater pretreatment on nanofiltration membrane performance', *Journal of Water Reuse and Desalination*, 7(1), pp. 45–52.

Hiebert, L.S., Vieira, E.A., Dias, G.M., Tiozzo, S. & Brown, F.D. (2019) 'Colonial ascidians strongly preyed upon, yet dominate the substrate in a subtropical fouling community', *Proceedings of the Royal Society B*, 286(1899), p. 20190396.

Hijmans, R.J. & van Etten, J. (2011) 'Geographic analysis and modeling with raster data', *R package version*, pp. 0–2.

Hinds, L.M., O'Donnell, C.P., Akhter, M. & Tiwari, B.K. (2019) 'Principles and mechanisms of ultraviolet light emitting diode technology for food industry applications', *Innovative Food Science and Emerging Technologies*, 56.

Hirose, E., Ohtsuka, K., Ishikura, M. & Maruyama, T. (2004) 'Ultraviolet absorption in ascidian tunic and ascidian-Prochloron symbiosis', *Journal of the Marine Biological Association of the United Kingdom*, 84(4), pp. 789–794.

Hoagland, K.D., Rosowski, J.R., Gretz, M.R. & Roemer, S.C. (1993) 'Diatom extracellular polymeric substances: function, fine structure, chemistry, and physiology', *Journal of phycology*, 29(5), pp. 537–566.

Hong, Y., Hu, H.-Y. & Li, F.-M. (2008) 'Physiological and biochemical effects of allelochemical ethyl 2-methyl acetoacetate (EMA) on cyanobacterium *Microcystis aeruginosa*', *Ecotoxicology and environmental safety*, 71(2), pp. 527–534.

Hopkins, G., Davidson, I., Georgiades, E., Floerl, O., Morrisey, D. & Cahill, P. (2021) 'Managing biofouling on submerged static artificial structures in the marine environment – assessment of current and emerging approaches', *Frontiers in Marine Science*, 8.

Howland, G.P. (1975) 'Dark-repair of ultraviolet-induced pyrimidine dimers in the DNA of wild carrot protoplasts', *Nature*, 254(5496), pp. 160–161.

Hsissou, R., Seghiri, R., Benzekri, Z., Hilali, M., Rafik, M. & Elharfi, A. (2021) 'Polymer composite materials: A comprehensive review', *Composite structures*, 262p. 113640.

Hu, P., Xie, Q., Ma, C. & Zhang, G. (2020) 'Silicone-based fouling-release coatings for marine antifouling', *Langmuir*, 36(9), pp. 2170–2183.

Huesemann, M.H., Hausmann, T.S., Bartha, R., Aksoy, M., Weissman, J.C. & Benemann, J.R.

(2009) ‘Biomass productivities in wild type and pigment mutant of *Cyclotella* sp.(Diatom)’, *Applied biochemistry and biotechnology*, 157(3), pp. 507–526.

Hung, O.S., Thiyagarajan, V., Wu, R.S.S. & Qian, P.Y. (2005) ‘Effect of ultraviolet radiation on biofilms and subsequent larval settlement of *Hydroides elegans*’, *Marine Ecology Progress Series*, 304pp. 155–166.

Hunsucker, K.Z., Braga, C., Gardner, H., Jongerius, M., Hietbrink, R., Salters, B. & Swain, G. (2019) ‘Using ultraviolet light for improved antifouling performance on ship hull coatings’, *Biofouling*, 35(6), pp. 658–668.

Hunsucker, K.Z., Koka, A., Lund, G. & Swain, G. (2014) ‘Diatom community structure on in-service cruise ship hulls’, *Biofouling*, 30(9), pp. 1133–1140.

Hunsucker, K.Z. & Swain, G.W. (2016) ‘In situ measurements of diatom adhesion to silicone-based ship hull coatings’, *Journal of Applied Phycology*, 28(1), pp. 269–277.

Icoglu Aksakal, F. & Ciltas, A. (2018) ‘The impact of ultraviolet B (UV-B) radiation in combination with different temperatures in the early life stage of zebrafish (*Danio rerio*)’, *Photochemical & Photobiological Sciences*, 17(1), pp. 35–41.

Iervolino, G., Zammit, I., Vaiano, V. & Rizzo, L. (2020) ‘Limitations and prospects for wastewater treatment by UV and visible-light-active heterogeneous photocatalysis: A critical review’, *Topics in Current Chemistry*, 378(1), .

Ikehata, H. & Ono, T. (2011) ‘The mechanisms of UV mutagenesis’, *Journal of radiation research*, 52(2), pp. 115–125.

Ikenaga, M. & Mabuchi, T. (1966) ‘Photoreactivation of endosperm mutations induced by ultraviolet light in maize’, *Radiation Botany*, 6(2), pp. 165–169.

IMO, I. (2008) ‘Summary of the Status of Conventions as at 31 May 2007’, *Organization IM, United Kingdom*,

Ingalls, A.E., Whitehead, K. & Bridoux, M.C. (2010) ‘Tinted windows: The presence of the UV absorbing compounds called mycosporine-like amino acids embedded in the frustules of marine diatoms’, *Geochimica et Cosmochimica Acta*, 74(1), pp. 104–115.

Ishii, H., Ohba, T. & Kobayashi, T. (2008) ‘Effects of low dissolved oxygen on planula settlement, polyp growth and asexual reproduction of *Aurelia aurita*’, *Plankton and Benthos Research*, 3(Supplement), pp. 107–113.

Islam, M.T., Huda, N., Abdullah, A.B. & Saidur, R. (2018) 'A comprehensive review of state-of-the-art concentrating solar power (CSP) technologies: Current status and research trends', *Renewable and Sustainable Energy Reviews*, 91pp. 987–1018.

Isomura, N. & Nishihira, M. (2001) 'Size variation of planulae and its effect on the lifetime of planulae in three pocilloporid corals', *Coral Reefs*, 20(3), pp. 309–315.

Janasie, C., Deans, O. & Harris, T. (2021) 'Legal extension strategies to increase awareness of drinking water contaminant regulatory framework', *Journal of Contemporary Water Research & Education*, 174(1), pp. 106–119.

Jebaraj, C.S., Forster, D., Kauff, F. & Stoeck, T. (2012) 'Molecular diversity of fungi from marine oxygen-deficient environments (ODEs)', in *Biology of marine fungi*. [Online]. Springer. pp. 189–208.

Jeffrey, S.W., MacTavish, H.S., Dunlap, W.C., Vesk, M. & Groenewoud, K. (1999) 'Occurrence of UVA-and UVB-absorbing compounds in 152 species (206 strains) of marine microalgae', *Marine Ecology Progress Series*, 189pp. 35–51.

Johnston, I.D., McCluskey, D.K., Tan, C.K.L. & Tracey, M.C. (2014) 'Mechanical characterization of bulk Sylgard 184 for microfluidics and microengineering', *Journal of Micromechanics and Microengineering*, 24(3), .

Jonsson, P.R., Berntsson, K.M. & Larsson, A.I. (2004) 'Linking larval supply to recruitment: flow-mediated control of initial adhesion of barnacle larvae', *Ecology*, 85(10), pp. 2850–2859.

Joux, F., Jeffrey, W.H., Lebaron, P. & Mitchell, D.L. (1999) 'Marine bacterial isolates display diverse responses to UV-B radiation', *Applied and Environmental Microbiology*, 65(9), pp. 3820–3827.

Kao, Y.-T., Saxena, C., Wang, L., Sancar, A. & Zhong, D. (2005) 'Direct observation of thymine dimer repair in DNA by photolyase', *Proceedings of the National Academy of Sciences*, 102(45), pp. 16128–16132.

Kardela, J.H., Millichamp, I.S., Ferguson, J., Parry, A.L., Reynolds, K.J., Aldred, N. & Clare, A.S. (2019) 'Nonfreezable water and polymer swelling control the marine Antifouling performance of polymers with limited hydrophilic content', *ACS Applied Materials and Interfaces*, 11(33), pp. 29477–29489.

Karentz, D. (2001) 'Chemical defenses of marine organisms against solar radiation exposure:

UV-absorbing mycosporine-like amino acids and scytonemim', *Marine chemical ecology*, pp. 481–520.

Karentz, D., Cleaver, J.E. & Mitchell, D.L. (1991) 'Cell survival characteristics and molecular responses of antarctic phytoplankton to ultraviolet-B radiation', *Journal of Phycology*, 27(3), pp. 326–341.

Kasting, J.F. (1987) 'Theoretical constraints on oxygen and carbon dioxide concentrations in the Precambrian atmosphere', *Precambrian research*, 34(3–4), pp. 205–229.

Kavanagh, C.J., Quinn, R.D. & Swain, G.W. (2005) 'Observations of barnacle detachment from silicones using high-speed video', *The Journal of Adhesion*, 81(7–8), pp. 843–868.

Kelly, M.R., Whitworth, P., Jamieson, A. & Burgess, J.G. (2022) 'Bacterial colonisation of plastic in the Rockall Trough, North-East Atlantic: An improved understanding of the deep-sea plastisphere', *Environmental Pollution*, 305(305), pp. 119–314.

Keshavarzfathy, M., Malayeri, A.H., Mohseni, M. & Taghipour, F. (2020) 'UV-LED fluence determination by numerical method for microbial inactivation studies', *Journal of Photochemistry and Photobiology A: Chemistry*, 392(July 2019), p. 112406.

Khosravi, S., Khodabandeh, S., Agh, N. & Bakhtiarian, M. (2013) 'Effects of salinity and ultraviolet radiation on the bioaccumulation of mycosporine-like amino acids in artemia from Lake Urmia (Iran)', *Photochemistry and Photobiology*, 89(2), pp. 400–405.

Kiil, S., Dam-Johansen, K., Weinell, C.E., Pedersen, M.S. & Codolar, S.A. (2002) 'Dynamic simulations of a self-polishing antifouling paint exposed to seawater', *Journal of Coatings Technology*, 74(929), pp. 45–54.

Kingsford, M.J., Pitt, K.A. & Gillanders, B.M. (2000) *Management of jellyfish fisheries, with special reference to the Order Rhizostomeae*. Vol. 38.

Kirstein, I. V, Wichels, A., Krohne, G. & Gerdts, G. (2018) 'Mature biofilm communities on synthetic polymers in seawater-Specific or general?', *Marine Environmental Research*, 142pp. 147–154.

Kitchener, B.G.B., Wainwright, J. & Parsons, A.J. (2017) 'A review of the principles of turbidity measurement', *Progress in Physical Geography*, 41(5), pp. 620–642.

Klein, S.G., Pitt, K.A. & Carroll, A.R. (2016) 'Surviving but not thriving: inconsistent responses of zooxanthellate jellyfish polyps to ocean warming and future UV-B

scenarios', *Scientific reports*, 6(1), pp. 1–9.

Koo, H.-J. & Kim, Y.-K. (2005) 'Reliability assessment of seat belt webbings through accelerated life testing', *Polymer Testing*, 24(3), pp. 309–315.

Koutchma, T. (2009) 'Advances in ultraviolet light technology for non-thermal processing of liquid foods', *Food and Bioprocess Technology*, 2(2), pp. 138–155.

Kozich, J., Schloss, P., Baxter, N., Jenior, M., Koumpouras, C. & Bishop, L. (2013) *16S rRNA sequencing with the Illumina MiSeq: library generation, QC, & sequencing*,

Kuffner, I.B. (2001) 'Effects of ultraviolet (UV) radiation on larval settlement of the reef coral *Pocillopora damicornis*', *Marine Ecology Progress Series*, 217(July 2001), pp. 251–261.

Kuipers, J., Bruning, H., Yntema, D. & Rijnaarts, H. (2015) 'Wirelessly powered ultraviolet light emitting diodes for photocatalytic oxidation', *Journal of Photochemistry and Photobiology A: Chemistry*, 299pp. 25–30.

Kumar, A., Tyagi, M.B., Singh, N., Tyagi, R., Jha, P.N., Sinha, R.P. & Häder, D.-P. (2003) 'Role of white light in reversing UV-B-mediated effects in the N2-fixing cyanobacterium *Anabaena BT2*', *Journal of Photochemistry and Photobiology B: Biology*, 71(1–3), pp. 35–42.

Lakretz, A., Ron, E.Z. & Mamane, H. (2011) 'Biofilm control in water by a UV-based advanced oxidation process', *Biofouling*, 27(3), pp. 295–307.

Lakretz, A., Ron, E.Z. & Mamane, H. (2010) 'Biofouling control in water by various UVC wavelengths and doses', *Biofouling*, 26(3), pp. 257–267.

Langenkämper, D., Zurowietz, M., Schoening, T. & Nattkemper, T.W. (2017) 'BIIGLE 2.0 - browsing and annotating large marine image collections', *Frontiers in Marine Science*, 4(MAR), pp. 1–10.

Larsson, A.I. & Jonsson, P.R. (2006) 'Barnacle larvae actively select flow environments supporting post-settlement growth and survival', *Ecology*, 87(8), pp. 1960–1966.

Laurion, I. & Vincent, W.F. (1998) 'Cell size versus taxonomic composition as determinants of UV-sensitivity in natural phytoplankton communities', *Limnology and Oceanography*, 43(8), pp. 1774–1779.

Lawrence, K.P., Delinasios, G.J., Premi, S., Young, A.R. & Cooke, M.S. (2022) 'Perspectives on cyclobutane pyrimidine dimers—Rise of the dark dimers', *Photochemistry and*

Photobiology, 98(3), pp. 609–616.

Lebret, K., Thabard, M. & Hellio, C. (2009) 'Algae as marine fouling organisms: Adhesion damage and prevention', *Advances in Marine Antifouling Coatings and Technologies*, pp. 80–112.

Lee, S.D., Yun, S.M., Cho, P.Y., Yang, H.W. & Kim, O.J. (2019) 'Newly recorded species of diatoms in the source of Han and Nakdong rivers, South Korea', *Phytotaxa*, 403(3), pp. 143–170.

Leeuw, T., Boss, E.S. & Wright, D.L. (2013) 'In situ measurements of phytoplankton fluorescence using low cost electronics', *Sensors*, 13(6), pp. 7872–7883.

Lei, H., He, D., Guo, Y., Tang, Y. & Huang, H. (2018) 'Synthesis and characterization of UV-absorbing fluorine-silicone acrylic resin polymer', *Applied Surface Science*, 442pp. 71–77.

Lejars, M., Margaillan, A. & Bressy, C. (2012) 'Fouling release coatings: A nontoxic alternative to biocidal antifouling coatings', *Chemical Reviews*, 112(8), pp. 4347–4390.

Lemaire, P. (2011) 'Evolutionary crossroads in developmental biology: the tunicates', *Development*, 138(11), pp. 2143–2152.

Lesser, M.P. (1997) 'Oxidative stress causes coral bleaching during exposure to elevated temperatures', *Coral reefs*, 16(3), pp. 187–192.

Li, C., Wang, G., Chen, K., Jia, P., Wang, L., Wang, X. & Yun, F. (2020) 'Analysis of removing barnacles attached on rough substrate with cleaning robot', *Journal of Marine Science and Engineering*, 8(8), .

Li, J., Liu, Z., Tan, C., Guo, X., Wang, L., Sancar, A. & Zhong, D. (2010) 'Dynamics and mechanism of repair of ultraviolet-induced (6-4) photoproduct by photolyase', *Nature*, 466(7308), pp. 887–890.

Li, J., Uchida, T., Todo, T. & Kitagawa, T. (2006) 'Similarities and differences between cyclobutane pyrimidine dimer photolyase and (6-4) photolyase as revealed by resonance raman spectroscopy: Electron transfer from the FAD cofactor to ultraviolet-damaged DNA', *Journal of Biological Chemistry*, 281(35), pp. 25551–25559.

Lin, S.H. & Chen, M.L. (1997) 'Treatment of textile wastewater by chemical methods for reuse', *Water research*, 31(4), pp. 868–876.

Lin, Y.-H., You, J.P., Lin, Y.-C., Tran, N.T. & Shi, F.G. (2010) 'Development of high-performance optical silicone for the packaging of high-power LEDs', *IEEE Transactions on Components and Packaging Technologies*, 33(4), pp. 761–766.

Lindegarth, M., Jonsson, P.R. & André, C. (2002) 'Physical and numerical modeling of the role of hydrodynamic processes on adult-larval interactions of a suspension-feeding bivalve', *Journal of marine research*, 60(3), pp. 499–516.

Liu, M., Li, S., Wang, H., Jiang, R. & Zhou, X. (2021) 'Research progress of environmentally friendly marine antifouling coatings', *Polymer Chemistry*, 12(26), pp. 3702–3720.

Llabrés, M., Agustí, S., Alonso-Laita, P. & Herndl, G.J. (2010) 'Synechococcus and Prochlorococcus cell death induced by UV radiation and the penetration of lethal UVR in the Mediterranean Sea', *Marine Ecology Progress Series*, 399pp. 27–37.

Lobban, C.S., Hallam, S.J., Mukherjee, P. & Petrich, J.W. (2007) 'Photophysics and multifunctionality of hypericin-like pigments in heterotrich ciliates: A phylogenetic perspective', *Photochemistry and Photobiology*, 83(5), pp. 1074–1094.

Lomonaco, T., Manco, E., Corti, A., La Nasa, J., Ghimenti, S., Biagini, D., Di Francesco, F., Modugno, F., Ceccarini, A. & Fuoco, R. (2020) 'Release of harmful volatile organic compounds (VOCs) from photo-degraded plastic debris: a neglected source of environmental pollution', *Journal of Hazardous Materials*, 394p. 122596.

Long, L.J., Lee, P.H., Small, E.M., Hillyer, C., Guo, Y. & Osley, M.A. (2020) 'Regulation of UV damage repair in quiescent yeast cells', *DNA Repair*, 90(April), p. 102861.

Lorenz, G. & Kandelbauer, A. (2022) 'Silicones', in *Handbook of thermoset plastics*. [Online]. Elsevier. pp. 659–677.

Lowe, A.J. (2002) *Microcosmus sqamiger, a solitary ascidian introduced to southern California harbors and marinas: Salinity tolerance and phylogenetic analysis*. [Online]. California State University, Fullerton.

Lowry, M.S., Hubble, D.R., Wressell, A.L., Vratsanos, M.S., Pepe, F.R. & Hegedus, C.R. (2008) 'Assessment of UV-permeability in nano-ZnO filled coatings via high throughput experimentation', *Journal of Coatings Technology and Research*, 5(2), pp. 233–239.

MacKenzie, A.F., Maltby, E.A., Harper, N., Bueley, C., Olender, D. & Wyeth, R.C. (2019) 'Periodic ultraviolet-C illumination for marine sensor antifouling', *Biofouling*, 35(5), pp. 483–493.

MacroTrends (2021) *WTI Crude Oil Prices*. [Online] [online]. Available from: https://www.macrotrends.net/2516/wti-crude-oil-prices-10-year-daily-chart (Accessed 30 September 2021).

Maguire, R.J. (1987) 'Environmental aspects of tributyltin', *Applied Organometallic Chemistry*, 1(6), pp. 475–498.

Mann, D.G. (1993) 'Patterns of sexual reproduction in diatoms', *Hydrobiologia*, 269(1), pp. 11–20.

Mann, R. & Harding, J.M. (2003) 'Salinity tolerance of larval *Rapana venosa*: Implications for dispersal and establishment of an invading predatory gastropod on the North American Atlantic coast', *The Biological Bulletin*, 204(1), pp. 96–103.

Maréchal, J.P. & Hellio, C. (2009) 'Challenges for the development of new non-toxic antifouling solutions', *International Journal of Molecular Sciences*, 10(11), pp. 4623–4637.

Matin, A., Laoui, T., Falath, W. & Farooque, M. (2021) 'Fouling control in reverse osmosis for water desalination & reuse: Current practices & emerging environment-friendly technologies', *Science of the Total Environment*, 765p. 142721.

Maxwell, J.C. (1865) *A dynamical theory of the electromagnetic field*. The Royal Society London.

McGreer, M. (2021) 'Testing the Effects of UV-C Radiation on Materials', *IST International Surface Technology*, 14(2), pp. 46–47.

McKenzie, C., Reid, V., Lambert, G., Matheson, K., Minchin, D., Pederson, J., Brown, L., Curd, A., Gollasch, S. & Goulletquer, P. (2017) 'Alien species alert: *Didemnum vexillum* Kott, 2002: Invasion, impact, and control', *ICES Cooperative Research Report*, (335), .

Meunier, S.M., Todorovic, B., Dare, E. V, Begum, A., Guillemette, S., Wenger, A., Saxena, P., Campbell, J.L., Sasges, M. & Aucoin, M.G. (2016) 'Impact of dissolved oxygen during UV-irradiation on the chemical composition and function of CHO cell culture media', *PloS one*, 11(3), .

Mihm, J.W., Banta, W.C. & Loeb, G.I. (1981) 'Effects of adsorbed organic and primary fouling films on bryozoan settlement', *Journal of Experimental Marine Biology and Ecology*, 54(2), pp. 167–179.

Miller, M.A., Gardner, I.A., Kreuder, C., Paradies, D.M., Worcester, K.R., Jessup, D.A., Dodd, E., Harris, Md., Ames, J.A. & Packham, A.E. (2002) 'Coastal freshwater runoff is a risk factor for *Toxoplasma gondii* infection of southern sea otters (Enhydra lutris nereis)', *International journal for parasitology*, 32(8), pp. 997–1006.

Mineur, F., Cook, E.J., Minchin, D., Bohn, K., MacLeod, A. & Maggs, C.A. (2012) 'Changing coasts: Marine aliens and artifcial structures', in *Oceanography and Marine Biology*. [Online]. CRC Press. pp. 198–243.

Miyake, A., Harumoto, T., Salvi, B. & Rivola, V. (1990) 'Defensive function of pigment granules in *Blepharisma japonicum*', *European journal of protistology*, 25(4), pp. 310–315.

Moe, C.G., Sugiyama, S., Kasai, J., Grandusky, J.R. & Schowalter, L.J. (2018) 'AlGaN light-emitting diodes on AlN substrates emitting at 230 nm', *physica status solidi (a)*, 215(10), p. 1700660.

Montero, C.I., Johnson, M.R., Chou, C.-J., Conners, S.B., Geouge, S.G., Tachdjian, S., Nichols, J.D. & Kelly, R.M. (2007) 'Responses of wild-type and resistant strains of the hyperthermophilic bacterium *Thermotoga maritima* to chloramphenicol challenge', *Applied and environmental microbiology*, 73(15), pp. 5058–5065.

Morton, B. (1981) 'The biology and functional morphology of *Mytilopsis sallei* (Recluz)(Bivalvia: Dreissenacea) fouling Visakhapatnam Harbour, Andhra Pradesh, India', *Journal of Molluscan Studies*, 47(1), pp. 25–42.

Moser, C.S., Wier, T.P., First, M.R., Grant, J.F., Riley, S.C., Robbins-Wamsley, S.H., Tamburri, M.N., Ruiz, G.M., Miller, A.W. & Drake, L.A. (2017) 'Quantifying the extent of niche areas in the global fleet of commercial ships: the potential for "super-hot spots" of biofouling', *Biological Invasions*, 19(6), pp. 1745–1759.

Moshchenko, A. V & Zvyagintsev, A.Y. (2004) 'Composition, structure and some distribution features of fouling community in the water intake tunnel of Vladivostok Heat and Power Plant', *Ocean and Polar research*, 26(4), pp. 619–633.

Mourya, M., Khan, M.J., Ahirwar, A., Schoefs, B., Marchand, J., Rai, A., Varjani, S., Rajendran, K., Banu, J.R. & Vinayak, V. (2022) 'Latest trends and developments in microalgae as potential source for biofuels: The case of diatoms', *Fuel*, 314p. 122738.

Mullenders, L.H.F., Hazekamp-van Dokkum, A.-M., Kalle, W.H.J., Vrieling, H., Zdzienicka,

M.Z. & van Zeeland, A.A. (1993) ‘UV-induced photolesions, their repair and mutations’, *Mutation Research/Genetic Toxicology*, 299(3–4), pp. 271–276.

Mullenders, L.H.F., Hoffen, A. van, Vreeswijk, M.P.G., Ruven, H.-J., Vrieling, H. & Van Zeeland, A.A. (1997) ‘UItraviolet-induced photolesions: repair and mutagenesis’, *Risk and Progression Factors in Carcinogenesis*, pp. 89–99.

Mullineaux, L.S. & Butman, C.A. (1991) ‘Initial contact, exploration and attachment of barnacle (*Balanus amphitrite*) cyprids settling in flow’, *Marine Biology*, 110(1), pp. 93–103.

Munk, T., Kane, D. & Yebra, D.M. (2009) ‘The effects of corrosion and fouling on the performance of ocean-going vessels: A naval architectural perspective’, *Advances in Marine Antifouling Coatings and Technologies*, pp. 148–176.

Muramoto, Y., Kimura, M. & Nouda, S. (2014) ‘Development and future of ultraviolet light-emitting diodes: UV-LED will replace the UV lamp’, *Semiconductor Science and Technology*, 29(8), .

Nair, P.S.R., Krishnamurthy, K. & Mawatari, S.F. (1992) ‘Salinity Tolerance in Four Estuarine Species of Bryozoa.’, *Marine fouling*, 9(1/2), pp. 15–20.

le Norcy, T., Niemann, H., Proksch, P., Tait, K., Linossier, I., Réhel, K., Hellio, C. & Faÿ, F. (2017) ‘Sponge-inspired dibromohemibastadin prevents and disrupts bacterial biofilms without toxicity’, *Marine drugs*, 15(7), p. 222.

Nurioglu, A.G. & Esteves, A.C.C. (2015) ‘Non-toxic, non-biocide-release antifouling coatings based on molecular structure design for marine applications’, *Journal of Materials Chemistry B*, 3(32), pp. 6547–6570.

O’Toole, G., Kaplan, H.B. & Kolter, R. (2000) ‘Biofilm formation as microbial development’, *Annual review of microbiology*, 54p. 49.

Olivier, F., Tremblay, R., Bourget, E. & Rittschof, D. (2000) ‘Barnacle settlement: field experiments on the influence of larval supply, tidal level, biofilm quality and age on *Balanus amphitrite* cyprids’, *Marine Ecology Progress Series*, 199pp. 185–204.

Orgel, L.E. (1994) ‘The origin of life on the earth’, *Scientific American*, 271(4), pp. 76–83.

Ou, Y. & Petersen, P.M. (2021) ‘Application of ultraviolet light sources for in vivo disinfection’, *Japanese Journal of Applied Physics*, (60), .

Palai, G., Nayyar, A., Solanki, A. & Tripathy, S.K. (2019) 'Generation of ultra violet signal from visible light using photonic crystal fiber: A realization of PCF based UV torch', *Optik*, 180pp. 913–916.

Parida, B., Iniyan, S. & Goic, R. (2011) 'A review of solar photovoltaic technologies', *Renewable and sustainable energy reviews*, 15(3), pp. 1625–1636.

Patel, D.K., Sakhaei, A.H., Layani, M., Zhang, B., Ge, Q. & Magdassi, S. (2017) 'Highly stretchable and UV curable elastomers for digital light processing based 3D printing', *Advanced Materials*, 29(15), .

Paul, V.J. (2008) 'Global warming and cyanobacterial harmful algal blooms', *CAdvances in Experimental Medicine and Biology*, pp. 239–257.

Peng, W. & Shaw, B.R. (1996) 'Accelerated deamination of cytosine residues in UV-induced cyclobutane pyrimidine dimers leads to CC→ TT transitions', *Biochemistry*, 35(31), pp. 10172–10181.

Pernet, F., Tremblay, R. & Bourget, E. (2003) 'Settlement success, spatial pattern and behavior of mussel larvae *Mytilus spp*. in experimental'downwelling'systems of varying velocity and turbulence', *Marine Ecology Progress Series*, 260pp. 125–140.

Pestana, D., Ostrensky, A., Boeger, W.A.P. & Pie, M.R. (2009) 'The effect of temperature and body size on filtration rates of *Limnoperna fortunei* (Bivalvia, Mytilidae) under laboratory conditions', *Brazilian Archives of Biology and Technology*, 52pp. 135–144.

Phukan, T., Rai, A.N. & Syiem, M.B. (2018) 'Dose dependent variance in UV-C radiation induced effects on carbon and nitrogen metabolism in the cyanobacterium *Nostoc muscorum Meg1*', *Ecotoxicology and Environmental Safety*, 155(November 2017), pp. 171–179.

Phukan, T., Rai, A.N. & Syiem, M.B. (2019) 'Unstandardized UV-C dose used for killing harmful cyanobacteria may instead initiate accelerated growth in the target organisms', *Ecotoxicology and Environmental Safety*, 181(April), pp. 274–283.

Pierri, C., Colangelo, P., Del Pasqua, M., Longo, C. & Giangrande, A. (2019) 'Consequences of the experimental removal of *Sabella spallanzanii* (Gmelin, 1791) from the fouling assemblage of a Mediterranean harbour', *Mediterranean Marine Science*, 20(3), pp. 476–486.

Pinnacle, F. (2016) 'Foul free for over two years-Presentation of results from AML

Oceanographic UV•Xchange biofouling control experiment at Folger Pinnacle', *IEEE Monterey*, (Sept), pp. 19–23.

Piola, R., Salters, B., Grandison, C., Ciacic, M. & Hietbrink, R. (2016) 'Assessing the use of low voltage UV-light emitting miniature LEDs for marine biofouling control', *DST-Group-TR-3266*, pp. 2–28.

Piola, R.F. & Hopkins, G.A. (2012) 'Thermal treatment as a method to control transfers of invasive biofouling species via vessel sea chests', *Marine Pollution Bulletin*, 64(8), pp. 1620–1630.

Pistone, A., Scolaro, C. & Visco, A. (2021) 'Mechanical properties of protective coatings against marine fouling: A review', *Polymers*, 13(2), pp. 1–19.

Pitt, K.A. & Kingsford, M.J. (2000) 'Reproductive biology of the edible jellyfish *Catostylus mosaicus* (Rhizostomeae)', *Marine Biology*, 137(5), pp. 791–799.

Ponnusamy, K., Paul, D. & Kweon, J.H. (2009) 'Inhibition of quorum sensing mechanism and *Aeromonas hydrophila* biofilm formation by vanillin', *Environmental Engineering Science*, 26(8), pp. 1359–1363.

Poore, A.G.B. & Steinberg, P.D. (1999) 'Preference–performance relationships and effects of host plant choice in an herbivorous marine amphipod', *Ecological monographs*, 69(4), pp. 443–464.

Premi, S., Wallisch, S., Mano, C.M., Weiner, A.B., Bacchiocchi, A., Wakamatsu, K., Bechara, E.J.H., Halaban, R., Douki, T. & Brash, D.E. (2015) 'Chemiexcitation of melanin derivatives induces DNA photoproducts long after UV exposure', *Science*, 347(6224), pp. 842–847.

Pritchard, A.M. (1988) 'The economics of fouling', in *Fouling Science and Technology*. [Online]. Springer. pp. 31–45.

Raikow, D.F., Reid, D.F., Blatchley, E.R., Jacobs, G. & Landrum, P.F. (2007) 'Effects of proposed physical ballast tank treatments on aquatic invertebrate resting eggs', *Environmental Toxicology and Chemistry*, 26(4), pp. 717–725.

Railkin, A.I. (2003) *Marine biofouling: colonization processes and defenses*. CRC press.

Rastogi, R.P., Kumar, A., Tyagi, M.B. & Sinha, R.P. (2010) 'Molecular mechanisms of ultraviolet radiation-induced DNA damage and repair', *Journal of Nucleic Acids*, 2010.

Rastogi, R.P., Madamwar, D., Nakamoto, H. & Incharoensakdi, A. (2020) 'Resilience and self-regulation processes of microalgae under UV radiation stress', *Journal of Photochemistry and Photobiology C: Photochemistry Reviews*, 43p. 100322.

Rauer, C., Nogueira, J.J., Marquetand, P. & González, L. (2016) 'Cyclobutane thymine photodimerization mechanism revealed by nonadiabatic molecular dynamics', *Journal of the American Chemical Society*, 138(49), pp. 15911–15916.

Readman, J.W. (2006) 'Development, occurrence and regulation of antifouling paint biocides: historical review and future trends', *Antifouling paint biocides*, pp. 1–15.

Ribeiro, S., Berge, T., Lundholm, N., Andersen, T.J., Abrantes, F. & Ellegaard, M. (2011) 'Phytoplankton growth after a century of dormancy illuminates past resilience to catastrophic darkness', *Nature communications*, 2(1), pp. 1–7.

Richard, K.N., Hunsucker, K.Z., Gardner, H., Hickman, K. & Swain, G. (2021) 'The application of UVC used in synergy with surface material to prevent marine biofouling', *Journal of Marine Science and Engineering*, 9(6), .

Richmond, M.D. & Seed, R. (1991) 'A review of marine macrofouling communities with special reference to animal fouling', *Biofouling*, 3(2), pp. 151–168.

Rijstenbil, J.W. (2001) 'Effects of periodic, low UVA radiation on cell characteristics and oxidative stress in the marine planktonic diatom *Ditylum brightwellii*', *European Journal of Phycology*, 36(1), pp. 1–8.

Rivero, N.K., Dafforn, K.A., Coleman, M.A. & Johnston, E.L. (2013) 'Environmental and ecological changes associated with a marina', *Biofouling*, 29(7), pp. 803–815.

Roberts, D., Rittschof, D., Holm, E. & Schmidt, A.R. (1991) 'Factors influencing initial larval settlement: temporal, spatial and surface molecular components', *Journal of Experimental Marine Biology and Ecology*, 150(2), pp. 203–221.

Rochette, P.J., Therrien, J.P., Drouin, R., Perdiz, D., Bastien, N., Drobetsky, E.A. & Sage, E. (2003) 'UVA-induced cyclobutane pyrimidine dimers form predominantly at thymine-thymine dipyrimidines and correlate with the mutation spectrum in rodent cells', *Nucleic Acids Research*, 31(11), pp. 2786–2794.

Ross, B.J. & Hallock, P. (2019) 'Survival and recovery of the foraminifer *Amphistegina gibbosa* and associated diatom endosymbionts following up to 20 months in aphotic conditions', *Marine Micropaleontology*, 149pp. 35–43.

Rye, R. & Holland, H.D. (1998) ‘Paleosols and the evolution of atmospheric oxygen: a critical review.’, *American Journal of Science*, 298(8), pp. 621–672.

Sagan, C. & Chyba, C. (1997) ‘The early faint sun paradox: Organic shielding of ultraviolet-labile greenhouse gases’, *Science*, 276(5316), pp. 1217–1221.

Salau, A.O., Deshpande, D.S., Adaramola, B.A. & Habeebullah, A. (2020) ‘Design and construction of a multipurpose solar-powered water purifier’, in *International Conference on Information and Communication Technology for Intelligent Systems*. [Online]. 2020 Springer. pp. 377–387.

Saleh, T.A., Al-Tikrity, E.T.B., Ahmed, D.S., El-Hiti, G.A., Kariuki, B.M., Yaseen, A.A., Ahmed, A. & Yousif, E. (2022) ‘Monitoring physicochemical properties of transparent PVC films containing captopril and metal oxide nanoparticles to assess UV blocking’, *Journal of Polymer Research*, 29(6), pp. 1–10.

Salta, M., Wharton, J.A., Blache, Y., Stokes, K.R. & Briand, J.-F. (2013) ‘Marine biofilms on artificial surfaces: structure and dynamics’, *Environmental Microbiology*, 15(11), pp. 2879–2893.

Sancar, A. (2003) ‘Structure and function of DNA photolyase and cryptochrome blue-light photoreceptors’, *Chemical reviews*, 103(6), pp. 2203–2238.

Sangermano, M., Razza, N. & Crivello, J.V. (2014) ‘Cationic UV-curing: Technology and applications’, *Macromolecular Materials and Engineering*, 299(7), pp. 775–793.

Santos, A.L., Oliveira, V., Baptista, I., Henriques, I., Gomes, N., Almeida, A., Correia, A. & Cunha, Â. (2013) ‘Wavelength dependence of biological damage induced by UV radiation on bacteria’, *Archives of microbiology*, 195(1), pp. 63–74.

Sarathy, S.R. & Mohseni, M. (2006) ‘An overview of UV-based advanced oxidation processes for drinking water treatment’, *IUVA News*, 8(2), pp. 16–27.

Sayed, A.M., Hassan, M.H.A., Alhadrami, H.A., Hassan, H.M., Goodfellow, M. & Rateb, M.E. (2020) ‘Extreme environments: microbiology leading to specialized metabolites’, *Journal of Applied Microbiology*, 128(3), pp. 630–657.

Scheer, T. (1943) ‘The development of marine fouling communities’, *The Biological Bulletin*, 89.1pp. 103–121.

Scheltema, R.S. (1974) ‘Biological interactions determining larval settlement of marine

invertebrates.', *Woods Hole Oceanography Institute*, 10pp. 263–296.

Schreiber, A., Kühn, B., Arnold, E., Schilling, F.J. & Witzke, H.D. (2005) 'Radiation resistance of quartz glass for VUV discharge lamps', *Journal of Physics D: Applied Physics*, 38(17), p. 3242.

Schreier, W.J., Kubon, J., Regner, N., Haiser, K., Schrader, T.E., Zinth, W., Clivio, P. & Gilch, P. (2009) 'Thymine dimerization in DNA model systems: Cyclobutane photolesion is predominantly formed via the singlet channel', *Journal of the American Chemical Society*, 131(14), pp. 5038–5039.

Schreier, W.J., Schrader, T.E., Koller, F.O., Gilch, P., Crespo-Hernández, C.E., Swaminathan, V.N., Carell, T., Zinth, W. & Kohler, B. (2007) 'Thymine dimerization in DNA is an ultrafast photoreaction', *Science*, 315(5812), pp. 625–629.

Schuch, A.P., Moreno, N.C., Schuch, N.J., Menck, C.F.M. & Garcia, C.C.M. (2017) 'Sunlight damage to cellular DNA: Focus on oxidatively generated lesions', *Free Radical Biology and Medicine*, 107pp. 110–124.

Schultz, M.P., Bendick, J.A., Holm, E.R. & Hertel, W.M. (2011) 'Economic impact of biofouling on a naval surface ship', *Biofouling*, 27(1), pp. 87–98.

Schultz, M.P., Walker, J.M., Steppe, C.N. & Flack, K.A. (2015) 'Impact of diatomaceous biofilms on the frictional drag of fouling-release coatings', *Biofouling*, 31(9), pp. 759–773.

Seed, R. & Richardson, C.A. (1999) 'Evolutionary traits in *Perna viridis* (Linnaeus) and *Septifer virgatus* (Wiegmann)(Bivalvia: Mytilidae)', *Journal of Experimental Marine Biology and Ecology*, 239(2), pp. 273–287.

Segev, E., Wyche, T.P., Kim, K.H., Petersen, J., Ellebrandt, C., Vlamakis, H., Barteneva, N., Paulson, J.N., Chai, L. & Clardy, J. (2016) 'Dynamic metabolic exchange governs a marine algal-bacterial interaction', *eLife*, 18;5.

Selim, M.S., Shenashen, M.A., El-Safty, S.A., Higazy, S.A., Selim, M.M., Isago, H. & Elmarakbi, A. (2017) 'Recent progress in marine foul-release polymeric nanocomposite coatings', *Progress in Materials Science*, 87pp. 1–32.

Shaban, A.M., El-Taweel, G.E. & Ali, G.H. (1997) 'UV ability to inactivate microorganisms combined with factors affecting radiation', *Water Science and Technology*, 35(11–12), pp. 107–112.

Sharma, V.K. & Demir, H.V. (2022) ‘Bright future of deep-ultraviolet photonics: Emerging UVC chip-scale light-source technology platforms, benchmarking, challenges, and outlook for UV disinfection’, *ACS Photonics*,

Shaw, K., Sesardić, I., Bristol, N., Ames, C., Dagnall, K., Ellis, C., Whittaker, F. & Daniel, B. (2008) ‘Comparison of the effects of sterilisation techniques on subsequent DNA profiling’, *International Journal of Legal Medicine*, 122(1), pp. 29–33.

Shick, J.M., Dunlap, W.C., Pearse, J.S. & Pearse, V.B. (2002) ‘Mycosporine-like amino acid content in four species of sea anemones in the genus *Anthopleura* reflects phylogenetic but not environmental or symbiotic relationships’, *The Biological Bulletin*, 203(3), pp. 315–330.

Shick, W. & Dunlap, J.M. (2002) ‘Mycosporine-like amino acids and related gradusols: biosynthesis, accumulation, and UV-protective functions in aquatic organisms’, *Annu Rev Physiol*, 64pp. 223–262.

Shukla, V., Bajpai, M., Singh, D.K., Singh, M. & Shukla, R. (2004) ‘Review of basic chemistry of UV-curing technology’, *Pigment & Resin Technology*, 33(5), pp. 272–279.

Sies, H. & Stahl, W. (2004) ‘Carotenoids and UV protection’, *Photochemical & Photobiological Sciences*, 3(8), pp. 749–752.

Sinha, R.P. & Häder, D.-P. (2008) ‘UV-protectants in cyanobacteria’, *Plant Science*, 174(3), pp. 278–289.

Sinha, R.P., Rastogi, R.P., Ambasht, N.K. & Häder, D.P. (2008) ‘Life of wetland cyanobacteria under enhancing solar UV-B radiation’, *Proc Natl Acad Sci India B*, 78pp. 53–65.

Skolimowski, M., Nielsen, M.W., Emnéus, J., Molin, S., Taboryski, R., Sternberg, C., Dufva, M. & Geschke, O. (2010) ‘Microfluidic dissolved oxygen gradient generator biochip as a useful tool in bacterial biofilm studies’, *Lab on a Chip*, 10(16), pp. 2162–2169.

Smith, R.J. & Facts, A. (2019) *The ostracod carapace*. [Online] [online]. Available from: https://www.biwahaku.jp/smith/ostracod_carapace.html (Accessed 27 July 2022).

Sneha, N. & Patil, B.M. (2022) ‘The impact of UV-C treatment on fruits and vegetables for quality and shelf life improvement using internet of things’, in *Computational Intelligence in Data Mining*. [Online]. Springer. pp. 235–247.

Solomon, K.R. (2008) ‘Effects of ozone depletion and UV-B radiation on humans and the

environment', *Atmosphere-Ocean*, 46(1), pp. 185–202.

Sommer, R., Cabaj, A., Pribil, W. & Haider, T. (1997) 'Influence of lamp intensity and water transmittance on the UV disinfection of water', *Water science and technology*, 35(11–12), pp. 113–118.

Sommer, R., Haider, T., Cabaj, A., Heidenreich, E. & Kundi, M. (1996) 'Increased inactivation of *Saccharomyces cerevisiae* by protraction of UV irradiation', *Applied and Environmental Microbiology*, 62(6), pp. 1977–1983.

Sommer, R., Haider, T., Cabaj, A., Pribil, W. & Lhotsky, M. (1998) 'Time dose reciprocity in UV disinfection of water', *Water Science and Technology*, 38(12), pp. 145–150.

Song, K., Mohseni, M. & Taghipour, F. (2016) 'Application of ultraviolet light-emitting diodes (UV-LEDs) for water disinfection: A review', *Water Research*, 94pp. 341–349.

Song, L., Li, W., He, J., Li, L., Li, T., Gu, D. & Tang, H. (2020) 'Development of a pulsed xenon ultraviolet disinfection device for real-time air disinfection in ambulances', *Journal of Healthcare Engineering*, 2020.

Spampinato, C.P. (2017) 'Protecting DNA from errors and damage: an overview of DNA repair mechanisms in plants compared to mammals', *Cellular and Molecular Life Sciences*, 74(9), pp. 1693–1709.

Stefaniak, L., Lambert, G., Gittenberger, A., Zhang, H., Lin, S. & Whitlatch, R.B. (2009) 'Genetic conspecificity of the worldwide populations of *Didemnum vexillum* Kott, 2002', *Aquatic Invasions*, 4(1), pp. 29–44.

Stroben, E., Schulte-Oehlmann, U., Fioroni, P. & Oehlmann, J. (1995) 'A comparative method for easy assessment of coastal TBT pollution by the degree of imposex in prosobranch species', *Haliotis. Paris*, 24pp. 1–12.

Suwarno, S.R., Hanada, S., Chong, T.H., Goto, S., Henmi, M. & Fane, A.G. (2016) 'The effect of different surface conditioning layers on bacterial adhesion on reverse osmosis membranes', *Desalination*, 387pp. 1–13.

Swalla, B.J. & Smith, A.B. (2008) 'Deciphering deuterostome phylogeny: molecular, morphological and palaeontological perspectives', *Philosophical Transactions of the Royal Society B: Biological Sciences*, 363(1496), pp. 1557–1568.

Sylvester, F., Kalaci, O., Leung, B., Lacoursière-Roussel, A., Murray, C.C., Choi, F.M., Bravo,

M.A., Therriault, T.W. & Macisaac, H.J. (2011) ‘Hull fouling as an invasion vector: Can simple models explain a complex problem?’, *Journal of Applied Ecology*, 48(2), pp. 415–423.

Sylvester, F. & MacIsaac, H.J. (2010) ‘Is vessel hull fouling an invasion threat to the Great Lakes?’, *Diversity and Distributions*, 16(1), pp. 132–143.

Szabó, C. & Ohshima, H. (1997) ‘DNA damage induced by peroxynitrite: Subsequent biological effects’, *Nitric Oxide - Biology and Chemistry*, 1(5), pp. 373–385.

Szeto, W., Yam, W.C., Huang, H. & Leung, D.Y.C. (2020) ‘The efficacy of vacuum-ultraviolet light disinfection of some common environmental pathogens’, *BMC Infectious Diseases*, 20(1), pp. 1–9.

Taghipour, F. & Mohseni, M. (2005) ‘CFD simulation of UV photocatalytic reactors for air treatment’, *AIChE journal*, 51(11), pp. 3039–3047.

Tait, L., Inglis, G., Seaward, K., Spong, K. & Wilkens, S. (2016) ‘Optimising settlement arrays for surveillance of non-indigenous biofouling species’, *MPI Information-Paper*, (2016/71), p. 74.

Takada, K., Shiba, T., Yamaguchi, T., Akane, Y., Nakayama, Y., Soda, S., Inoue, D. & Ike, M. (2018) ‘Cake layer bacterial communities during different biofouling stages in full-scale membrane bioreactors’, *Bioresource technology*, 259pp. 259–267.

Tedetti, M. & Semperv, R. (2006) ‘Invited review penetration of ultraviolet radiation in the marine environment. A review’, *Photochemistry and Photobiology*, 82pp. 389–397.

Thimijan, R.W. & Heins, R.D. (1983) ‘Photometric, radiometric, and quantum light units of measure: a review of procedures for interconversion’, *HortScience*, 18(6), pp. 818–822.

Thiyagarajan, V., Harder, T. & Qian, P.-Y. (2003) ‘Combined effects of temperature and salinity on larval development and attachment of the subtidal barnacle *Balanus trigonus* Darwin’, *Journal of Experimental Marine Biology and Ecology*, 287(2), pp. 223–236.

Thomas, A. (2016) *Microorganisms in sea ice melt pools as a source of ultraviolet radiation absorbing metabolites*. [Online]. University of Prince Edward Island.

Thorne, R.S.W. (1961) ‘Application of formazin standards to nephelometric estimation of beer turbidity’, *Journal of the Institute of Brewing*, 67(2), pp. 191–199.

Tiemeyer, M., Selleck, S.B. & Esko, J.D. (2009) ‘Arthropoda’, *Essentials of Glycobiology. 2nd*

edition,

de Tommasi, E., Congestri, R., Dardano, P., De Luca, A.C., Managò, S., Rea, I. & De Stefano, M. (2018) 'UV-shielding and wavelength conversion by centric diatom nanopatterned frustules', *Scientific Reports*, 8(1), pp. 1–14.

Tonzani, S. (2009) 'Time to change the bulb', *Nature*, 459(7245), p. 312.

Toonen, R.J. & Pawlik, J.R. (1996) 'Settlement of the tube worm *Hydroides dianthus* (Polychaeta: Serpulidae): cues for gregarious settlement', *Marine Biology*, 126(4), pp. 725–733.

Trani, R., Corriero, G., de Pinto, M.C., Mercurio, M., Pazzani, C., Pierri, C., Scrascia, M. & Longo, C. (2021) 'Filtering activity and nutrient release by the keratose sponge *Sarcotragus Spinosulus* Schmidt, 1862 (Porifera, Demospongiae) at the laboratory scale', *Journal of Marine Science and Engineering*, 9(2), p. 178.

Tree, J.A., Adams, M.R. & Lees, D.N. (1997) 'Virus inactivation during disinfection of wastewater by chlorination and UV irradiation and the efficacy of F+ bacteriophage as a "viral indicator"', *Water Science and Technology*, 35(11–12), pp. 227–232.

Vansteenbrugge, L., Ampe, B., De Troch, M., Vincx, M. & Hostens, K. (2015) 'On the distribution and population dynamics of the ctenophore *Mnemiopsis leidyi* in the Belgian part of the North Sea and Westerschelde estuary', *Marine Environmental Research*, 110pp. 33–44.

Vasilets, V.N., Nakamura, K., Uyama, Y., Ogata, S. & Ikada, Y. (1998) 'Improvement of the micro-wear resistance of silicone by vacuum ultraviolet irradiation', *Polymer*, 39(13), pp. 2875–2881.

Vernberg, W.B. & Vernberg, F.J. (1972) 'The synergistic effects of temperature, salinity, and mercury on survival and metabolism of the adult fiddler crab, *Uca pugilator*', *Fishery Bulletin*, (2), .

Vidal-Liñán, L., Villaverde-de-Sáa, E., Rodil, R., Quintana, J.B. & Beiras, R. (2018) 'Bioaccumulation of UV filters in *Mytilus galloprovincialis* mussel', *Chemosphere*, 190pp. 267–271.

de Vries, H.J., Kleibusch, E., Hermes, G.D.A., van den Brink, P. & Plugge, C.M. (2021) 'Biofouling control: the impact of biofilm dispersal and membrane flushing', *Water Research*, 198p. 117163.

van de Waal, D.B. & Litchman, E. (2020) 'Multiple global change stressor effects on phytoplankton nutrient acquisition in a future ocean', *Philosophical Transactions of the Royal Society B: Biological Sciences*, 375(1798), pp. 1–8.

Wahl, M. (2020) 'Living attached: aufwuchs, fouling, epibiosis', in *Fouling Organisms of the Indian Ocean*. [Online]. CRC Press. pp. 31–83.

Wahl, M. (1989) 'Marine epibiosis. I. Fouling and antifouling: some basic aspects', *Marine Ecology Progress Series*, 58pp. 175–189.

Wahl, M. & Lafargue, F. (1990) 'Marine epibiosis', *Oecologia*, 82(2), pp. 275–282.

Waite, J.H. (2017) 'Mussel adhesion–essential footwork', *Journal of Experimental Biology*, 220(4), pp. 517–530.

Waldfried, C., Sakthivel, P., Frisella, P., Moore, D., Berry, I., Durr, K. & Han, Q. (2006) 'UV curing technology for advanced device fabrication: challenges and solutions', in *2006 8th International Conference on Solid-State and Integrated Circuit Technology Proceedings*. [Online]. 2006 IEEE. pp. 513–516.

Walters, L.J., Miron, G. & Bourget, E. (1999) 'Endoscopic observations of invertebrate larval substratum exploration and settlement', *Marine ecology progress series*, 182pp. 95–108.

Wang, J., Rong, H. & Zhang, C. (2018) 'Evaluation of the impact of dissolved oxygen concentration on biofilm microbial community in sequencing batch biofilm reactor', *Journal of bioscience and bioengineering*, 125(5), pp. 532–542.

Wang, X., Niu, X., Chen, Y., Sun, Z., Han, A., Lou, X., Ge, J., Li, X., Yang, Y., Jian, J., Gonçalves, R.J. & Guan, W. (2019) 'Transcriptome sequencing of a toxic dinoflagellate, *Karenia mikimotoi* subjected to stress from solar ultraviolet radiation', *Harmful Algae*, 88(July), p. 101640.

Watnick, P. & Kolter, R. (2000) 'Biofilm, city of microbes', *Journal of bacteriology*, 182(10), pp. 2675–2679.

Weber, S.D., Hofmann, A., Pilhofer, M., Wanner, G., Agerer, R., Ludwig, W., Schleifer, K.-H. & Fried, J. (2009) 'The diversity of fungi in aerobic sewage granules assessed by 18S rRNA gene and ITS sequence analyses', *FEMS microbiology ecology*, 68(2), pp. 246–254.

Welch, D., Buonanno, M., Grilj, V., Shuryak, I., Crickmore, C., Bigelow, A.W., Randers-Pehrson, G., Johnson, G.W. & Brenner, D.J. (2018) 'Far-UVC light: A new tool to control

the spread of airborne-mediated microbial diseases', *Scientific Reports*, 8(1), pp. 1–7.

Werschkun, B., Sommer, Y. & Banerji, S. (2012) 'Disinfection by-products in ballast water treatment: An evaluation of regulatory data', *Water Research*, 46(16), pp. 4884–4901.

Wetherbee, R., Lind, J.L., Burke, J. & Quatrano, R.S. (1998) 'The first kiss: Establishment and control of initial adhesion by raphid diatoms', *Journal of Phycology*, 34(1), pp. 9–15.

Whitworth, P., Aldred, N., Reynolds, K.J., Plummer, J., Duke, P. & Clare, A.S. (2022) 'Importance of duration, duty-cycling and thresholds for the implementation of ultraviolet C in marine biofouling control', *Frontiers in Marine Science*, 8pp. 1–14.

Wickham, H., Navarro, D. & Pedersen, T.L. (2016) *Elegant graphics for data analysis (ggplot2)*. Third. Springer-Verlag New York.

Wieczorek, S.K. & Todd, C.D. (1998) 'Inhibition and facilitation of settlement of epifaunal marine invertebrate larvae by microbial biofilm cues', *Biofouling*, 12(1–3), pp. 81–118.

Williamson, C.E., Stemberger, R.S., Morris, D.P., Frost, T.M. & Paulsen, S.G. (1996) 'Ultraviolet radiation in North American lakes: attenuation estimates from DOC measurements and implications for plankton communities', *Limnology and Oceanography*, 41(5), pp. 1024–1034.

Wilson, N., Corbett, S. & Tovey, E. (2020) 'Airborne transmission of covid-19', *bmj*, 370.

Winward, G.P., Avery, L.M., Stephenson, T. & Jefferson, B. (2008) 'Ultraviolet (UV) disinfection of grey water: Particle size effects', *Environmental Technology*, 29(2), pp. 235–244.

Worrest, R.C., Dyke, H. Van & Thomson, B.E. (1978) 'Impact of enhanced simulated solar ultraviolet radiation upon a marine community', *Photochemistry and Photobiology*, 27(4), pp. 471–478.

Wu, S., Guttmann, M., Lobo-Ploch, N., Gindele, F., Susilo, N., Knauer, A., Kolbe, T., Raß, J., Hagedorn, S. & Cho, H.K. (2022) 'Enhanced light extraction efficiency of UV LEDs by encapsulation with UV-transparent silicone resin', *Semiconductor Science and Technology*, 37(6), .

Wu, Y., Li, Z., Du, W. & Gao, K. (2015) 'Physiological response of marine centric diatoms to ultraviolet radiation, with special reference to cell size', *Journal of Photochemistry and Photobiology B: Biology*, 153pp. 1–6.

Yamano, N., Kunisada, M., Kaidzu, S., Sugihara, K., Nishiaki-Sawada, A., Ohashi, H., Yoshioka, A., Igarashi, T., Ohira, A., Tanito, M. & Nishigori, C. (2020) 'Long-term effects of 222-nm ultraviolet radiation C sterilizing lamps on mice susceptible to ultraviolet radiation', *Photochemistry and Photobiology*, 96(4), pp. 853–862.

Yaseen, A.A., Al-Tikrity, E.T.B., Yousif, E., Ahmed, D.S., Kariuki, B.M. & El-Hiti, G.A. (2021) 'Effect of ultraviolet irradiation on polystyrene containing cephalexin Schiff bases', *Polymers*, 13(17), .

Ye, X., Grube, W. & Zhu, H. (2022) 'UV tunable light source and its potential applications for UVC virus inactivation research', in *Photonic Instrumentation Engineering IX*. [Online]. 2022 SPIE. pp. 135–140.

Yebra, D.M., Kiil, S. & Dam-Johansen, K. (2004) 'Antifouling technology - Past, present and future steps towards efficient and environmentally friendly antifouling coatings', *Progress in Organic Coatings*, 50(2), pp. 75–104.

Yim, S., Lee, J., Jo, H., Scholten, J., Willingham, R., Nicoll, J. & Baswan, S.M. (2019) '*Chrysanthemum morifolium* extract and ascorbic acid-2-glucoside (AA2G) blend inhibits UVA-induced delayed cyclobutane pyrimidine dimer (CPD) production in melanocytes', *Clinical, cosmetic and investigational dermatology*, 12p. 823.

Yoshikawa, A., Hasegawa, R., Morishita, T., Nagase, K., Yamada, S., Grandusky, J., Mann, J., Miller, A. & Schowalter, L.J. (2020) 'Improve efficiency and long lifetime UVC LEDs with wavelengths between 230 and 237 nm', *Applied Physics Express*, 13(2), p. 22001.

You, F.M., Huo, N., Deal, K.R., Gu, Y.Q., Luo, M.-C., McGuire, P.E., Dvorak, J. & Anderson, O.D. (2011) 'Annotation-based genome-wide SNP discovery in the large and complex *Aegilops tauschii* genome using next-generation sequencing without a reference genome sequence', *BMC genomics*, 12(1), pp. 1–19.

Youn, B.-H. & Huh, C.-S. (2005) 'Surface degradation of HTV silicone rubber and EPDM used for outdoor insulators under accelerated ultraviolet weathering condition', *IEEE Transactions on Dielectrics and Electrical Insulation*, 12(5), pp. 1015–1024.

Zabihi, Z., Homayoonfal, M. & Davar, F. (2020) 'Application of UV irradiation enhanced by CuS photosensitive nanoparticles to mitigate polysulfone membrane fouling', *Journal of Photochemistry and Photobiology A: Chemistry*, 390(December 2019), p. 112304.

Zamir Bin Alam, M., Otaki, M., Furumai, H. & Ohgaki, S. (2001) 'Direct and indirect

inactivation of *Microcystis aeruginosa* by UV-radiation', *Water Research*, 35(4), pp. 1008–1014.

Zargiel, K.A., Coogan, J.S. & Swain, G.W. (2011) 'Diatom community structure on commercially available ship hull coatings', *Biofouling*, 27(9), pp. 955–965.

Zelle, M.R. (1960) 'Biological effects of ultraviolet radiation', *IRE Transactions on Medical Electronics*, ME-7(3), pp. 130–135.

Zhang, M., Wang, L. & Zhong, D. (2017) 'Photolyase: Dynamics and electron-transfer mechanisms of DNA repair', *Archives of biochemistry and biophysics*, 632pp. 158–174.

Supplementary material

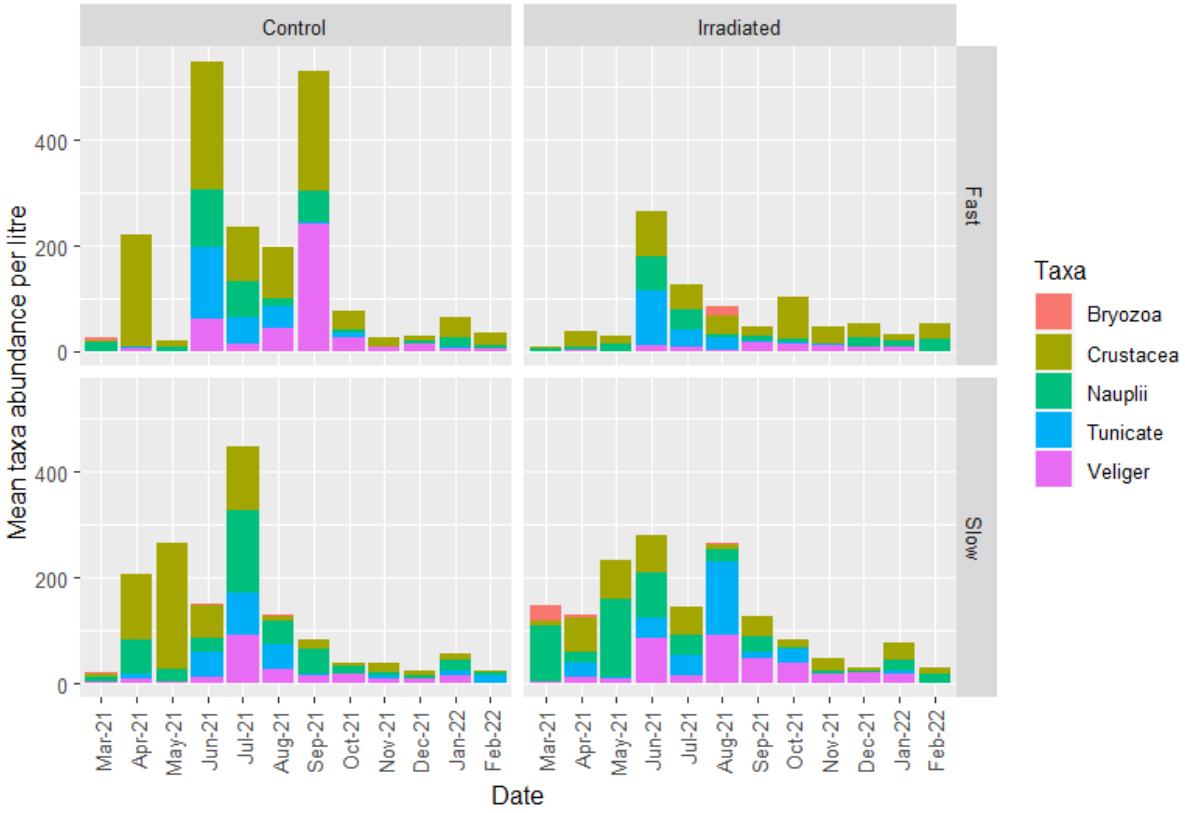

Supplementary Figure 1. Planktonic abundances from field deployed experimental chambers over 12-months.

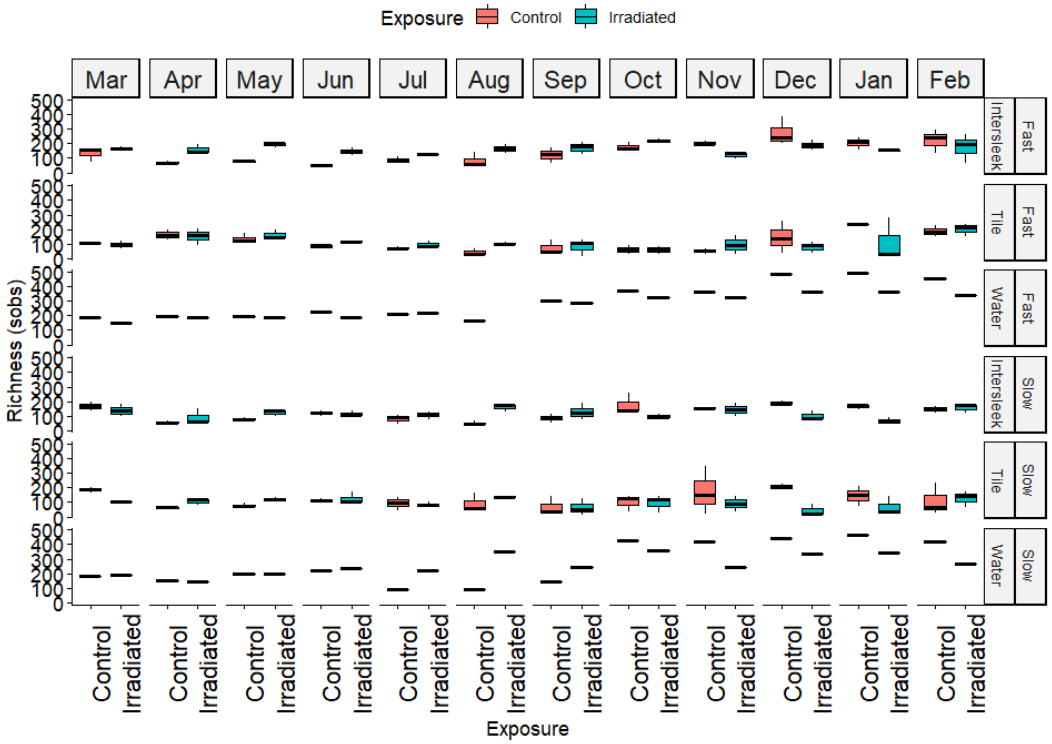

Supplementary Figure 4 Sobs diversity indices of OTUs identified from 18S metagenetic analysis. Samples were deployed for 12 months in Hartlepool. UK.

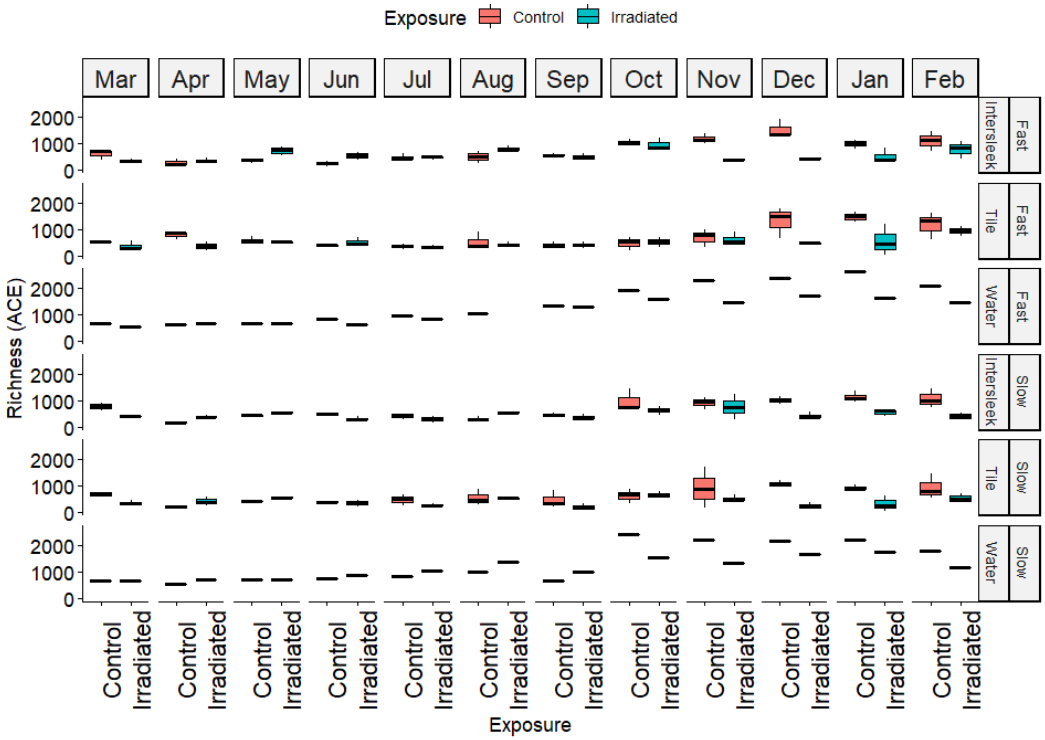

Supplementary Figure 7 ACE diversity indices of OTUs identified from 18S metagenetic analysis. Samples were deployed for 12 months in Hartlepool. UK.

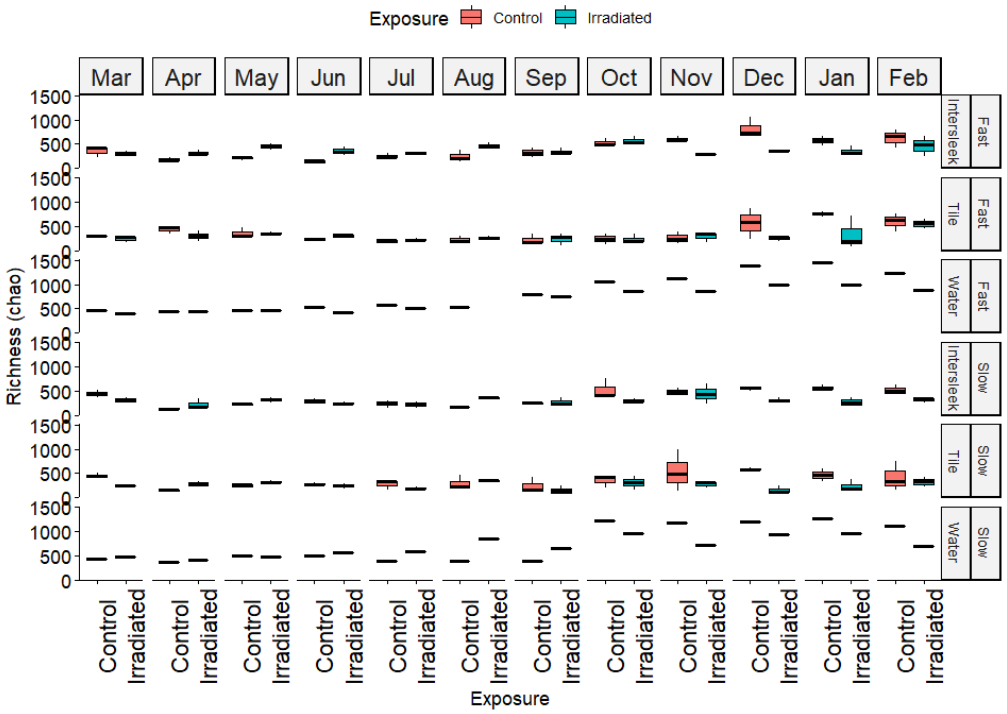

Supplementary Figure 10. Chao diversity indices of OTUs identified from 18S metagenetic analysis. Samples were deployed for 12 months in Hartlepool. UK.

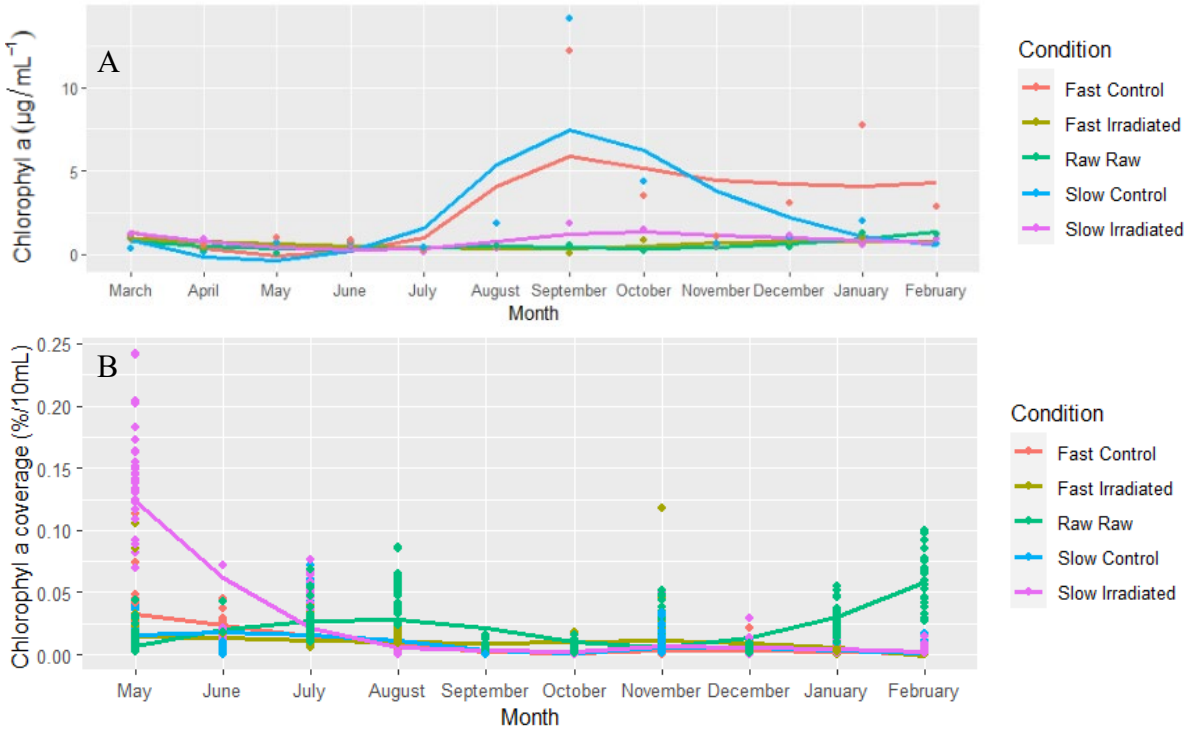

Supplementary Figure 11 Planktonic Chl-a abundance, sampled from five chambers at Hartlepool marina from March 2021- February 2022. A). DMSO extraction and fluorescence method attaining quantitation in µg/mL. B). Epifluorescent microscopy method attaining quantitation in photograph percentage coverage of filter per 10mL of raw sample. Samples collected using a 50-micron net and determined via DMSO extraction and fluorescence. Photographs of March and April for B were corrupt and omitted.